SYNTHESIS AND PHOTOPHYSICAL STUDIES OF CROWN ETHER-BODIPY DYES AND THE FABRICATION OF BODIPY EMBEDDED FLUORESCENT NANOFIBERS.

A thesis submitted in fulfilment of the requirements for the degree of

MASTERS OF SCIENCE

OF RHODES UNIVERSITY

BY

JUSTIN STONE

FEBRUARY 2016

I dedicate this thesis to

My parents

Mark and Brenda Stone

None of this could have been possible without your infinite patience and support. I am eternally grateful, for everything that you have done for me.

ACKNOWLEDGMENTS

I would like to express my deepest appreciation to my thesis supervisor Dr John Mack of the chemistry department at Rhodes University. Working with him has been an invaluable experience and I will forever be grateful for the opportunities that he has given me. Without his guidance, dedication and tenacity this thesis would not have been possible.

I would like to give a special thanks to Professor Tebello Nyokong for her unwavering faith, support and encouragement throughout the course of my studies. I will be forever in your debt.

I would like to give an extra special thank you to Ms Gail Cobus for being the silent glue that holds our entire lab together and for her help with the administration work.

In addition, I would like to thank Dr Jonathon Britton for countless insightful conversations throughout my studies. And a special thank you to the students of the S22 research group for putting up with my craziness and for being an absolute pleasure to work beside.

To Professor Nagao Kobayashi and Kimura Sensei of Shinshu University who were kind enough to allow me to visit Japan on a research exchange and who were critical for the success of the work doumo arigatou gozaimashita. This thank you extends to all of the students in Kimura-lab for their warm hospitality and invaluable assistance during my stay in Japan.

I would be remiss not to thank the amazing administration, technical and support staff of the Rhodes chemistry department whose moral support, and rapid responses with regards to equipment repair and coffee delivery, enabled the success of this work.

I am grateful to all of my friends, especially my brothers at The KEG. I thank you for the great times; the interesting conversations and for always having my back. Thank you for keeping me sane, keep being awesome.

I am eternally grateful to my family for making this all possible and for being the source of my motivation. This work is as much yours as it is mine. Thank you.

To Alison Geddie, I thank you for always being there to help pick me up and dust me off. Her support means more to me than she could ever know.

Abstract:

This study has three major objectives: 1) to synthesize a series of structurally related BODIPY dyes, 2) to fabricate BODIPY embedded electrospun nanofibers, and 3) to investigate and characterize the photophysical properties of all synthesized BODIPY dyes with a special focus on their ability to generate singlet oxygen.

This thesis first explores the acid catalysed condensation reaction to produce two structurally analogous meso-substituted BODIPY dyes based on cuminaldehyde and 4-dimethylaminobenzaldehdye. In order to enhance the rate of ISC and promote the generation of reactive oxygen species bromine atoms were then attached to the BODIPY 2,6-positions. These BODIPY dyes were then embedded in a polystyrene solution and electrospun into nanofibers. The resulting nanofibers were found to be highly fluorescent, but were no longer able to generate singlet oxygen.

Ion-sensitive BODIPYs were prepared from the dibrominated BODIPY dyes by employing a modified Knoevenagel condensation reaction to form a styryl bond with 4'-formylbenzo-15-crown-5 at the 3,5-position of the BODIPY core.

Changes in the morphology and position of the absorption and emission spectra of these crown ether-styryl BODIPY dyes were observed in the presence of sodium ions. These results imply that crown ether-substituted BODIPY dyes could function as ion sensors

Table of Contents

List of Schemes:

List of Tables:

List of Figures:

List of Equations:

List of Symbols:

S_0	Singlet ground state
S_1	First singlet excited state
T_1	First triplet excited state
$^1O_2$	Singlet oxygen
Å	Angstrom
K_s	Stability constant
S_2	Second singlet excited state
T_2	Second triplet excited state
$^3O_2$	Triplet oxygen
Φ_F	Fluorescence quantum yield
k_f	Rate of fluorescence
k_d	Rate of excited state depopulation processes
η	Refractive index
F	Integrated fluorescence emission
A	Absorbance maxima at excitation wavelength
τ_F	Fluorescence lifetime
τ_d	Phosphorescence decay lifetime
T_τ	Triplet lifetime
B	Sensitizer coefficient
Φ_Δ	Singlet oxygen quantum yield
W	sensitizer photobleaching rate

I	Rate of absorption
^{1}H	Proton NMR
SDD	Gaussian09 default basis set
ε	Molar extinction coefficient
λ_{max}	Absorption maxima

List of Abbreviations:

A	Absorption
Abs	Absorption
ADMA	Anthracene-9, 10-bis-methylmalonate
B3LYP	Becke, three-parameter, Lee-Yang-Parr
Benz	4-Meso benzaldehyde substituted BODIPY dye
CHNS	Carbon, hydrogen, nitrogen, sulfur
DCM	Dichloromethane
DDQ	2, 3-Dichloro-5, 6-dicyano-1, 4-benzoquinone
DMF	Dimethylformamide
DMSO	Dimethyl sulfoixde
DPBF	1,3-Diphenylisobenzofuran
EDG	Electron donating group
Em	Emission
ESI	Electron spray ionization
EWG	Electron withdrawing group
Ex	Excitation
FT-IR	Fourier transformation Infra-red spectroscopy
HOMO	Highest occupied molecular orbital
HSAB	Hard and soft acid and base
ISC	Intersystem-crossing
LED	Light emitting diode
LUMO	Lowest unoccupied molecular orbital
MALDI	Matrix-assisted laser desorption/ionization
MS	Mass spectrometry
NBS	N-bromosuccinamide
Nd:YAG	Neodynium-doped yttrimium aluminium garnet
NMR	Nuclear magnet resonance spectroscopy

OPO	Optical parametric oscillator
Pc	Phthalocyanine
PDT	Photodynamic therapy
PET	Photon-induced electron transfer
PMT	Photomultiplier tube
PS	Polystyrene
R6G	Rhodamine-6 G
RB	Rose Bengal
r.t.	Room temperature
SEM	Scanning electron microscopy
Std	Standard
TCSPC	Time-correlated single photon counter
TD-DFT	Time-dependant density functional theory
TEA	Triethylamine
TFA	Trifluoroacetic acid
THF	Tetrahydrofuran
TLC	Thin layer chromatography
TMS	Tetramethylsilane
TOF	Time-of-flight
Trans	Transition
XRD	X-ray diffraction

Chapter 1:

Introduction

Properties, Applications and Structure of BODIPY Dyes and Crown Ethers

1.1 4,4-Difluoro-4-bora-3a,4a-diaza-*s*-indacene (BODIPY) dyes

1.1.1 History and Applications

Difluoroboron-complexed dipyrrins were first identified by Treibs and Kreuzer in 1968.[1] These compounds were identified when the authors attempted the acylation of 2,4-dimethyl pyrrole with acetic anhydride using BF_3 as the catalyst. Instead of the desired pyrrole they noted the formation of a highly fluorescent product which resulted from the complexation of a boron atom following the acid catalyzed condensation of the two pyrrole units. They went on to synthesize a number of different difluoro-complex dipyrrins and noted that these new molecules have intense absorbance around 500 nm and are highly fluorescent.[1] After their initial paper very little research was reported on these dipyrrin complexes until 1989 when Monsma et al. demonstrated the potential of these dyes for the fluorescent imaging of cells **(Figure 1)**.[2]

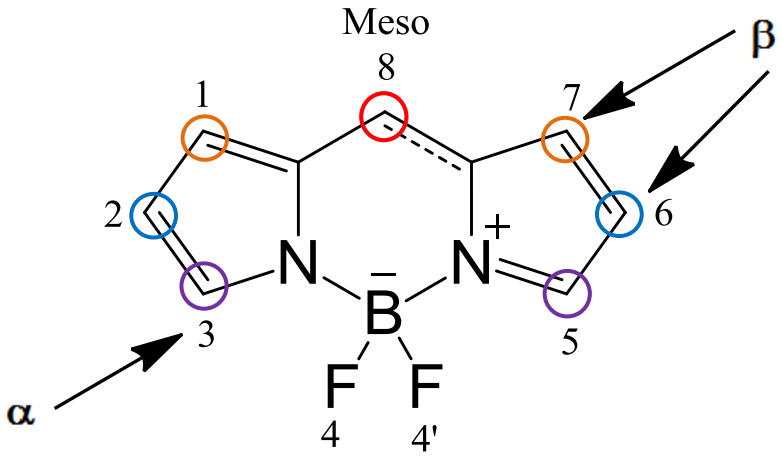

Figure 1: The 4,4-difluoro-4-bora-3a,4a-diaza-*s*-indacene (BODIPY) core including the IUPAC number sequence used for naming BODIPY dyes (unsubstituted BODIPY).

This resulted in a sharp rise in interest in these molecules and has led to their development for a number of applications beyond the staining of cells.[3] Monsma abbreviated the long name: 4,4-difluoro-4-bora-3a,4a-diaza-*s*-indacene to the more familiar BODIPY as these dyes are now usually known. It has been suggested that BODIPY dyes could replace fluoroscein for biolabelling due to their superior photostablity.[4] The utility of BODIPY dyes for use as lasers dyes[5,6,7] and solar collectors[8,9] was also explored due to their remarkable photophysical properties. In recent years there has been a strong focus on the synthesis of water soluble and near infrared (NIR) region BODIPY dyes for use as biolabels[10,11] and in cellular imaging **(Figure 2)**.[12,13,14]

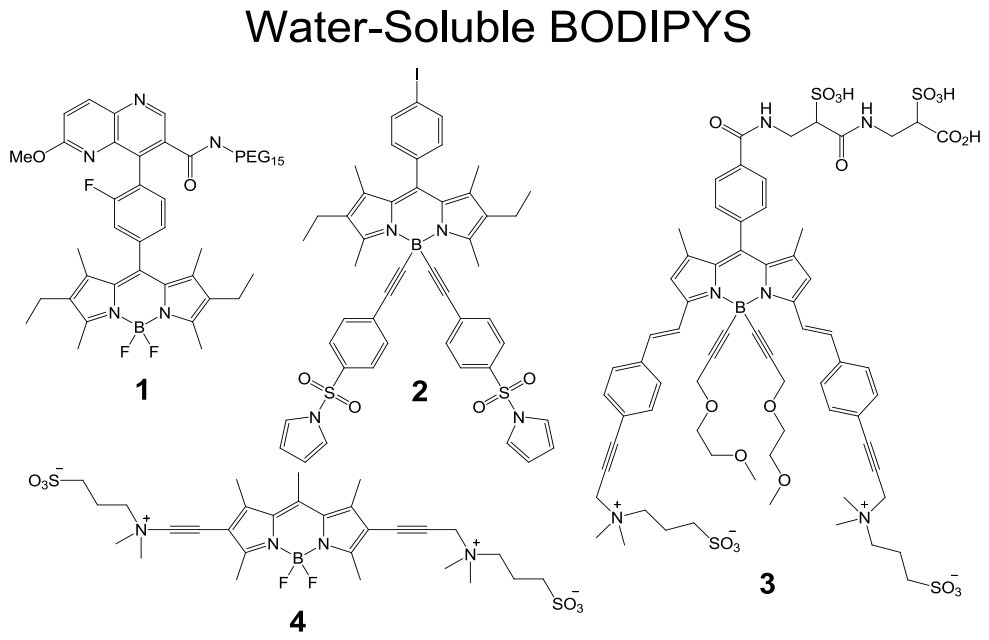

Figure 2: Strategies to improve the water solubility of BODIPY dyes target virtually every position of the BODIPY core. (See **Table 1** for a summary of photophysical data.)

While having the ability to absorb red light is an important characteristic for biological applications it was rather incidental in this work and was used as a diagnostic indicator rather than a required property.

Figure 3 highlights examples from the literature of BODIPY dyes that have been used for various applications. Amongst the most important in this regard are their use as fluorescent sensors for pH[15,16,17] and the detection of a number of environmentally significant cations, such as Hg^{2+}, Cu^{2+}, $Cr^{3+}$and Zn^{2+}).[12,18,19,20] The detection of anions[21] and biomolecules[22] are still being investigated by a number of groups due to the huge structural diversity afforded by the BODIPY core **(Figure 4)**. The initial report by Nagano's group, that the BODIPY core could be modified to enhance the generation of cytotoxic singlet oxygen has led to research exploring their potential as photodynamic therapy (PDT) agents.[23,24,25,26,27]

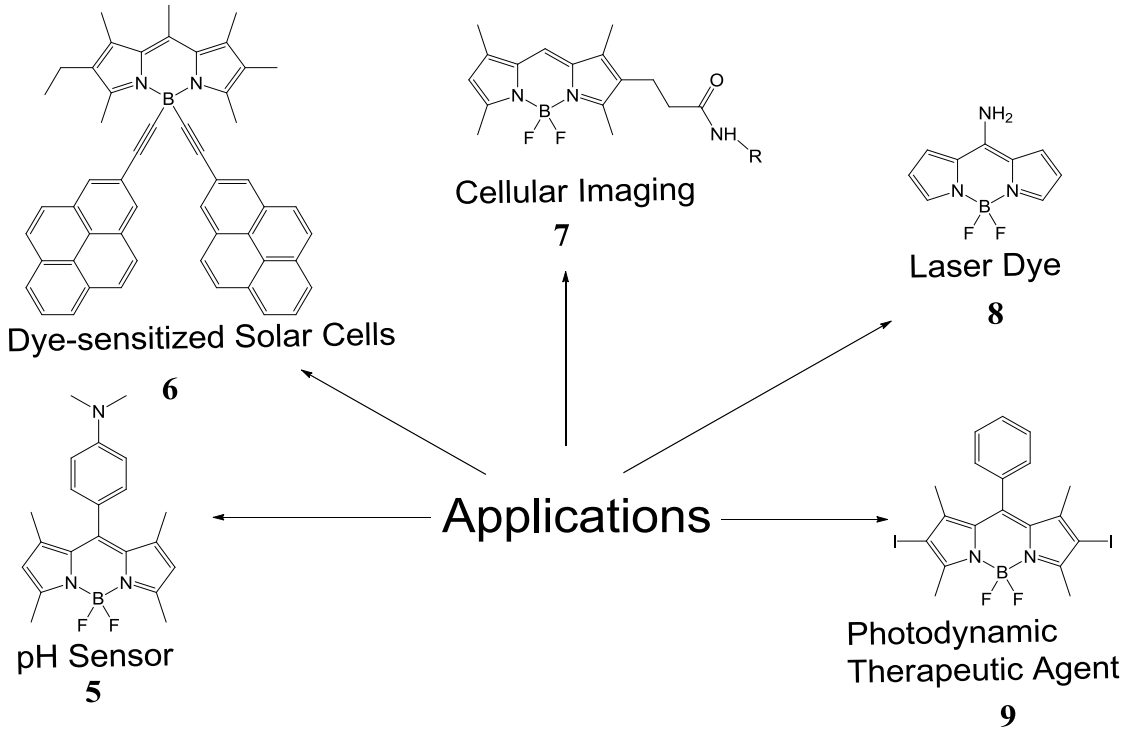

Figure 3: Applications highlighting the versatility of substituted BODIPY dyes. (See **Table 1** for a summary of photophysical data.)

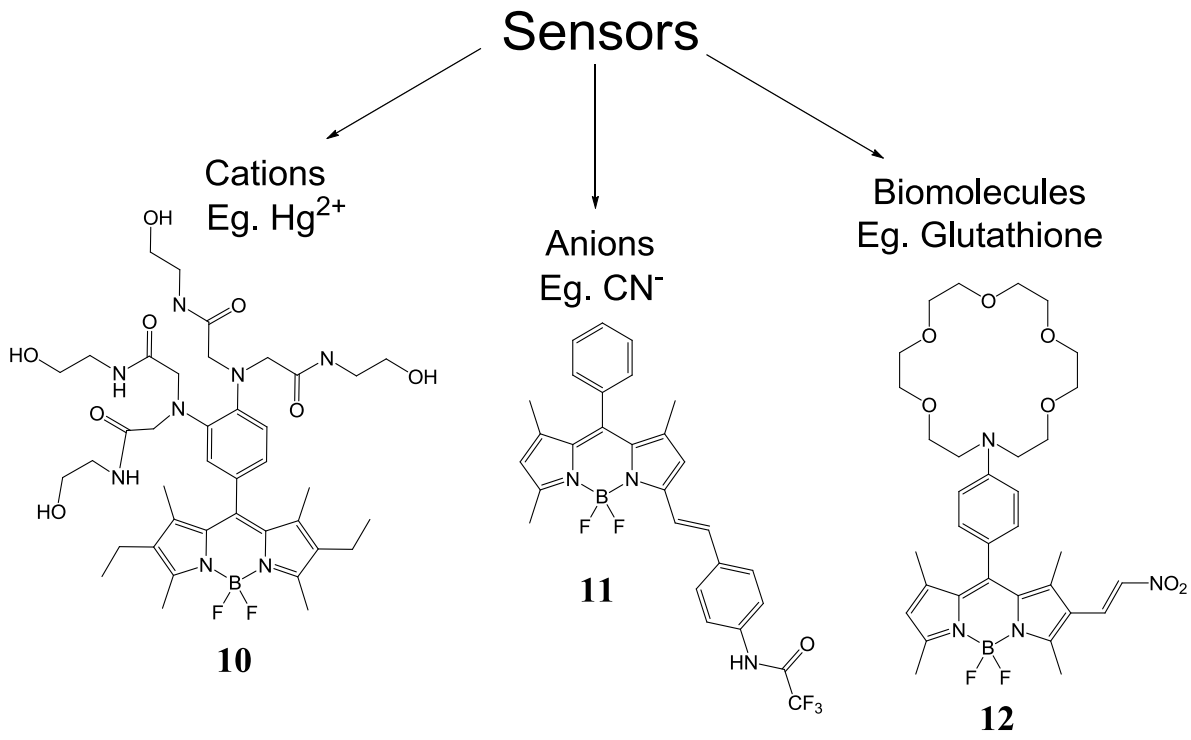

Figure 4: Examples from the literature of BODIPY dye-based sensors. (See **Table 1** for a summary of photophysical data.)

1.1.2 General Properties of BODIPY dyes

BODIPY dyes possess a number of favourable photochemical properties. They are intensely coloured with high molar extinction of coefficients between 40,000–100,000 M^{-1} cm^{-1} being widely reported.[28] Unfunctionalized BODIPY dyes typically absorb in the of 490–520 nm region and are usually resistant to changes in solvent polarity due to their rigid structure and internal zwitter ionic configuration **(Figure 5)**.[28,29] The absorption spectrum of a BODIPY dye tends to be dominated by a single absorption band that is associated almost entirely with the $S_0 \rightarrow S_1$ ($\pi \rightarrow \pi^*$) transition. A shoulder is typically observed on the high-energy side of the main absorption band in the 475–485 nm region due to a 01 vibrational transition.[30] A weak transition has also

been observed as a weak absorption band in the 300–400 nm region and has been attributed to the $S_0 \rightarrow S_2$ ($\pi \rightarrow \pi^*$) transition.[30] The band maxima in the electronic absorption and emission spectra can be shifted by attaching substituents at various positions of the BODIPY core. BODIPY dyes can be synthesized for biological applications such as photodynamic therapy, provided that their main spectral band is shifted enough to allow them to absorb light in the NIR region.[31]

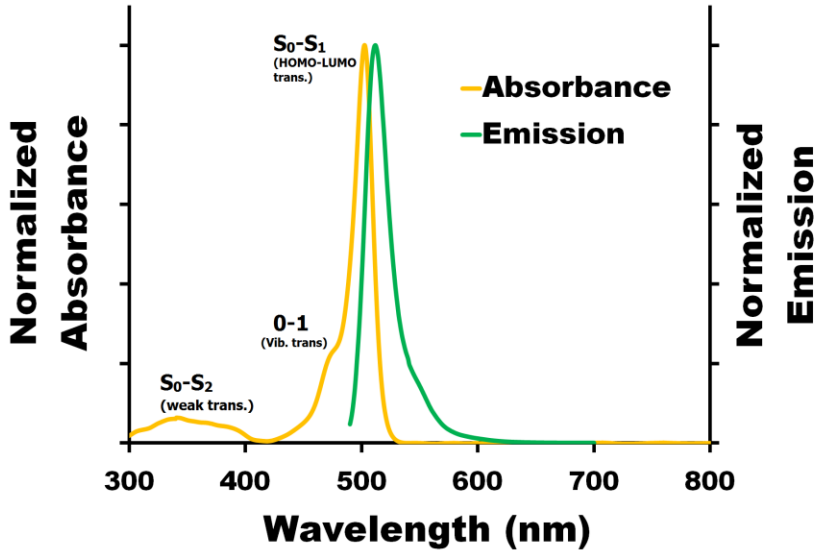

Figure 5: Ground state electronic absorption (yellow) and fluorescence emission (green) spectra of a meso-substituted BODIPY dye.

The intense colours of BODPIY dyes are often clearly distinct from those of the starting materials which make it possible to qualitatively assess the success of synthetic reactions based on the colour of the solution. Reactions involving BODIPYs are therefore relatively easy to monitor and purification using chromatography is relatively straightforward given their high solubility in a wide range of organic solvents. Another characteristic commonly observed with BODIPY dyes is their high fluorescence emission intensity **(Figure 6)**. The ability of BODIPY dyes to fluoresce has been extensively studied and has generally been considered to be the single most

important characteristic that the dyes possess.[3,32] Typically BODIPYs have narrow emission bands in the 500–550 nm region, but as with their absorption properties this band can be red shifted into the 700 nm range [3,31] after structural modification. Solid state fluorescence is observed in BODIPYs that have bulky substituents at the boron or meso-positions. This is attributed to steric hindrance between BODIPY dye molecules in solution which reduces aggregation and thus concentration based quenching of their fluorescent state when the solvent is removed. [33] Some BODIPY dyes are such potent fluorophores that it is possible to observe their fluorescence even in ambient light.[34] Fluorescence quantum yields for BODIPY dyes can vary from near zero to almost 1.0 depending on the nature of the substituents on the core and the chemical environment.[35] (see section 1.4.3). This has enabled for the development of a number of "off-on" fluorescent sensors. The characteristically small Stokes shift (ca. 300 cm^{-1}), the difference in wavelength between the band maxima of the absorbed and emitted light for the $S_0 \rightarrow S_1$ transition, observed for BODIPY dyes arise as a result of their rigid structure which prevents non-radiative deactivation of the excited state and results in the S_0 and S_1 states having similar potential energy surfaces.[35,36] The fluorescence lifetime of BODIPY dyes is typically in the single digit nanosecond (3–7 x 10^{-9} s) range.[37] High fluorescence quantum yields and short lifetimes make BODIPY dyes highly suitable for imaging and sensing applications.[38] Unsubstituted BODIPY dyes do not phosphoresce due to a low rate of intersystem crossing (ISC). But, Nagano et al. were able to demonstrate that the spin-selection rule could be relaxed by attaching a halogen atom to the BODIPY core and that halogenated BODIPY dyes do phosphoresce (see section 1.4.1).[23] BODIPYs are renowned for being highly stable chemically and

thermally, and are unusually photostable due to their high oxidation potentials and their neutral charge.[23,39]

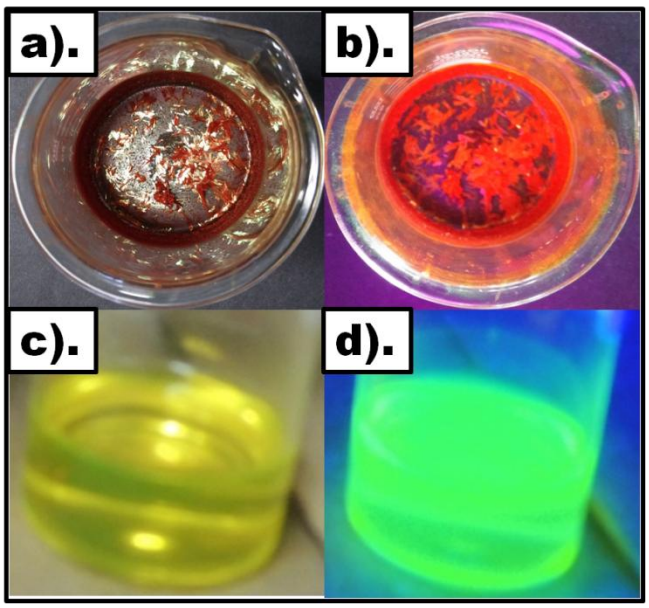

Figure 6: **(a)** Fine crystals of meso-phenyl BODIPY dye. **(b)** Solid state orange fluorescence observed upon irradiated by UV light. **(c)** A solution of yellow meso-phenyl BODIPY in $CHCl_3$. **(d)** The intense green fluorescence of meso-phenyl BODIPY under UV irradiation.

Unlike porphyrins and pthalocyanines BODIPY dyes are not prone to aggregation.[35] Although BODIPYs are highly soluble in most organic solvents, they tend to be insoluble in aqueous solutions. A number of water soluble BODIPYs have been synthesized to address this shortcoming for those applications that require water solubility.[14,40,41,42,43]

1.1.3 BODIPY Structure

BODIPY dyes are heterocyclic molecules with core structures that are comprised of two carbon atom linked pyrrole rings that are complexed by a BF_2 moiety. An interpyrrolic methine bridge (referred to as the meso-carbon) joins the two pyrrole

groups to form the dipyrromethene.[44] Despite displaying properties that are typical of aromatic compounds, BODIPY dyes are not aromatic as they do not obey Hückel's rule. Their pseudo-aromatic behaviour arises as a result of coordination with a boron atom which forces the dipyrromethene into a rigid planar conformation.[29,30] BODIPY dyes are structural analogues of porphyrins **(Figure 1 and Figure 7)** and are numbered according to the IUPAC nomenclature for porphyrins. For this reason, they have sometimes been referred to as "porphyrins little sister" by some researchers.[3] The versatility of BODIPY dyes can be attributed to the ease with which structural changes can be made to the unsubstituted core.[35]

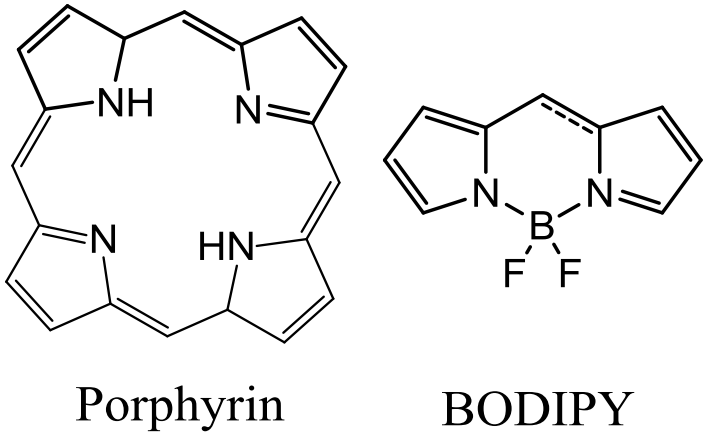

Figure 7: A structural comparison of an unsubstituted BODIPY dye to that of free base porphyrin.

1.1.4 Synthesis of BODIPY dyes

The synthesis of BODIPY dyes is often based on pyrrole condensation reactions, which have been extensively studied in the context of porphyrin chemistry **(Scheme 1)**.[45] Acid catalysis of an acid anhydride **(a)**[1], aldehyde **(b)**[46], or acid chloride[47], in the presence of excess pyrrole leads to the formation of dipyrromethane. The resulting dipyrromethane is highly unstable, so it is important to carry out the oxidation

reaction and complex the dipyrromethene that is formed with $BF_3{\cdot}OEt_2$ as soon as possible to form the BODIPY dye. Oxidation is usually carried out with 2,3-dichloro-5,6-dicyano-1,4-benzoquinone (DDQ) or *p*-chloranil and since basic conditions are required for boron complexation, a tertiary amine is usually employed as the base.[35] Synthesis of the unsubstituted BODIPY core is complicated by the instability of the required dipyrromethene.[36] It is far easier to start with a substituted pyrrole which can prevent tripyrromethane or porphyrin formation by blocking polymerization of the pyrrole units. A vast number of substituted BODIPYs can be synthesized through careful consideration of the starting pyrrole. Post-synthetic structural modifications are possible due to the stability of the BODIPY core.[32] The zwitterion caused by electronegativity differences between the heteroatoms within the BODIPY core provides sites that are vulnerable to both electrophilic and nucleophilic attack[29] **(Figure 1)**.

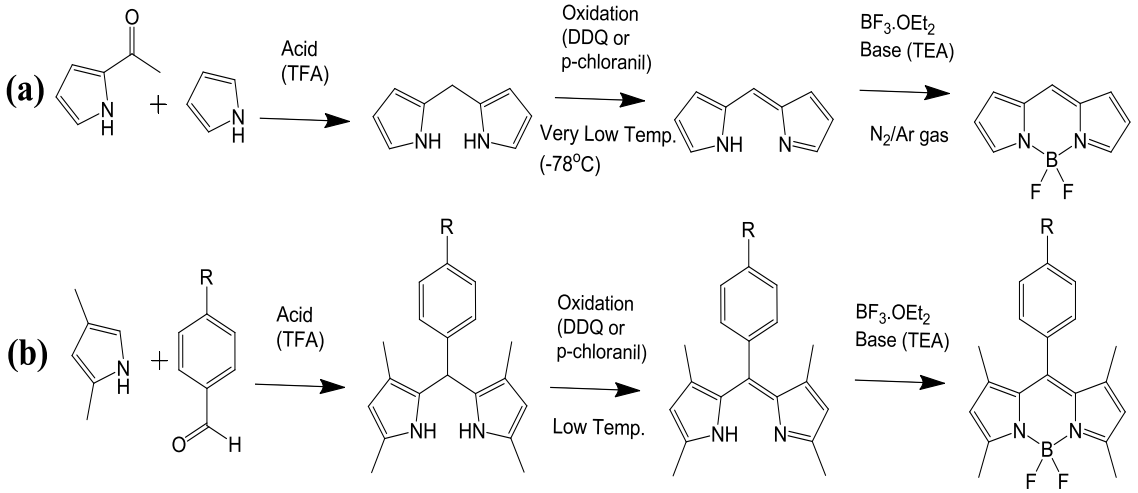

Scheme 1: The acid-catalysis of acid anhydride **(a)**, or aldehyde **(b)** with pyrrole to enable the synthesis of basic BODIPY dyes.

1.1.5 Functionalization of the BODIPY Core

BODIPY dyes are well known for their structural diversity which is due to the stability of the BODIPY core. As a result, substituents have been attached to virtually every position of the BODIPY core **(Figure 1)**. This section seeks to explore the structural and photophysical properties of each of these positions.

C8 or meso-position:

The bridging carbon at the 8-position of the BODIPY core is referred to as the meso–carbon.[48] The easiest method for substitution at the meso-position is via the acid catalysed condensation of pyrrole with an aromatic aldehyde followed by oxidation and BF_3 complexation (see section 1.1.4). A wide variety of meso-substituted BODIPYs have been synthesised in this manner by changing the starting aldehyde. **Figure 8** provides some examples of these BODIPYs and highlights one of the novel BODIPYs that was synthesized in this work. Substitution at this position often has little to no effect on the UV-visible absorption spectrum because they lie out of the plane of the BODIPY core resulting in poor conjugation with the π-system, but can greatly affect the fluorescence emission of the dye through photon-induced electron transfer (PET) processes.[16,30] Adding a substituent at this position can lead to a quenching of fluorescence emission, due to the presence of low lying charge transfer states between the BODIPY core and the meso-substituent.[32,49,50] When bulky groups are added at the ortho-positions intense fluorescence is observed, as the steric hindrance caused by the bulky groups prevents the non-radiative decay that is caused by free rotation.[4,35] The para-position of the meso-substituent is ideal for linking the BODIPY dye with other macromolecules;[27] water solubilising groups;[14] or

nanomaterials as substituents at this position have little effect on the absorbance properties of the BODIPY dye.[51] The effect of replacing the meso-carbon with a nitrogen atom has also been explored. The resulting aza-BODIPY dyes have excellent NIR absorption properties.[24,52]

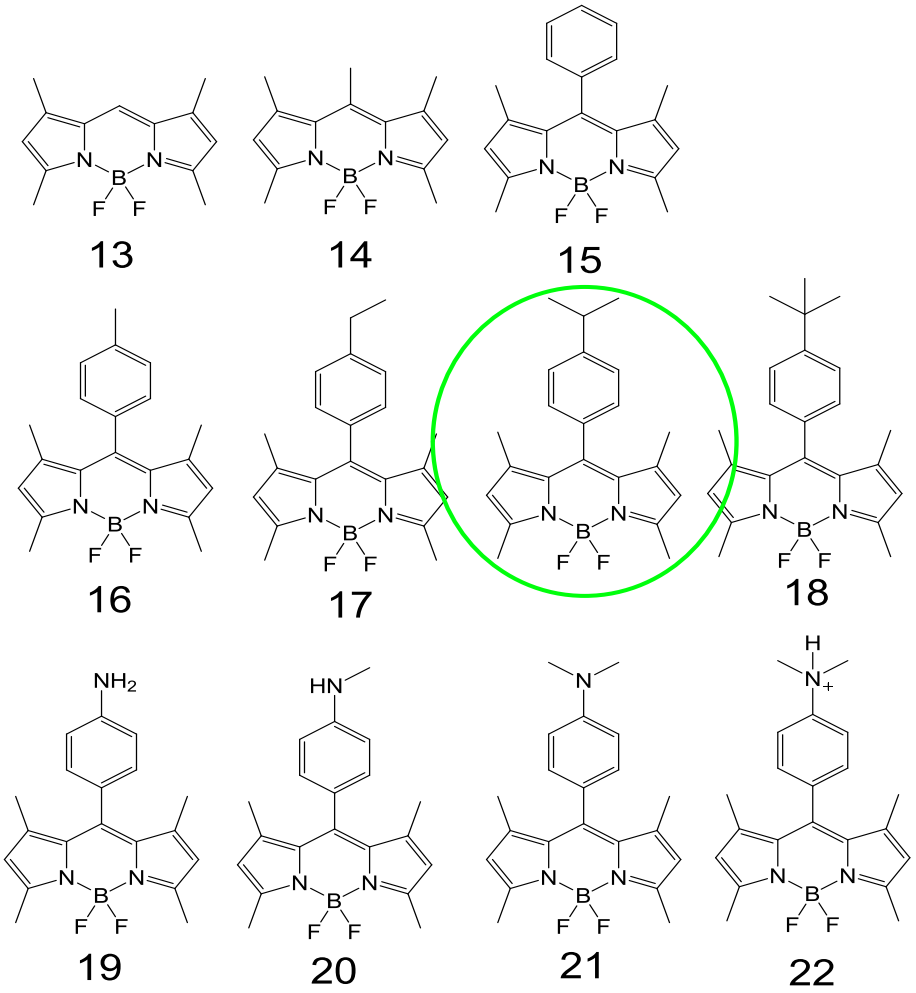

Figure 8: A selection of meso-BODIPY dyes taken from the literature highlighting the novel meso-(p-isopropylphenyl) BODIPY synthesized in this work. (See **Table 1** for a summary of photophysical data).

C1 and C7:

These positions lie next to the carbon atoms directly adjacent to the meso-carbon and are of least interest when attempting to change the photochemical properties of the BODIPY core.[54] They are, however, structurally significant positions which are most

commonly left unsubstituted or occupied by methyl groups. Halogen atoms and fused rings have also been incorporated at these positions and utilized to expand the π-conjugation of the BODIPY core.[4,39,55] Adding methyl groups, to the 1,7-positions serves a two-fold purpose. By blocking these positions the methyl groups can eliminate or reduce undesired polymerization of the dipyrromethene unit, to form tripyrrolemethene or porphyrins, leading to improved reaction yields.[45] The methyl groups also prevent rotation of phenyl rings at the meso-carbon. This causes a decrease of energy loss due to vibrational motion and an increase in fluorescence quantum yields **(Figure 9).**[32,49] Varying the starting pyrrole, or post-synthesis halogenation of unsubstituted BODIPYs, has been shown to be an effective method for functionalizing these positions.[56]

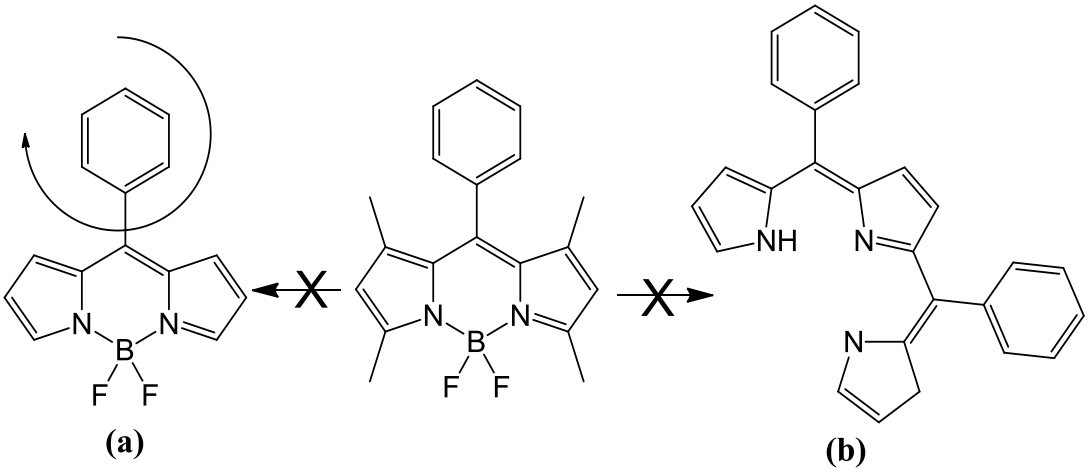

Figure 9: Steric hindrance caused by the methyl groups at the 1,7-positions minimizes energy loss from the meso-substituents to vibrational motion **(a)** and the methyl groups at the 3,5-positions prevent polymerization of the dipyrrin core **(b)**.

C2 and C6:

The carbons located at the middle of the pyrrole ring that lie furthest from each other are referred to as the 2,6-positions. In molecular modelling calculations these positions have been shown to have the least positive carbon atoms in the BODIPY core

and hence are the most susceptible to electrophilic attack.[23,57] The electronic structure of the BODIPY core reveals that the LUMO of the BODIPY π-system has a nodal plane at these positions, while the HOMO has a significant molecular orbital coefficient.[30] As a result, the addition of substituents at these positions can have a large effect on both the absorbance and emission properties of the BODIPY dye. Electron withdrawing groups (EWG) stabilize the HOMO orbital increasing the HOMO–LUMO band gap and hence cause a blue shift of the maxima of the main spectral bands, while electron donating groups (EDG) destabilize the HOMO orbital narrowing the HOMO–LUMO band gap resulting in a red shift of the main spectral bands.[30,58] Carboxylic[57], amino,[58], formyl,[59] nitro,[60] and sulphono[61] groups have all been added to these positions to impart different functionalities to the BODIPY core **(Figure 10)**. By fusing aromatic rings to these positions it is possible to further extend the π-system and rigidify the BODIPY core, resulting in a significant red shift of the maxima of the main spectral bands.[62] BODPIY units have also been linked at the 2,6-positions to form polymeric BODIPY dyes.[60,61] Of particular interest is halogenation at these positions. It has been shown that adding bromine or iodine atoms at these positions causes a red-shift of the BODIPY spectra.[23,39] Although the halogen atoms are EWGs they are resonance donators due to the lone pairs of electron pairs that they possess and this results in a net decrease in the HOMO–LUMO band gap. Halogenation at these positions causes a sharp decrease in the fluorescence quantum yields of the dyes due to heavy atom effect (see chapter 1.4.1).[56]

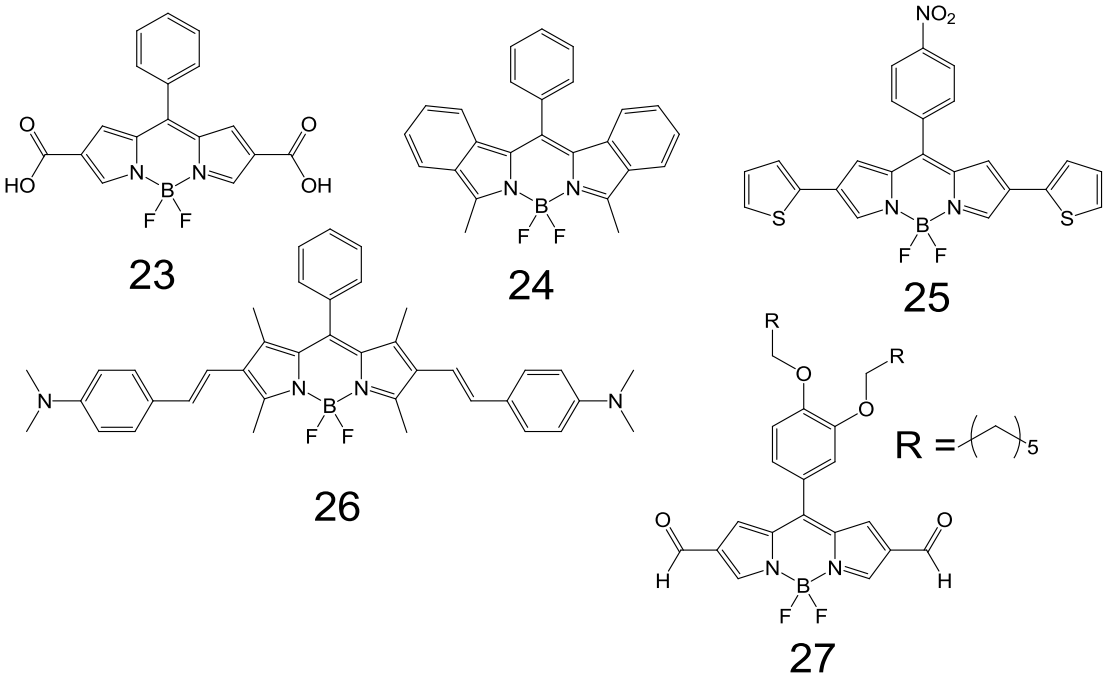

Figure 10: Some examples of BODIPY dyes substituted at the 2,6-positions. (See **Table 1** for a summary of photophysical data.)

C3 and C5:

The 3,5-position carbons lying closest to the boron atom are sometimes also referred to as the α-carbons. Both the HOMO and LUMO orbitals possess significant molecular orbital coefficients at these positions, however the molecular orbital coefficient of the HOMO is larger than that of the LUMO.[30] Substituents attached at these points affect the HOMO and LUMO orbitals to different degrees and thus have an effect on the photochemical properties of the dye **(Figure 11)**. If the BODIPY core is electron deficient, especially after 2,6-dihalogenation,[55] then these carbons are the most acidic and are vulnerable to Knoevenagel condensation reactions.[63] Water soluble substituents and substituents that extend the conjugation of the π-system are commonly attached at these positions.[64]

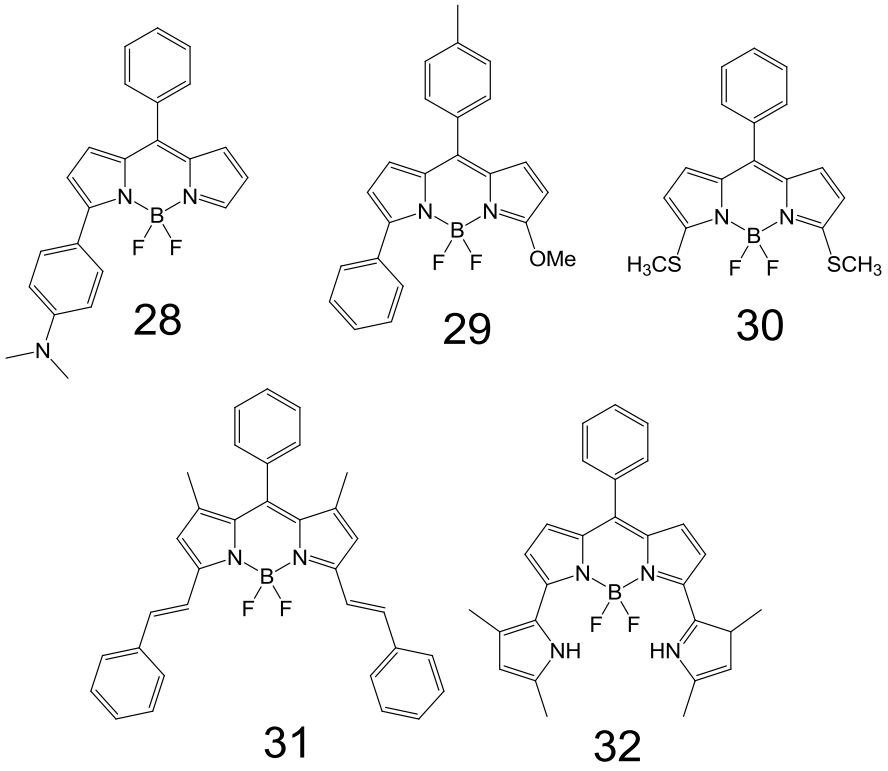

Figure 11: Some examples of BODIPY dyes substituted at the 3,5-positions. (See **Table 1** for a summary of photophysical data.)

4 and 4':

The fluorine atoms attached to the boron atom are denoted as the 4 and 4' positions. Since the fluorine atoms are hard according to hard and soft acid and base (HSAB) theory, it is possible to replace them with other hard ligands.[65] For example, ethanyl,[7,8] methoxy,[33] and various water solubilising groups[40] have been used to replace the fluorine atoms **(Figure 12)**. These compounds tend to have greater Stokes shifts and are markedly less stable than the fluorine derivatives.[28] Functionalization at these positions is often used to increase the light harvesting abilities of the BODIPY dye.[7,8] It has also been demonstrated that solid state fluorescence can be achieved in this manner.[33]

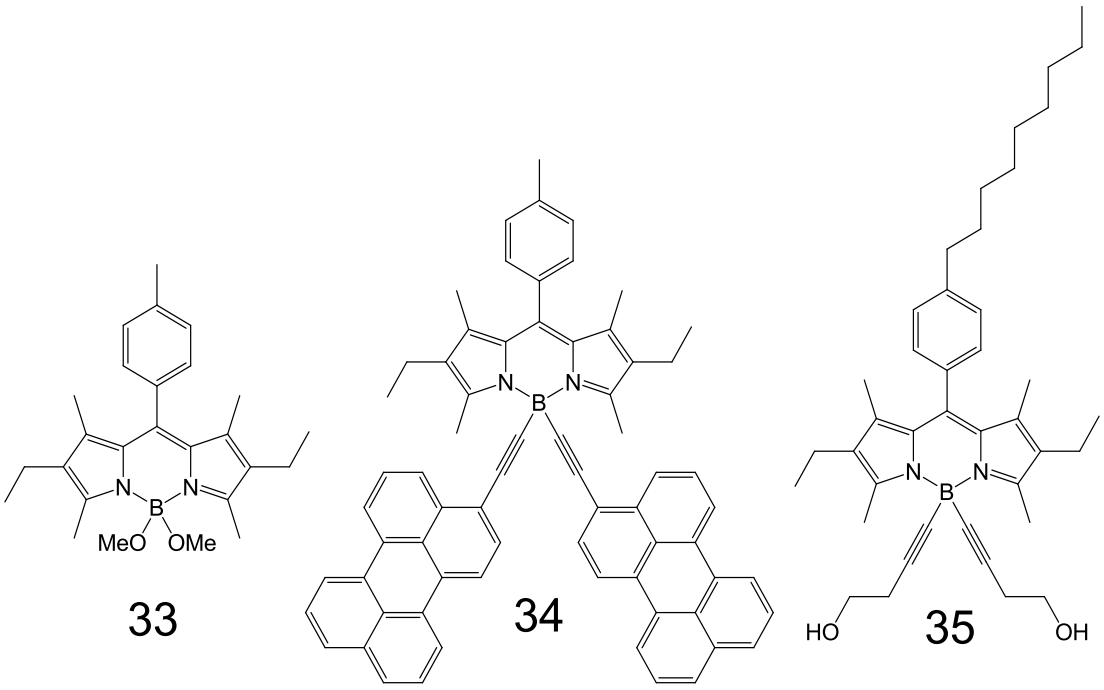

Figure 12: The replacement of the fluorine atoms at the boron centre of the BODIPY core have resulted in a number of highly conjugated BODIPY structures. (See **Table 1** for a summary of photophysical data.)

1.1.6 Halogenation of the BODIPY core

The addition of halogen atoms (Cl,[66] Br,[67] I[68]) to the BODIPY core has been an topic of great interest in BODIPY research due to the wide range of further reaction possibilities that they make available. Boens et al performed a number of nucleophilic substitution reactions, demonstrating the versatility of these halogenated BODIPYs.[69] These compounds have been employed in Pd catalysed coupling reactions[6] and have formed the foundation for synthesising polymeric BODIPY chains.[60] There are three commonly used strategies for introducing a halogen atom onto a BODIPY dye. Initially the halogens were incorporated directly onto the pyrrole starting materials prior to dipyrromethane formation.[70] The second method involves the incorporation of halogen atoms onto the dipyrrin precursors. This, however, has only been reported

for the halogenation of aza-BODIPYs. The third strategy involves the direct electrophilic addition of a halogen atom by taking advantage of the electron deficient nature of the BODIPY core.[67] Attaching halogen atoms to the BODIPY core can alter the photophysical properties of the BODIPY dye in a number of interesting ways. The incorporation of halogen atoms can red-shift the BODIPY main absorption and emission bands and tend to cause a decrease in the fluorescence quantum yield of the BODIPY dye. This allows for the fine tuning of the maxima of the main spectral bands, which can be useful for achieving the wavelengths required for biological or other applications.[71] Halogenation of the BODIPY core also causes an intensification of the absorption band in the. 350–400 nm region. This makes it possible to populate the triplet excited state of the halogenated BODIPY dyes which allows these dyes to generate singlet oxygen. Using larger halogens, or increasing the number of halogen atoms that are attached to the BODIPY core, increases the magnitude of these effects due to the heavy atom effect.[72] However, Lakshmi and Ravikanth have reported that the relationship between the number of halogen atoms and the magnitude of their effects is non-linear and that adding more than four halogen atoms results in no further change in the photophysical properties of the BODIPY dye.[39] It has been noted that after a certain number of halogen atoms has been exceeded, an increase in the fluorescence quantum yield is observed. [39,67] It has been suggested that the $T_1 \rightarrow S_1$ excited state transition competes with the $S_1 \rightarrow T_1$ transition as both ISC processes are enhanced.[73]

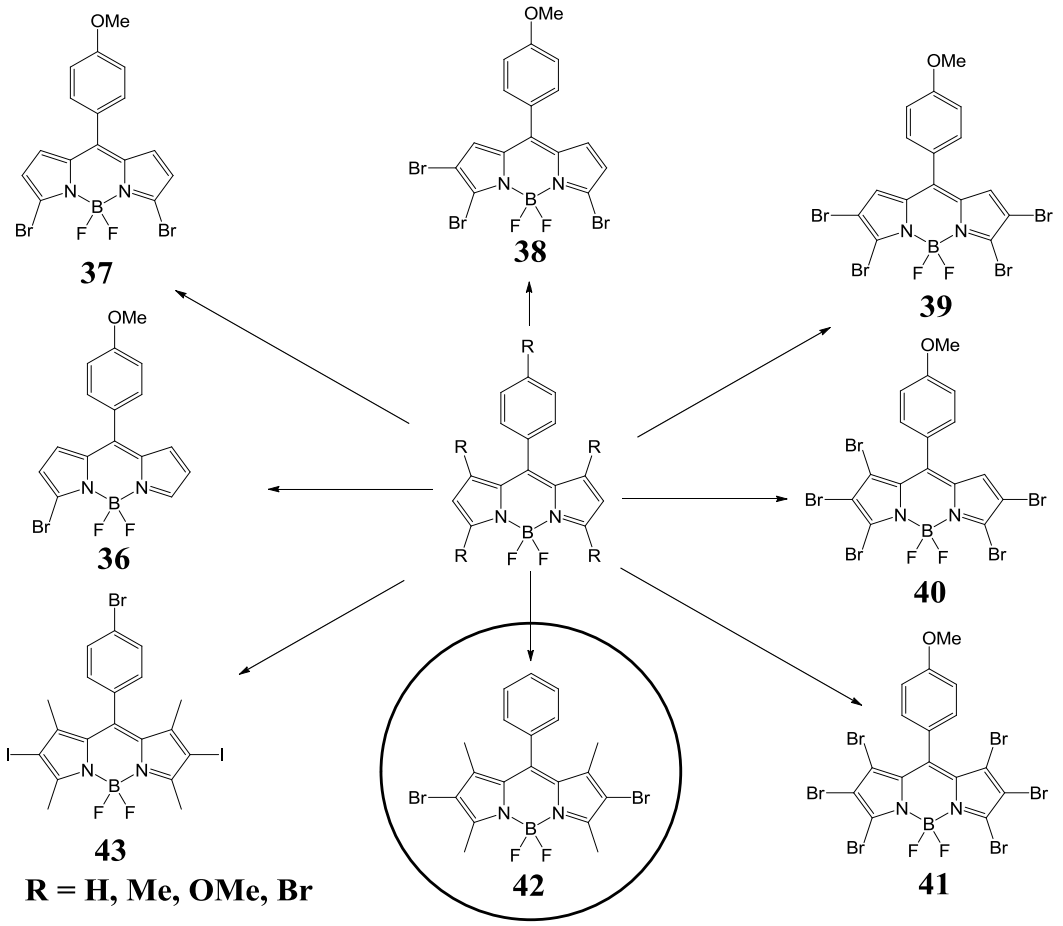

Figure 13: A series of halogenated BODIPY dyes highlighting the analogue chosen for this work. (See **Table 1** for a summary of photophysical data.)

Lakshmi and Ravikanth noted that halogens cause a decrease in the reduction potential of the BODIPYs.[39] Since there are only minor changes in the energy of the main absorption band for the $S_0 \rightarrow S_1$ transition, the converse also applies and the oxidation potential increases. This helps to stabilize BODIPY dyes from degradation due to $^1O_2$.[38]

Halogen atoms have been added to virtually every position on the BODIPY core **(Figure 13)**. In the absence of steric crowding the 3,5-positions have been shown to be the favoured positions for halogenation, followed by the 2,6- then the 1,7-positions. However in the context of 1,3,5,7-tetramethyl substituted BODIPY the 2,6-positions

are the most positive and were thus favoured for halogenation in the context of this study.[54]

1.1.7 Styryl BODIPY dyes

A useful method of adding functionality and extending π-conjugation in BODIPY dyes is through styryl bond formation. A styryl radical is comprised of an aromatic ring that is attached to an ethylene group and has the chemical formula C_6H_5–CH=CH–R **(Figure 14)**. Styryl BODIPYs incorporate one or more of these univalent styryl fragments.[74] These styryl fragments can be incorporated directly onto the starting pyrrole.[75] It is also possible to add one or more styryl groups to 1,3,5,7-tetramethyl-BODIPY due to the acidity of the methyl groups.[63]

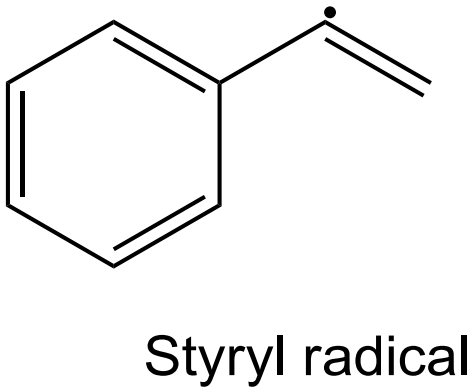

Figure 14: The structure of a styryl radical.

A styryl bond can be formed between the 3-position methyl of the BODIPY and an aromatic aldehyde using a modified Knoevenagel condensation reaction.[34] Mono-[76,77], di-[34,58] and tetra-styryl[55] BODIPYs have been synthesized in this manner **(Scheme 2)**. The main drawback of the Knoevenagel reaction is that water needs to be removed in order to drive the reaction equilibria forward to appreciable yields. This can be

achieved through the use of a Dean-Stark trap or molecular sieves.[78] Microwave-assisted synthesis has been employed in order to reduce the normally long reaction times as well as to improve the reaction yields when preparing styryl-BODIPY dyes.[77] The introduction of styryl groups at the 3,5-positions modifies the absorption and emission properties of the BODIPY, making these positions important points of attachment for the development of molecular sensors.[21,78,79,80] The addition of styryl fragments to the 3,5-positions of BODIPY dyes results in large red-shifts of the main bands in the BODIPY spectra with shifts of ca. 60 nm per styryl group commonly reported in the literature.[31] In contrast, the introduction of styryl groups at the 2,6-positions results in a marked decrease in fluorescence quantum yield and smaller red shift effects.[58] Styryl groups are able to extend the π-conjugation system of a BODIPY dye which can prove useful for conjugating the BODIPY core to other light harvesting substituents, such as porphyrins, to the BODIPY core.[38,81]

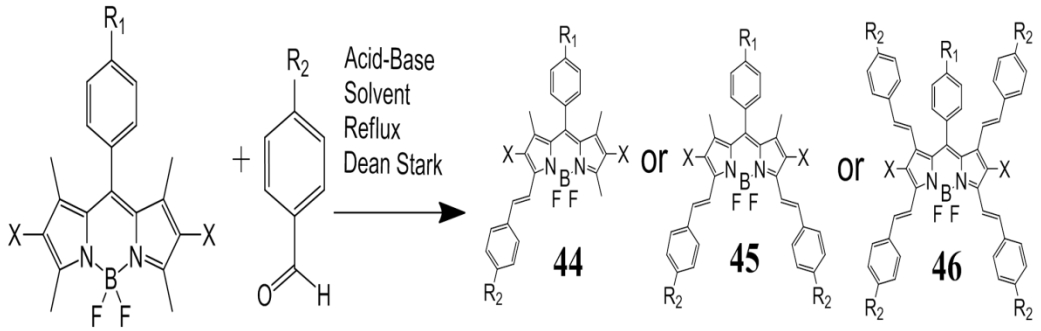

Scheme 2: The Knoevenagel condensation of an aldehyde and a BODIPY dye.

1.1.8 Crown ether BODIPY dyes

There has been comparatively little research on the photophysical effects of attaching crown ether moieties onto BODIPY dyes. Most of the research on BODIPY-crown complexes involves substituting a formyl crown ether unit at the 3- and/or 5-positions by introducing crown-ether-substituted styryl groups through Knoevenagel condensation-type reactions[82] or at the meso-position, through direct incorporation onto a benzaldehyde during the dipyrromethane synthesis step.[83] Chelation of a cation by a meso-crown ether causes almost no change in the absorption spectra of BODIPY dyes since the phenyl crown lies out of the BODIPY plane,[84] but significant effects are observed in the fluorescence emission spectra.[22] Crown-ether-substituted styryl groups introduced at the 3,5-positions can affect both the absorption and emission spectra of the BODIPY.[85] As with other styryl groups, crown ethers generally cause a red-shift of the main BODIPY spectral bands.[86] Crown ethers can transform BODIPYs into powerful molecular platforms for detecting a number of environmentally significant cations by taking advantage of competing PET and intermolecular charge transfer (ICT) processes.[87] To this end a number of aza (nitrogen containing)[85] and thia (sulfur containing)[87] crown ethers have been appended to various BODIPYs **(Figure 15)**.[82,88]

Ozlem and Akkaya synthesized a BODIPY that consisted of 3,5-di-styryl amino groups; a meso position benzo-crown ether; and 2,6-substituted di-iodo groups.[84] They were able to demonstrate that this BODIPY behaved as a molecular AND logic gate that was able to produce a signal only when the two specific analytes (Na^+ and H^+) were present in solution. The authors were the first to explore control of the singlet oxygen

generated by BODIPY by using crown ethers. However they did not explore the fluorescence properties of this multi-functional dye.

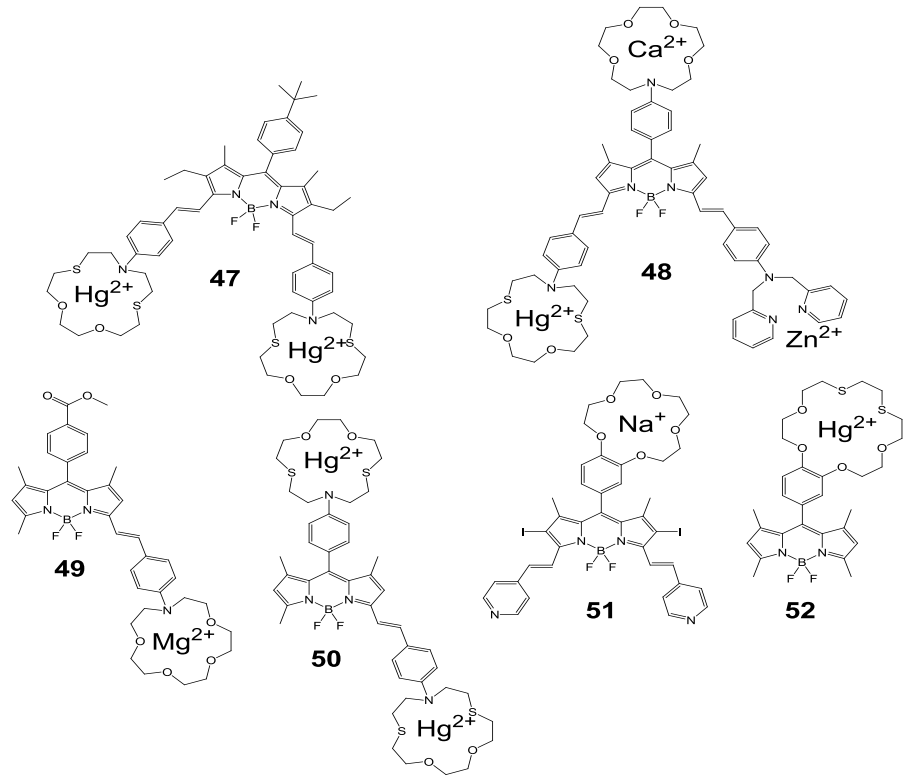

Figure 15: Some examples of crown ether-BODIPY dyes, including their target cations, taken from the literature. (See **Table 1** for a summary of photophysical data.)

Table 1: Photophysical data for selected BODIPY dyes taken from literature.

Dye	Solvent*	λ_{Abs} (nm)	Log ε ($M^{-1}.cm^{-1}$)	λ_{Em} (nm)	Φ_F	τ_F (ns)	Φ_Δ	Reference
Unsub BODIPY	DCM	503	4.70	512	0.90	7.2	---	
1	H_2O	528	---	552	0.41	4.71 (17.96)	---	14
2	DCM	522	5.01	534	0.50	6.9	---	40
3	PBS	642	4.89 (4.74)	655	0.22	---	---	41
4	PBS	521	---	540	0.78	---	---	43
5	MeOH-TFA	500	---	514	0.35	---	---	17
6	THF	525	4.90	530	0.90	6.5	---	8
7	No data reported.							2
8	EtOAc	406	2.9	444	1.00	4.25	---	5
9	DCM (DCM-TFA)	534 (533)	4.97 (4.92)	550 (546)	0.05 (0.04)	---	0.76	23
10	THF	490	---	512	---	---	---	18
11	MeCN (MeCN-CN^-)	561 (594)	4.92 (4.75)	571	0.2 (0.01)	---	---	12
12	---	---	---	---	---	---	---	21
13	---	500	---	506	---	5.7	---	4
14	---	494	---	519	---	5.8	---	4
15	DCM (THF)	501 (501)	4.98 (4.84)	511 (509)	0.63 (0.79)	-	-	4
16	---	---	---	---	---	---	---	---
17	---	---	---	---	---	---	---	---
18	EtOH	500	4.67	513	0.71	---	---	53
19	H_2O (H_2O-NO_2^-)	497 (507)	---	510 (521)	0.32 (0.84)	---	---	32
20	---	---	---	----	---	---	---	---
21	MeOH/H_2O	500	---	512	---	---	---	17
22	---	---	---	---	---	---	---	---
23	---	510	---	525	0.66	---	---	56
24	DCM	542	4.68	562	0.60	---	---	61
25	---	---	---	---	---	---	---	60
26	DCM (DCM-TFA)	616 (578)	---	(619)	(0.01)	2.46	---	57
27	DCM	505	12.3	538	0.60	---	---	58
28	MeCN	597	---	731	0.13	---	---	31
29	$CHCl_3$	530	---	557	0.38	2.49	---	37
30	MeOH	571	4.04	585	0.34	---	---	63
31	Toluene	629	---	641	0.59	---	---	57
32	DCM	700	4.93	739	0.18	---	---	65
33	Hexane	524	4.90	538	0.56	---	---	33
34	No data available.							7
35	DCM	516	4.92	525	0.83	---	---	64
36	$CHCl_3$ (EtOAc)	509 (504)	4.75 (4.76)	523 (519)	0.19 (0.06)	1.21 (0.64)	---	39
37	$CHCl_3$ (EtOAc)	521 (515)	4.91 (4.87)	532 (528)	0.25 (0.14)	1.30 (0.73)	---	39
38	$CHCl_3$ (EtOAc)	536 (529)	4.81 (4.82)	550 (544)	0.33 (0.14)	1.83 (1.02)	---	39
39	$CHCl_3$ (EtOAc)	553 (545)	---	568 (562)	0.22 (0.14)	2.14 (1.19)	---	39
40	$CHCl_3$ (EtOAc)	552 (545)	---	565 (560)	0.03 (<0.01)	---	---	39
41	$CHCl_3$ (EtOAc)	551 (545)	---	565 (559)	0.01 (<0.01	---	---	39

					)			
42	DCM	538	---	577	0.14	---	---	59
43	DCM (THF)	537 (536)	---	554 (553)	0.04 (0.03)	---	---	23
44	Isopropanol	589	---	608	---	---	---	34
45	Isopropanol	657	---	679	0.42	---	---	34
46	$CHCl_3$	700	---	727	0.12	---	---	54
47	THF (THF-Hg^{2+})	720 (630)	---	740 (650)	---	---	---	82
48	MeCN (MeCN-Ca^{2+}, Zn^{2+}, Hg^{2+})	692 (626)	---	(656)	---	0.04 (0.27)	---	78
49	MeCN (MeCN-Mg^{2+})	608 (562)	---	723 (573)	0.08 (0.80)	---	---	85
50	THF/H_2O (THF/H_2O-Hg^{2+})	606 (564)	---	668 (578)	0.04 (0.33)	---	---	87
51	MeCN (MeCN-TFA)	630 (660)	---	---	---	---	Rel. rate 1.0 (6.1)	84
52	MeCN/H_2O (MeCN/H_2O -Hg^{2+})	498 (500)	---	507	---	---	---	83

*Brackets indicate the use of a second solvent system or the presence of any additional analytes

1.2 Macrocyclic polyethers (Crown Ethers)

1.2.1 History and Applications

In the 1960s, Charles Pedersen managed to isolate small white crystals during an attempt to synthesize a ligand capable of binding divalent cations. These crystals showed the ability to complex with the potassium ion which was deemed unusual enough at the time to warrant further study.[89] Analysis revealed that these crystals were cyclic oligomers of dioxane. (-CH_2-CH_2-O-) now known as crown ethers. While similar molecules had been reported by a number of other groups prior to Pedersen's work,[90,91] the cation complexes of these polyethers had not been investigated.

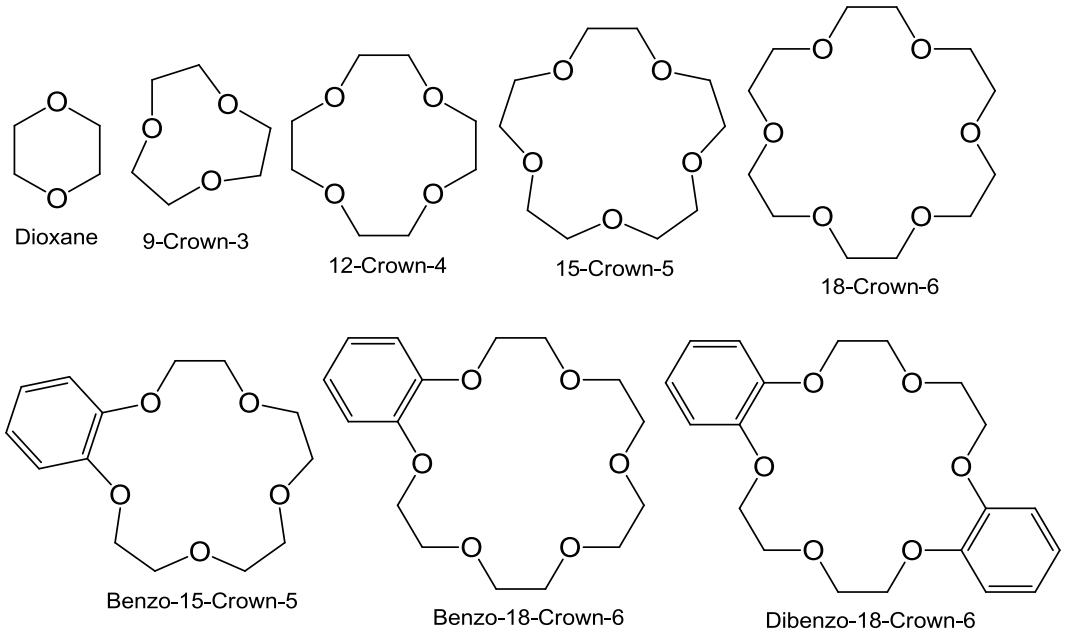

Figure 16: A series of increasingly complex polyethers named according to the nomenclature outlined by Pedersen.[89]

Pedersen abbreviated the complex standard names of polyethers, such as 2,3,11,12-dibenzo-1,4,7,10,13,16-hexaoxacyclooctadeca-2,I-1d iene, to shorter names such as

dibenzo-18-crown-6.[89] The names of the polyethers were split into four parts which followed a set of simple rules: the first part, e.g. dibenzo, refers to any hydrocarbon rings that are attached to the crown, the second part, e.g. 18, represents the total number of carbon atoms in the ring; the third part, e.g. crown, provided the class of crown structure; and the fourth part, e.g. 6, refers to the number of heteroatoms in the ring **(Figure 16)**.

Originally crown ethers were made using only oxygen atoms, but this was subsequently expanded to include nitrogen (classed as aza crown in the third part of the nomenclature system)[92] and sulphur (classed as thia crown)[83] atoms. What made crown ethers particularly interesting was their ability to bind to a number of different alkali and alkali-earth cations despite being neutral molecules.[92] Pederson outlined the synthesis, properties and complexes of over thirty of these macrocycles, including the benzo-15-crown-5 used in this study.[89] The subsequent intense research focus that followed, resulted in a large number of papers and patents.[93] Pedersen, Lehn and Cram shared the 1987 Nobel Peace Prize for Chemistry for their contributions to the fields of macrocycles and the complexation of metal ions.[93]

1.2.2 General Properties and Applications

Crown ethers are particularly important in both colorimetric and fluorescent sensor applications as they offer a binding platform for various analytes, primarily cations. The binding of a cation by a crown ether unit can result in the formation of stable complexes. This is often accompanied by detectable changes in optical or redox properties of the molecule. A number of fluorescent dyes that incorporate crown

ether moieties have been reported, **(Figure 17)** but the study of BODIPY crown ether dyes is still in its early stages. Another major application of crown ethers is in phase transfer catalysis, this makes crown ether conjugated molecules useful candidates as heterogeneous catalysts. Crown ethers have found use in a number of different applications as: ion selective electrodes; anti-microbial agents (for *E. coli)*, on nanotubes, and in organic LEDs.[93] Crown ethers have been used in chromatography to successfully separate mixtures of enantiomers, drugs, and amino acids. A highly attractive property of crown ethers is their low toxicity in the human body as some simple crown ethers have been shown to be less toxic than aspirin.[93]

1.2.3 Structure and synthesis

Crown ether macrocycles that contain as few as nine and as many as sixty carbon atoms have been reported in literature. By some estimates crown ether variants number well into the thousands.[91] Benzo derivatives are the most versatile because their aromatic ring is susceptible to electrophilic aromatic substitution. Formylbenzo crown ethers can be synthesized either by ring closure of substituted catechols with glycol derivatives, or by direct substitution onto the aromatic ring **(Scheme 3).**[91] These crown ethers possess cavity sizes between 1.7 and 2.2 Å which are ideal for complexing the small Na^+ ion.[94] A significant disadvantage of the benzo crown ether is that the carbon bond that is formed where the benzene ring and the crown ether moiety are fused is unusually long (highlighted in **Figure 17**) which causes the binding constant for the crown ether to be lower than it otherwise would be.[91]

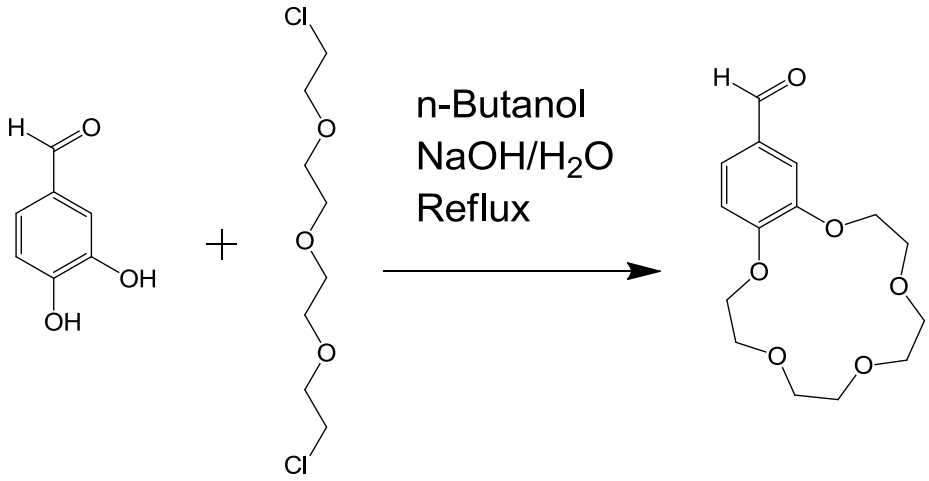

Scheme 3: The ring closure synthesis of 4-formylbenzo-15-crown-5.

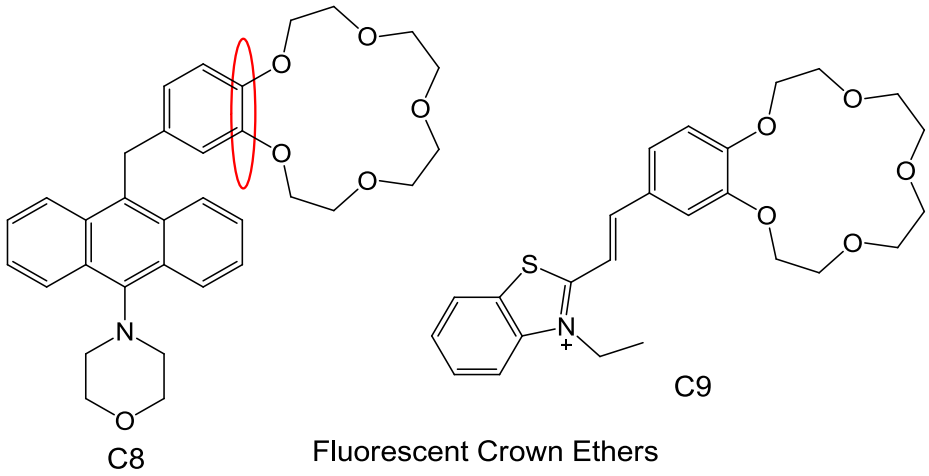

Figure 17: Examples of fluorescent sensors based on crown ether moieties.

1.2.4 Crown Ethers with Heteroatoms other than Oxygen (Figure 18)

Thia crowns are crown ethers that have had one or more of their oxygen atoms replaced by divalent sulphur atoms.[93] These crown ethers bind poorly with alkali and alkali earth metals, but bind mercury and silver ions more selectively.[93] The sulfur atom, points away from the centre of the ring, which causes the crown ether to be

distorted. Therefore, the ions that are complexed by a thia-crown ether tend to lie outside of the crown cavity.

Phosphorous crowns have been synthesized, but are rare due to air-sensitivity and difficulty of synthesis.[91] They are more selective towards cobalt and nickel.

The nitrogen atom is the most commonly substituted heteroatom because it is trivalent. Therefore, the nitrogen atom can be directly functionalized without affecting the crown ether ring. The lone pair of electrons on the nitrogen atom can be used to provide an off-on switch for fluorescent dyes that are attached to the crown by taking advantage of PET/ICT processes.[78,85] Phenyl aza-crowns have low stability constants when complexing with metal ions.[92]

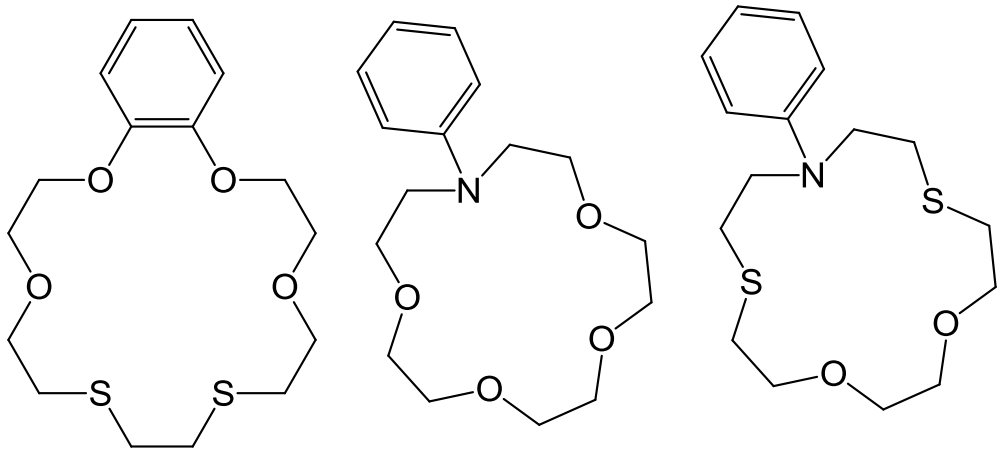

(a) 79 (b) 82 (c) 83

Figure 18: Some examples of crown ethers containing heteroatoms other than oxygen. **(a)** thia-crown; **(b)** aza-crown; and **(c)** aza-thia-crown ether.

1.2.5 Complexation of Cations (Figure 19)

The ability of crown ethers to form stable complexes with alkali earth and transition metal ions has been the central focus of research on these molecules since these were first discovered. Solvent effects are important when dealing with crown ethers as stable complexes will generally only form in the solvents from which the complex is stable enough to crystallize. While crown ethers are neutral molecules their complexes are typically positively charged as the most commonly chelated materials include inorganic (such as Na^+ or NH_4^+) and biological cations (such as glutathione or lysine).[22] Negatively charged crown ethers complexes have also been reported after chelation of various anions, but these remain relatively rare. X-ray studies have revealed that crown ether complexes are typically 2D structures that possess D_{3d} symmetry.[95] Two of the most important aspects of crown ether chemistry are their complexation strength and selectivity. Oxygen based crown ether rings tend to be highly selective only towards alkali and alkali-earth metal cations. The most effective method for changing the selectivity of crown ethers is by replacing these oxygen atoms with other heteroatoms, such as nitrogen or sulfur, as these atoms are able to impart their affinity for different types of cations onto the crown ether.

Another method for controlling the selectivity of crown ethers is by adjusting their cavity size. Due to the hole size relationship the closer in size that the cation ionic radii is to the cavity radii of the crown ether, the easier it is for a complex to form. Therefore 15-crown-5 binds Na^+ ions preferentially over K^+ (and other group one cations) ions as the ionic radii of Na^+ is similar in size to the cavity radii (1.7–2.2 Å), while the larger cavity radii of 18-crown-6 preferentially binds the larger K^+ ions.

Crown ethers possess the ability to both bind and release cations. The ratio of the rate at which a crown ether binds a cation over the rate at which it releases said cation (k_s^{-1}) is known as the stability constant, k_s. The stability constant for crown ethers is determined by the stability of the crown ether, the stability of the salt in solution, and the stability of the resulting complex. k_s values for simple crown ethers are reported to lie in the range of 10^6 M^{-1} and are generally higher in low polarity solvents which cause stronger binding between the crown ether and the cation. Polar solvents result in weaker binding, which causes the release of cations to occur more rapidly.[93]

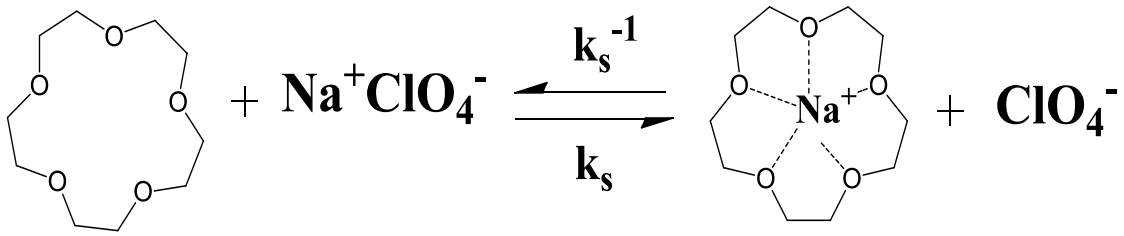

Figure 19: Sodium complex formation for 15-crown-5.

1.3 Nanofibers and Electrospinning

1.3.1 Nanofibers

Nanofibers are elongated threadlike objects (these can be organic or inorganic) that have been engineered to have diameters in the 40–2000 nm range.[96] They are one dimensional (1D) nanomaterials similar to nanowires and nanorods as only their diameters are confined to the nanometer range while the lengths are in the micron range. They are generally non-woven materials, but recent advances have facilitated the weaving of nanofibers.[97] Nanofibers have a higher surface area-to-volume ratios, smaller pore sizes, and higher tensile strength when compared to microfibers. They can be manufactured from a wide range of raw materials and are highly versatile. Nanofibers have found applications in a number of fields including air and water filtration and treatment, in tissue engineering for medical research, as drug delivery vehicles in pharmaceutics, as supports for various nanomaterials, in wound dressings, as various gas and chemical sensors, and in the textile industry.[98] Polystyrene was chosen as the base for the nanofibers that were fabricated in this work as it is a low cost material with many attractive qualities, such as chemical inertness; transparency; and low cost. While the electrospinning of various Pc Nanofibers has been extensively investigated[99,100,101] the electrospinning of BODIPY nanofibers is still a relatively unexplored field.

1.3.2 Electrospinning of Nanofibers

While nanofibers can be fabricated through a number of other techniques such as drawing, template synthesis, phase and self-assembly, electrospinning is by far the most commonly employed method.[98] Electrospinning is regarded as easy to use, relatively easy to scale up and cost effective method when compared to the other techniques.

Electrospinning involves passing a charged polymer solution through a high voltage electric field in order to collect fibers with nanoscale diameters **(Figure 20)**. Once the polymer solution reaches a certain charge a jet of polymer is ejected from the droplet that forms at the tip of the needle. The polymer jet travels to the low potential collector were it dries and gathers as a mat of nanofibers.

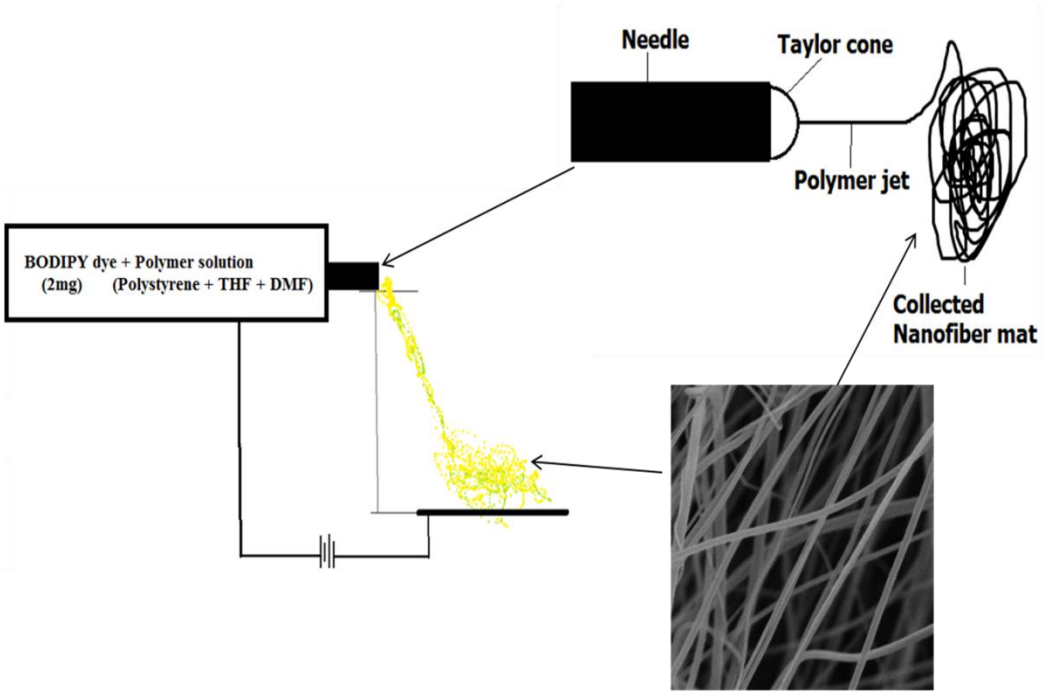

Figure 20: A schematic diagram detailing the electrospinning set-up.

1.4 Photophysical Properties of BODIPY dyes

1.4.1 Jablonski Diagram

The numerous photophysical processes that a BODIPY dye can undergo can be visualized using a Jablonski diagram, **Figure 21**. Fluorescence is particularly important when working with BODIPY dyes. The triplet excited state of BODIPY dyes are generally inaccessible as transitions from the singlet to the triplet state are spin forbidden. These ISC transitions are usually weak, but they can be enhanced by increasing the atomic number of the atom, due to spin-orbit coupling which links the spin of the electron to its orbital angular momentum. This phenomenon is termed the heavy atom effect. Halogen atoms have been shown to successfully promote ISC in BODIPY dyes. One of the aims of this project is to determine whether cation complexation by the crown ether unit has an effect on the rate of ISC.

1.4.2 Fluorescence and Phosphorescence

When a material absorbs electromagnetic radiation the electronic state of the material can be elevated from the ground state to an excited state. Following Kasha's rule relaxation from the lowest energy excited state back into the ground state can be accompanied by the emission of a photon if the spin multiplicity is retained. Fluorescence refers to the emission of a photon that accompanies the relaxation from the singlet excited state to the singlet ground state. One of the very first and most

important properties that researchers observed with BODIPY dyes was their ability to fluoresce intensely. Changes of solvent polarity or pH are less likely to affect BODIPY emission when compared to other fluorescent dyes as they are generally less sensitive to the chemical environment due to the rigid zwitter ionic structure of the BODIPY core.[29]

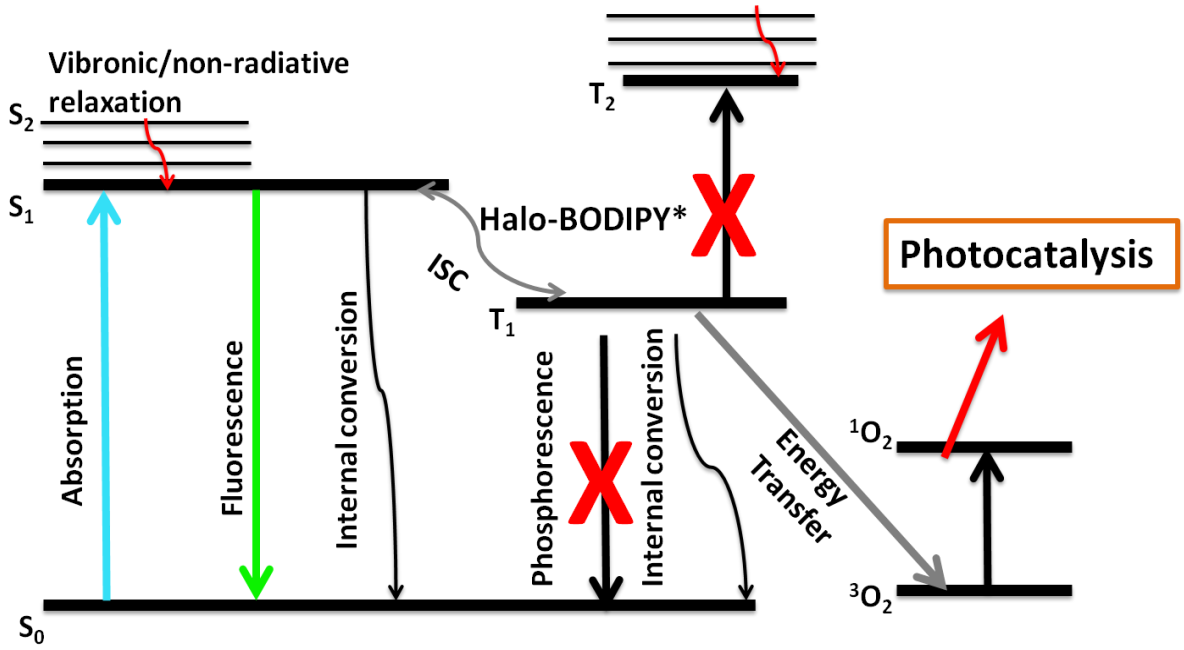

Figure 21: A Jablonski diagram showing the electronic transitions between the BODIPY ground (S_0) state and first excited (S_1) state. The presence of the heavy halogen atoms on the BODIPY core promotes intersystem crossing (ISC) from the S_1 state to the excited triplet (T_1) state. Energy transfer (ET) between the T_1 state and molecular oxygen results in the generation of singlet oxygen.

BODIPY fluorescence properties are highly dependent on the structure of the dye. The BODIPY emission spectra can be easily manipulated by changing the substituents that are attached to the core of the dye. Unsubstituted BODIPYs typically have an intense narrow emission spectra at ca. 510 nm, but a wide range of BOIDPY emission wavelengths have been reported, with some as low as 450 nm, and others extending well into the NIR region.

The process of photon emission from the relaxation of the triplet excited state to the triplet ground state is termed phosphorescence. With regards to BODIPY dyes, until recently phosphorescence has rarely been reported, since generally there is negligible triplet state formation. Heavy halogen atoms relax the spin-selection rule in turn enhancing the rate of ISC from the singlet to triplet excited state.[23] It has proven difficult to directly observe phosphorescence from BODIPYs as the energy is either transferred back to the singlet state or into the environment via non-radiative pathways, but BODIPY phosphorescence spectra have been recorded by attaching multiple halogens to the BODIPY core and using cold solvents (78 K).[73] Whilst direct phosphorescent properties are not reported in this work, ISC can be inferred indirectly from the detection of singlet oxygen radicals when the photosensitizer properties of the dyes are investigated.

1.4.3 Fluorescence Quantum Yields (Φ_F)

The definition of the fluorescence quantum yield from the IUPAC gold book is shown in **Equation 1**.[104] It is the number of measurable events (which can be spectral, such as emission; or physical, such as the formation of a product) relative to the number of photons absorbed by a given system.

Equation 1: Standard definition of fluorescence quantum yield (Φ_F).

$$\Phi_F = \frac{\text{Number of Defined Events}}{\text{Number of Photons Absorbed}}$$

When fluorescence emission is the event of interest the fluorescence quantum yield can also be expressed as shown in **Equation 2** which gives the fluorescence quantum yield as the rate of the emission process divided by the sum of the rates of all other deactivation processes.

Equation 2: Alternative definition of fluorescence quantum yield (Φ_F).

$$\Phi_F = k_f / \sum k_d$$

In **Equation 2**, k_f is the rate of fluorescence and Σk_d refers to the sum of the rate of all other processes, including fluorescence, that depopulate the excited state. It is usually determined using a comparative method in which the ratio of the number of emitted to absorbed photons of a known fluorophore standard are compared to the number of absorbed and emitted photons of the new compound **(Equation 3)**.

Equation 3: Fluorescence quantum yield (Φ_F) comparative method.

$$\Phi_F = \Phi_F^{std} . \left(\frac{F . A_{std} . \eta^2}{F_{std} . A . \eta_{std}^2} \right)$$

F and F_{std} are the integrals of the emission curves of the BODIPY and standard respectively. A and A_{std} are the respective absorbance values of the BODIPY and standard at the excitation wavelength. η and η_{std} refer to the refractive indices of the solvents used for the BODIPY and standard, respectively and Φ_F^{std} is the fluorescence quantum yield of the standard. The standards employed in this study were Rhodamine-6-G (Φ_F = 0.94 in ethanol)[102] and Zinc Pc (Φ_F = 0.20 in DMSO)[103]. The value obtained should lie between 0.0 and 1.0, with 0.0 being completely non-fluorescent

and 1.0 meaning that every photon absorbed is re-emitted. It can therefore be used as a measure for the efficiency of the fluorescence process being studied. Fluorescence quantum yields for BODIPY dyes are usually relatively high (Φ_F > 0.60) however the presence of halogen atoms on the BODIPY core can cause a large decrease in the fluorescence quantum yield.

1.4.4 Fluorescence Lifetime (τ_F)

The fluorescence lifetime is a parameter describing the time evolution of the decay of the fluorescent radiant intensity.[104] This provides a measure of the average amount of time between absorption and re-emission of a photon by the fluorophore based on the profile of the fluorescence decay curve. A time-correlated single photon counter (TCSPC) can be used to plot a decay curve of the population of fluorophores in solution, an example of which is provided in **Figure 22**. The value of the fluorescence lifetime for the given fluorophore can be determined by deconvolution of this decay curve. The fluorescence lifetimes of BODIPYs have been reported to be less than 10 nanoseconds.[37]

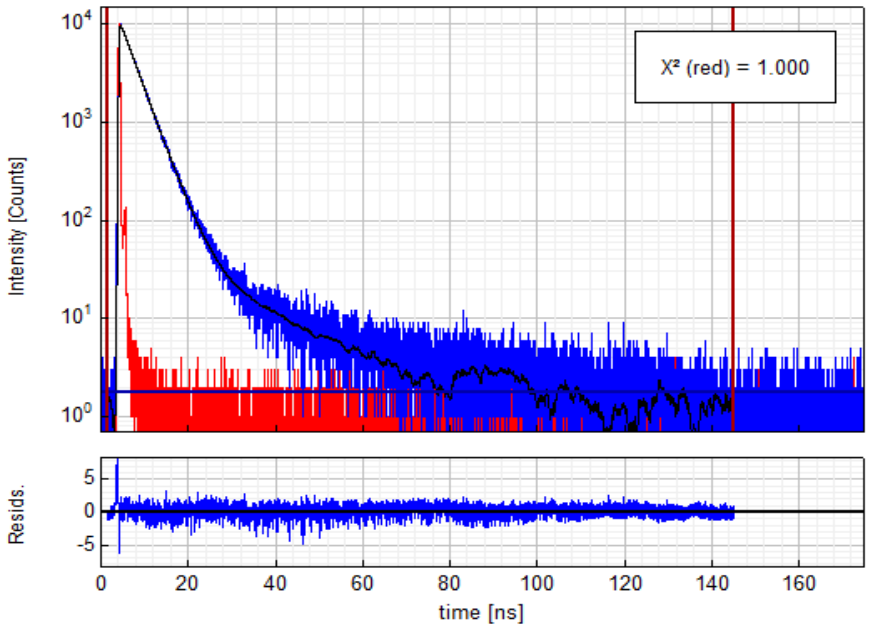

Figure 22: A BODIPY fluorescence decay curve (blue) measured using time-correlated single photon counting, including the internal response function (Red) (IRF: ludox in water) and the associated residuals.

1.4.5 Singlet Oxygen Quantum Yield (Φ_Δ)

The lowest energy state of molecular oxygen is the triplet ground state ($^3O_2$). It is possible to transfer energy from a triplet sensitizer (in this case a halogenated BODIPY dye) to molecular dioxygen **(Figure 21)**. This energy transfer process causes the electrons to undergo a spin state rearrangement to form a singlet excited state. The resulting singlet oxygen species ($^1O_2$) has been shown to be highly reactive and has been used in organic reactions to oxidize the *ene* functional group to an epoxide,[105] kill cells in a process called PDT, and in the photo-degradation of pollutants,[106] which is the aim of this work. The production of singlet oxygen by BODIPY predominantly follows the type 2 pathway[107] shown in **Figure 23**.

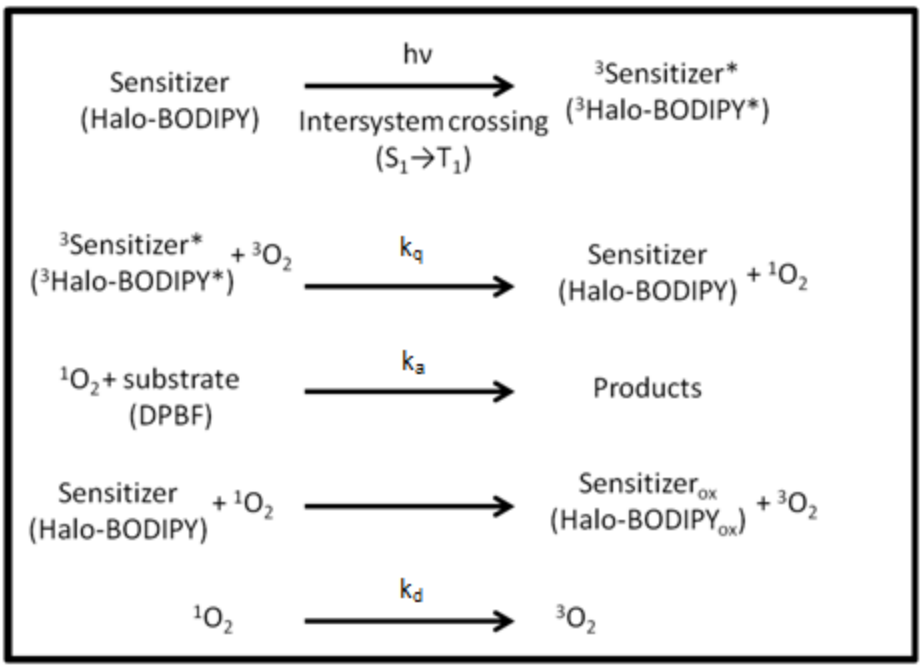

Figure 23: Singlet oxygen generation by irradiation of a halogenated BODIPY dye following the type II reaction mechanism.

There are two methods that can be used for detecting singlet oxygen:

1). *The physical/luminescence method*[108]

When singlet oxygen relaxes from the excited state back to the ground state it produces an infra-red decay curve at 1270 nm. It is possible to detect this emission by using a sensitive germanium detector. This data can be used to plot a time resolved phosphorescence decay curve of the singlet oxygen from which the singlet oxygen quantum yield can be obtained. This decay curves obeys **Equation 4.**

Equation 4: Singlet oxygen quantum yield (Φ_Δ) phosphorescence method.

$$I(t) = B.\frac{\tau_D}{\tau_T - \tau_D}.\left[e^{-t/\tau_T} - e^{-t/\tau_D}\right]$$

where I(t) is the phosphorescence intensity of $^1O_2$ at time t, τ_D is the lifetime of the $^1O_2$ phosphorescence decay, τ_T is the triplet state lifetime of the sample, and B is the coefficient related to sensitizer concentration and $^1O_2$ quantum yield.

The singlet oxygen quantum yield of the BODIPY can then be determined using a comparative method show by **Equation 5.**

Equation 5: Singlet oxygen quantum yield (Φ_Δ) comparative physical method.

$$\Phi_\Delta = \Phi_\Delta^{std} \cdot \frac{B}{B^{std}}$$

Φ_Δ^{std} is the singlet oxygen quantum yield of the standard, in this case it would be Rose Bengal (Φ_Δ = 0.86 in ethanol) or ZnPc (Φ_Δ = 0.67 in DMSO). B and B^{std} refer to the coefficient involved in sensitizer concentration and $^1O_2$ quantum yield for the sample and standard respectively.

2). *The chemical/scavenger method*

The chemical method makes use of a singlet oxygen quencher, such as 1,3-diphenylisobenzofuran (DPBF) for organic solvents or anthracene-9, 10-bis-methylmalonate (ADMA) for aqueous solutions.[109] By monitoring the absorption spectrum of these solutions before and after irradiation it is possible to measure the disappearance of the quencher as singlet oxygen is formed. The amount of quencher that is degraded is proportional to the amount of singlet oxygen produced. On this basis, the singlet oxygen quantum yield of the BODIPY can be determined by comparing the singlet oxygen generating ability of a known standard to that of the BODIPY sample using **Equation 6**. Φ_Δ^{std} refers to the singlet oxygen quantum yield for the standard, Rose Bengal (Φ_Δ = 0.86 in ethanol)[110] or ZnPc (Φ_Δ = 0.67 in DMSO)[111]. W

and W^{std} are the quencher (DPBF or ADMA) photobleaching rates in the presence of the BODIPY dye and standard respectively. $I_{abs}{}^{Std}$ and I_{abs} are the respective rates of light absorption by the BODIPY and standard.

Equation 6: Singlet oxygen quantum yield (Φ_{Δ}) comparative chemical method.

$$\Phi_{\Delta} = \Phi_{\Delta}^{std} . \frac{W . I_{Abs}^{Std}}{W^{std} . I_{Abs}}$$

1.5 Summary of Aims:

BODIPY dyes are small, highly fluorescent molecules with highly favourable photophysical properties. Unsubstituted BODIPY dyes are, however, not able to generate any radical species and are thus poor photocatalysts. The value of a BODIPY dye as a photocatalyst can be realized through the addition of halogen atoms to the core of the BODIPY dye as heavy atoms, such as bromine, are known to enhance the rate of ISC and hence enable the generation of reactive singlet oxygen. It may be possible to further increase the singlet oxygen generating ability of a BODIPY dye by introducing other groups, such as crown ethers, that can complex heavy atoms onto the core of the BODIPY, since this should have a significant effect on the photophysical properties. Crown ether-BODIPY dye conjugates could prove useful in applications, such as bioimaging and sensors, as they would result in BODIPY dyes that are sensitive to ions in solution.

Another disadvantage is the difficulty of recovering a homogeneous catalyst from a solution after a reaction has taken place. It would be advantageous to fabricate a heterogeneous photocatalyst by embedding a halogenated BODIPY dye into a polymer support. These BODIPY photocatalysts could then be used, easily recovered from a reaction mixture, and recycled. To this end a key goal of the study was to prepare BODIPY-nanofiber composites. Embedding BODIPY dye into a nanofibers material should result in highly fluorescent nanofibers, so there is also scope for ion sensor applications.

The objectives of this project are as follows:

1. To complete the series of meso-methylphenyl-BODIPY dyes by synthesizing the novel meso-(p-isopropylphenyl) BODIPY **(1)** derivative **(Scheme 4)**.
2. A comparison of the novel BODIPY with a previously synthesized meso-(p-dimethylaminophenyl) **(4)** BODIPY dye **(Scheme 5)**.
3. To synthesize 2,6-dibrominated derivatives of both BODIPY **(1)** and meso-dimethylaminophenyl BODIPY **(4)** dyes in order to compare their photochemical properties, with special focus on their singlet oxygen generating abilities.
4. The fabrication and characterization of BODIPY embedded fluorescent polystyrene nanofibers to explore their potential as sensors or photocatalysts.
5. Attempt the photocatalytic degradation of azo-dyes (Tartrazine and Orange-G) by 2,6-dibrominated BODIPY dyes embedded in nanofibers.
6. To synthesize and characterize cation sensitive BODIPY dyes by introducing a crown ether moiety at the 3,5-positions of the dibrominated BODIPY core **(3a)** and **(3b)** for the cuminaldehyde based dye and **(6a)** and **(6b)** for the dimethylaminobenzaldehyde based dye) and to determine whether complexation of sodium ions has any measurable effect on the photophysical or photochemical properties (especially on singlet oxygen generation) of the novel crown ether-BODIPY dyes.
7. Analyze trends in all of the synthesized BODIPYs by carrying out theoretical calculations in order to obtain a better understanding of the structure-property relationship of these compounds.
8. Determination of the photophysical and photochemical parameters of all synthesized compounds including: fluorescence quantum yields; fluorescence lifetimes; and singlet oxygen quantum yields.

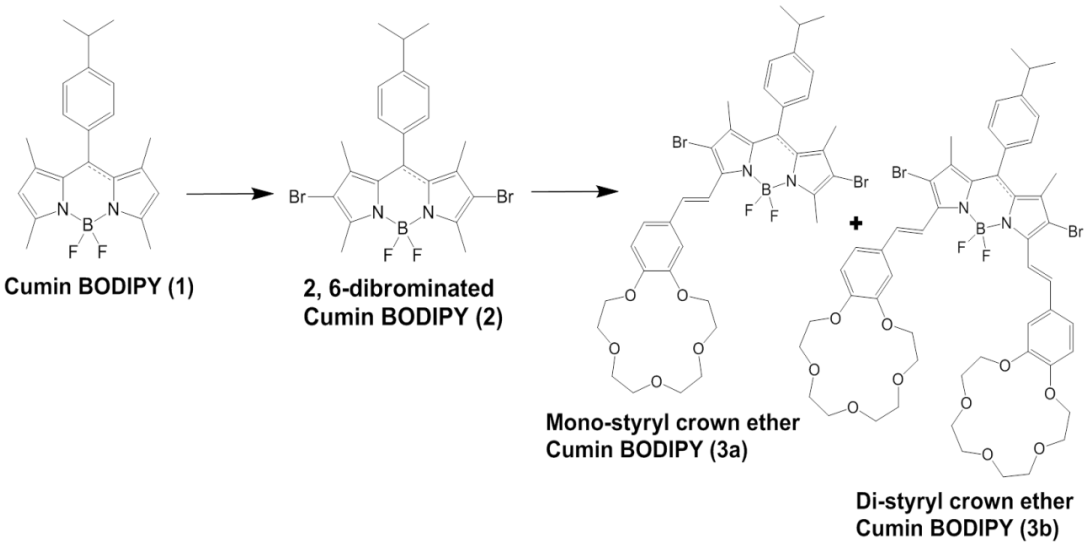

Scheme 4: A series of increasingly more complex BODIPY dyes formed by first preparing BODIPY dye **(1)** based on cuminaldehyde. Brackets indicate their assigned number.

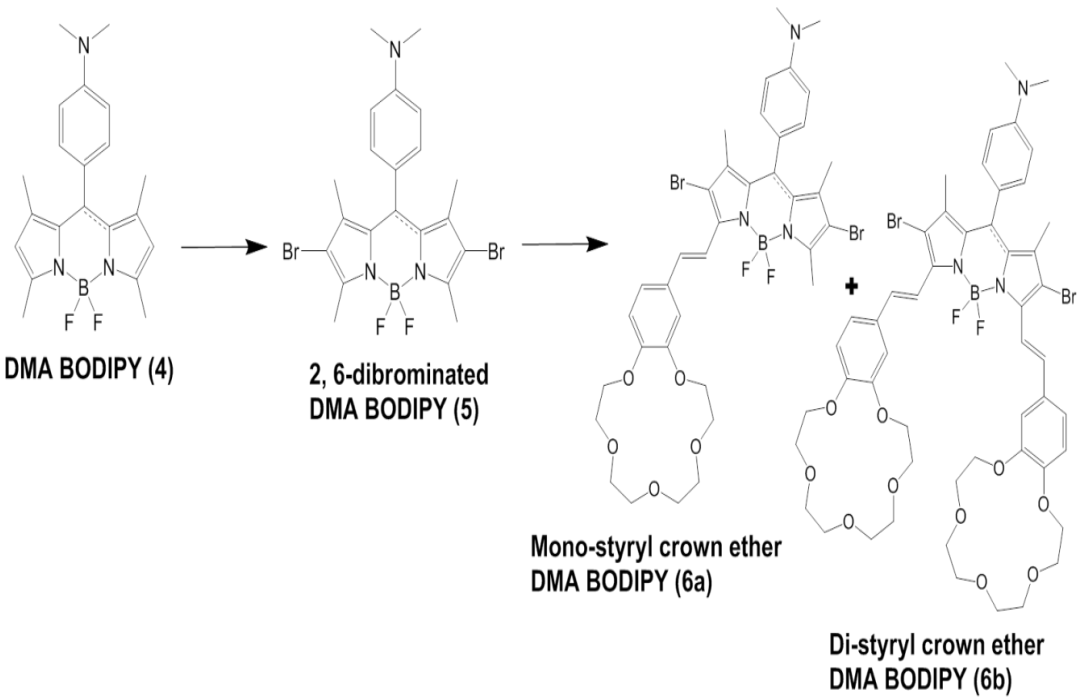

Scheme 5: A series of increasingly more complex BODIPY dyes formed by first preparing BODIPY dye **(4)** based on 4-dimethylamino benzaldehyde. Brackets indicate their assigned number.

Chapter 2:

Experimental

Equipment, Materials, Methods and Synthesis

- **Experimental**

2.1 Equipment

- UV-visible absorption spectra were recorded using either a JASCO V-650 or a Shimadzu UV-2550 UV-Vis spectrophotometer. Spectra were recorded in a quartz cell of 1 cm path-length
- Fluorescence emission and excitation spectra were obtained using a Varian Cary Eclipse spectrofluorimeter. The emission and excitation slit widths were set at 5 nm while a medium PMT voltage was maintained.
- Fluorescence lifetimes were measured using a time correlated single photon counting (TCSPC) setup (FluoTime 200, Picoquant GmbH). For the brominated and mono-crown BODIPYs, a LDH-P-C-485 laser head driven by PDL 800-B single channel driver and a 10MHz repetition rate was employed. A LDH-P-670 laser head with a 20MHz repetition rate was used for the di-crown BODIPY dyes. Fluorescence was detected under the magic angle with a Peltier cooled photomultiplier tube (PMT) (PMA-C 192-N M, Picoquant GmbH) and integrated electronics (PicoHarp 300E, Picoquant GmbH). A monochromator with a spectral width of about 4 nm was used to select the required emission wavelength band. The response function of the system, which was measured with a scattering Ludox solution (DuPont), had a full width at half maximum (FWHM) of about 300 ps. All fluorescence decay curves were measured at the emission peak maxima. The decay curves were analysed with the FluoFit program (Picoquant GmbH).

- Singlet oxygen experiments were conducted using an EKSPLA NT342B-20-AW – Nd:YAG laser (max output – 1J, pulse duration 3–6 ns) with parametric generation (max output – 50 mJ, pulse duration 3–5 ns, wavelength 400 – 2400 nm).
- IR spectra were recorded on a Bruker Alpha FT-IR spectrophotometer using a Platinum ATR accessory.
- ^{1}H Nuclear Magnetic Resonance (^{1}H NMR) spectra were obtained using a Bruker AMX 400 MHz spectrometer in chloroform-d_1. Resonances are reported at values in the ppm referenced to the methyl resonance of the internal standard, TMS, at 0.00 ppm.
- Mass spectra data were collected on a Bruker AutoFLEX III Smart-beam MALDI-TOF mass spectrometer using an α-cyano-4-hydroxycinnamic acid matrix and positive mode of operation for the heavier BODIPYs. The mass spectra for the lighter BODIPY dyes were analyzed using an Expressions CMS Advion ESI-MS with CAMAG TLC-MS interface.
- X-ray powder diffraction (XRD) patterns were recorded on a Bruker D8, Discover instrument equipped with a proportional counter, using Cu-Kα radiation (λ = 1.5405 A, nickel filter). Data was collected in the range from 2θ = 10^{o} to 100^{o}, scanning at 1^{o} min^{-1} with a filter time-constant of 2.5 s per step and a slit width of 6.0 mm. Samples were placed on a zero background silicon wafer. The X-ray diffraction data were treated using the freely-available Eva (evaluation curve fitting) software.[112] Baseline correction was performed on each diffraction pattern by subtracting a spline fitted to the curved background.
- Imaging of BODIPY crystals and various nanofibers were captured using a TESCAN Vega TS 5136LM scanning electron microscopy (SEM) (Jeol Quanta 200 F FE-SEM) at an

accelerating voltage of 20 kV. Before SEM analysis, non-conductive samples were coated with gold using a sputter coater (Balzers Union SKD 030).

- The fluorescence images were taken with a Direct Metal Laser Sintering (DMLS) Olympus BX series fluorescence photomicroscope. The excitation source was a high voltage mercury lamp. Images were captured using bright field and wide field UV (WU) filters at 10 x magnification.
- Irradiation of samples for photodegradation studies were carried out using a halogen lamp (300W) at 60 V; a 500-600 nm (Schott) glass UV filter; and a water filter, to filter off far infrared radiation.

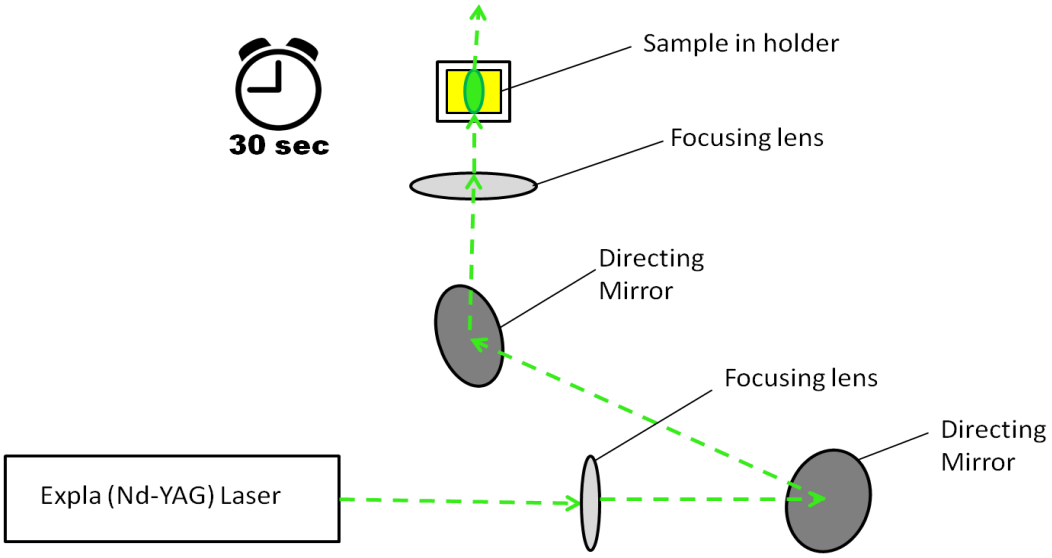

Figure 24: Laser set-up for singlet oxygen experiments.

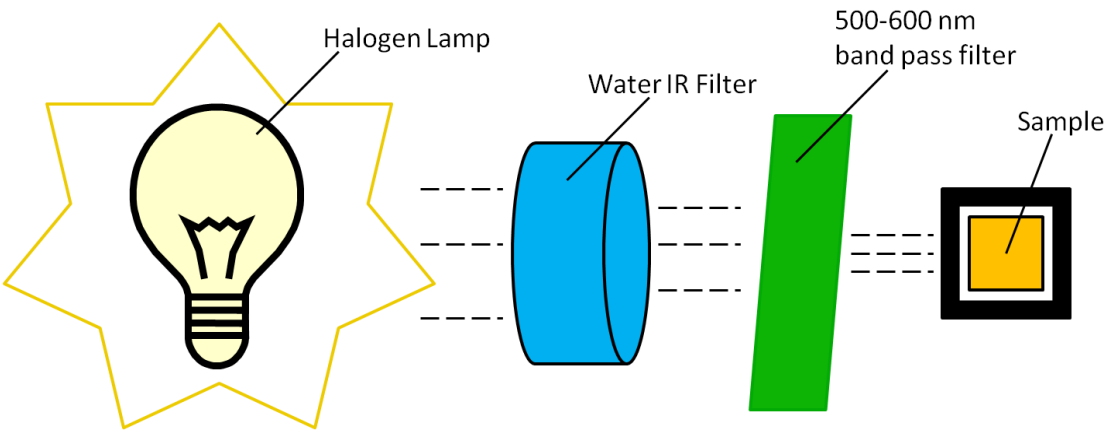

Figure 25: Experimental set-up used for photodegradation studies.

2.2 Materials

2.2.1 Reagents

2,4-Dimethyl pyrrole, cuminaldehyde, 4-dimethyl amino benzaldehyde, trifluoroacetic acid (TFA), 2,3-dichloro-5,6-dicyano-1,4-benzoquinone (DDQ), *p*-chlorinal, $BF_3.Et_2O$, triethylamine (TEA), N-iodosuccinamide, rhodamine-6-G and 1,3-diphenylisobenzofuran (DBPF) were purchased from Sigma Aldrich. Rose Bengal was obtained from Fluka. 3,4 dihydroxybenzaldehyde, diethylene glycol bis (2-chloroetyl) ether, piperidine, glacial acetic acid, N-bromosuccinamide, and sodium hydroxide and were obtained from Tokyo Chemical Industry Co. Ltd.

2.2.2 Solvents

DMF, THF, DCM, and ethanol were obtained from local suppliers. Benzene, n-butanol, n-heptane and methanol were purchased from Tokyo Chemical Industry. Ultrapure water was filtered from a Milli-Q Water System. Solvents were dried and stored over 4A molecular sieves as needed.

2.3 Methods

2.3.1 Fluorescence Quantum Yield (Φ_F)

Comparative determinations of fluorescence quantum yields can be derived from **Equation 3:**[113]

$$\Phi_F = \Phi_F^{std} . \left(\frac{F . A_{std} . \eta^2}{F_{std} . A . \eta_{std}^2} \right)$$

Φ_F^{std} refers to the fluorescence quantum yield of the standards. Rhodamine-6-G (Φ_F = 0.94 in ethanol)[102] was used for the lower wavelength BODIPYs while ZnPc (zinc phthalocyanine) (Φ_F = 0.20 in DMSO)[103] was used for dyes with spectral bands at longer wavelength with a maxima beyond 600 nm. η and η_{std} refer to the refractive indices of the solvents of the sample and standard, respectively. F and F_{std} refers to the integrated fluorescence emission of the sample and standard respectively, while A and A_{std} refer to the absorbance of the sample and standard at the excitation wavelength for the sample and standard respectively.

2.3.2 Fluorescence Titration

The acid dependent fluorescence emission of BODIPY **(4)** was investigated by titration with a solution of TFA (100 µL aliquots at ca. 1 x 10^{-6} M). The fluorescence emission spectra were recorded until emission intensity no longer increased upon addition of

another aliquot of the TFA solution. The instrument configuration and excitation wavelength for the sample and the standard were kept constant throughout the experiment.

2.3.3 Fluorescence Lifetimes (τ_F)

Fluorescence decay curves for each BODIPY were recorded at their respective emission maxima using a single photon counting technique (TCSPC) as outlined in section 2.1. Deconvolution of these decay curves using the Fluorfit[114] software yields the average time between absorption and emission of a photon by a fluorophore. This is termed the fluorescence lifetimes of a fluorophore which is typically in the 1–10 ns range for BODIPY dyes.[37]

2.3.4 Singlet Oxygen Quantum Yields (Φ_Δ)

Singlet oxygen quantum yields of BODIPY dyes were determined by a comparative method with a singlet oxygen scavenger **(Equation 6)**.The rate of singlet oxygen generation by the sample molecule is compared to that of a known standard by monitoring the absorption change of a singlet oxygen quencher, such as DPBF. Rose Bengal (Φ_Δ = 0.86 in ethanol)[110] and ZnPc (Φ_Δ = 0.67 in DMSO)[111] were used as the singlet oxygen standard and were irradiated, along with the samples, using an Ekspla NT 342B-20-AW laser (20 mJ/5 ns, 20 Hz) laser at various cross-over wavelengths for the absorption spectra of the sample and standard. The degradation of DPBF due to

singlet oxygen generation was monitored at 385 nm by UV-visible absorption spectroscopy.

2.3.5 Molecular Modelling

Geometry optimization and TD-DFT calculations were carried out using the method B3LYP of the Gaussian09 software packages with SDD basis sets.[115] The B3LYP optimized models were then used for TD-DFT calculations using the CAM-B3LYP functional, which has a long range correction that provides more accurate predictions for the relative energies of transitions with significant charge transfer character.[30] The Gaussian09 default basis set, SDD, was chosen for its ability to calculate reasonable trends when heavy atoms, such as bromine or iodine, are included in the BODIPY structure.

2.4 Synthesis

The synthesis of the meso-substituted BODIPY dyes followed a 1-pot reaction procedure adapted from literature.[116] Despite the apparent step-wise nature of these reactions only the final products were isolated and characterized.

2.4.1 4,4'-Difluoro-8-(4-isopropylphenyl)-1,3,5,7-tetramethyl-4-bora-3a,4a-diaza-*s*-indacene (1)

Cuminaldehyde (0.5 g, 1.0 mole eq.) and 2,4-dimethylpyrrole (2.0 mole eq., ρ = 0.924 $g.cm^{-3}$) was added to a DCM (48 mL) under Ar/N_2 with stirring. TFA (2–3 drops) was slowly added to the solution. The reaction was carried out at room temperature for 3 h under Ar/N_2 with vigorous stirring. Thin layer chromatography (TLC) confirmed the absence of the aldehyde and the formation of the appropriate dipyrromethane.

The mixture was cooled to 0°C after which a solution of *p*-chlorinal (1.2 mole eq.) dissolved in DCM (10 mL) was added dropwise. The solution was allowed to warm up to room temperature and the reaction was left to proceed for 30 min under Ar/N_2 with stirring. A deep purple colour was observed and TLC confirmed the synthesis of the dipyrromethene.

The mixture was again cooled to 0°C. TEA (7 mole eq.) and $BF_3{\cdot}Et_2O$ (11 mole eq.) were cooled to 0°C and added dropwise into the dipyrromethene solution. The mixture was left to stir under Ar/N_2 at room temperature for 12 h. The resulting mixture was filtered through a silica plug using DCM (30 mL) and then extracted with 0.1 M HCl.

The organic phase was dried over Na_2SO_4 and separated via flash column chromatography with ethyl acetate and hexane (1:14) as the eluent.

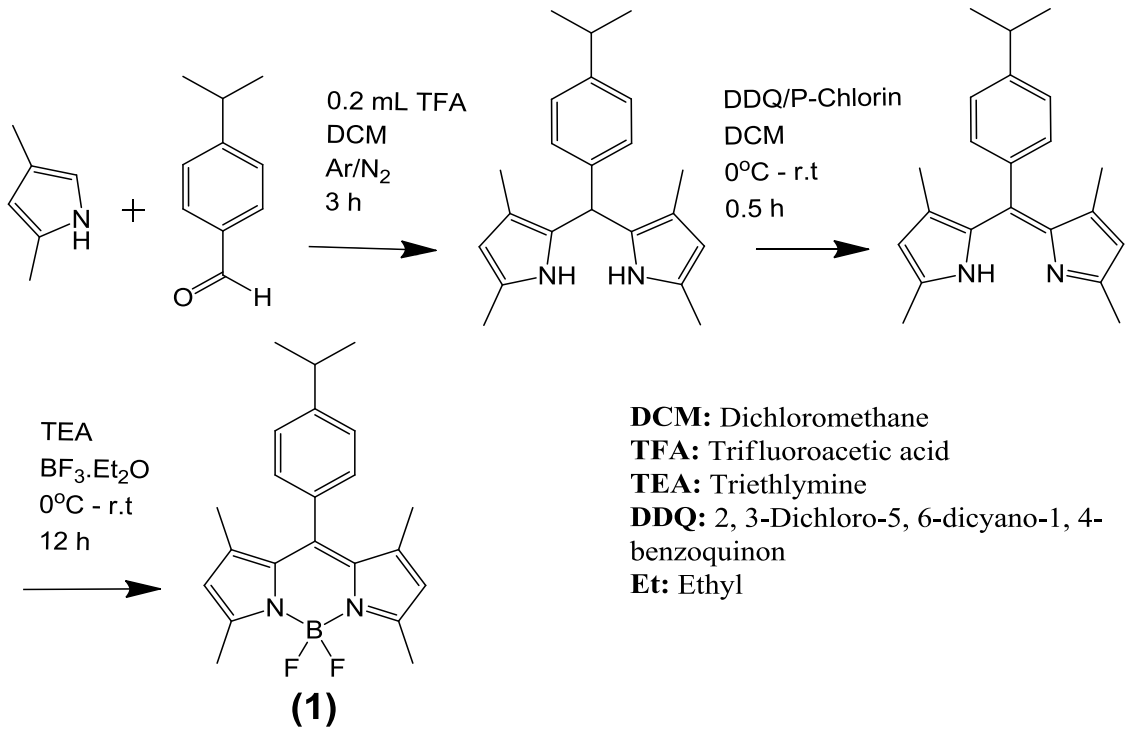

(1)

Scheme 6: Acid catalysed synthesis of 4,4'-difluoro-8-(4-isopropylphenyl)-1,3,5,7-tetramethyl-4-bora-3a,4a-diaza-*s*-indacene (BODIPY **(1)**) via the classic "1-pot" method.

(1): Eluent: chloroform/hexane (1:3). Obtained: Orange crystalline powder. Yield: (102 mg, 8.2%). FT-IR (cm^{-1}): 2957 (C-H stretch), 2922 (C-H stretch), 2861 (C-H stretch), 1541 (C-C in ring stretch), 1301 (C-N stretch), 1154 (C-N stretch), 1058 (C-N stretch), 970 (=C-H bend) 809, 711, 581, 475. ^{1}H-NMR: (Chloroform-d_1): δ, ppm 7.32–7.34 (2H, m, Ar-H), 7.16–7.18 (2H, m, Ar-H), 5.97(2H, s, py-H), 2.96–3.00 (1H, m, C-H), 2.55(6H, s, C-H_3), 1.36 (6H, s, -C-H_3), 1.28–1.30 (6H, d, C-H_3). Calc. for $C_{22}H_{25}BF_2N_2$: Expected: C, 72.15, H, 6.88, N, 7.65; Found: C, 72.23, H, 7.67, N, 6.94. ESI-MS m/z calc: 366.26 amu; Found: 366.2 amu.

2.4.2 4,4'-Difluoro-8-(4-isopropylphenyl)-1,3,5,7-tetramethyl-2,6-dibromo-4-bora-3a,4a-diaza-*s*-indacene (2)

(1) (50 mg) and N-bromosuccinimide (2.2 mole eq.) were dissolved in DMC (10 mL). The mixture was left to stir under Ar/N_2 at room temperature for 4 h. The reaction was quenched with sodium thiocyanate and the organic phase was dried over Na_2SO_4 and separated via flash column chromatography with chloroform and hexane (1:14) as the eluent.

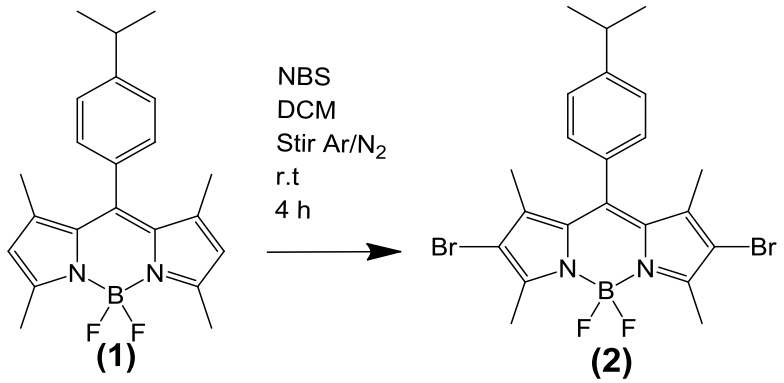

DCM: Dichloromethane
NBS: N-Bromosuccinamide
TEA: Triethlymine
DDQ: 2, 3-Dichloro-5, 6-dicyano-1, 4- benzoquinon
Et: Ethyl

Scheme 7: The synthesis of 4,4'-difluoro-8-(4-isopropylphenyl)-1,3,5,7 tetramethyl-2,6-dibromo-4-bora-3a,4a-diaza-*s*-indacene via nucleophilic addition of bromine to BODIPY (1).

(2): Obtained: deep red crystalline powder. Yield: (60 mg, 83.3%). FT-IR (cm^{-1}): 2959 (C-H stretch), 2920 (C-H stretch), 2851 (C-H stretch), 1529 (C-C in ring stretch), 1462 (C-H bend), 1309 (C-N stretch), 1174 (C-N stretch), 1085 (C-N stretch), 995 (=C-H bend), 711, 591, 530 (C-Br stretch). ^{1}H-NMR: (Chloroform-d_1): δ, ppm 7.36-740 (2H, m, Ar-H), 7.13-7.17 (2H, m, Ar-H), 2.99-3.04 (1H, m, C-H), 2.60-2.66 (6H, s,-C-H_3), 1.37 (6H, s, -C-H_3), 1.30-1.31 (6H, d, -C-H_3). MALDI TOF-MS m/z calc for $C_{22}H_{23}BF_2Br_2N_2$: Expected: 524.05 amu; Found: 525.7 amu (+1H).

2.4.3 4,4'-Difluoro-8-(4-isopropylphenyl)-1,7-dimethyl-2,6-dibromo -3,5-di-styryl-(4'-benzo-15-crown-5)-4-bora-3a,4a-diaza-*s*-indacene (3)

(2) (0.1 mmol, 1 mole eq.), 4-formylbenzo-15-crown-5 (0.13 mmol, 1.4 mole eq.) and glacial acetic acid (0.4 mL) were dissolved in dry benzene (20 mL) under Ar with stirring. Piperidine was added slowly and the solution was heated to reflux for 48 hours under Ar. A Dean-Stark trap was deployed for the azeotropic removal of water formed during the condensation reaction. The reaction was quenched with water and the organic phase was dried over $MgSO_4$. The desired products were obtained by column and flash chromatography. The blue fraction was separated with chloroform and hexane (2:3) as the eluent and the green fraction was separated with ethyl acetate and chloroform (1:1).

(3a): Eluent: chloroform/hexane (2:3). Obtained: deep blue ink colour powder. Yield: (8 mg, 10.5%). FT-IR (cm^{-1}): 3446 (N-H stretch), 2934 (C-H stretch), 2855 (C-H stretch), 1719 (C-H bend), 1709, 1619 (aromatic stretch), 1592 (C-C in ring stretch), 1441 (C-H bend), 1256 (C-O stretch), 1034 (C-N stretch), 987 (=C-H), 854, 717, 591, 541 (C-Br stretch). ^{1}H-NMR: (Chloroform-d_1): δ, ppm 7.94–7.98 (1H, m, Ar-H), 7.29–7.31 (4H, m, Ar-H), 7.07–7.11 (2H, m, Ar-H), 4.10–4.18 (2H, m, CH), 3.46–3.49 (4H, m, CH_2 crown ring), 3.31–3.33 (4H, m, CH_2 crown ring), 2.57 (1H, s, C-H), 2.00–2.02 (8H, d, CH_2 crown), 1.44–1.60 (12H, m, CH_3), 1.19–1.35 (3H, m, CH_3). MALDI TOF-MS m/z calc. for $C_{37}H_{41}BF_2Br_2N_2O_5$: 802.35 amu; Found: 825.3 amu (+ $1Na^+$).

(3b): Eluent: ethyl acetate/chloroform (1:1). Obtained: dark green powder. Yield: (12 mg, 11.2%). FT-IR (cm^{-1}): 3569 (N-H stretch), 2920 (C-H stretch), 2859 (C-H stretch), 1707 (C-H bend), 1592 (N-H bend), 1509, 1445 (C-H bend), 1260 (C-O stretch), 1109 (C-N stretch), 717 (=C-H), 597 (C-Br stretch). ^{1}H-NMR: (Chloroform-d_1): δ, ppm. 7.94–7.99 (2H, m, Ar-H), 7.48–7.60 (2H, m, Ar-H), 7.30–7.32 (4H, m, Ar-H), 7.07–7.13 (2H, m, Ar-H), 4.12–4.16 (4H, m, CH) 3.86–3.87 (8H, broad m, CH_2 crown ring), 3.57–3.71 (24H, broad m, CH_2 crown ring), 1.98–1.99 (1H, s, CH), 1.35 (3H, s, CH_3), 1.19–1.26 (9H, broad m, -CH_3). ESI-MS m/z calc. for $C_{52}H_{59}BF_2Br_2N_2O_{10}$: 1080.65; Found: 1083.24 amu (+ $3H^+$).

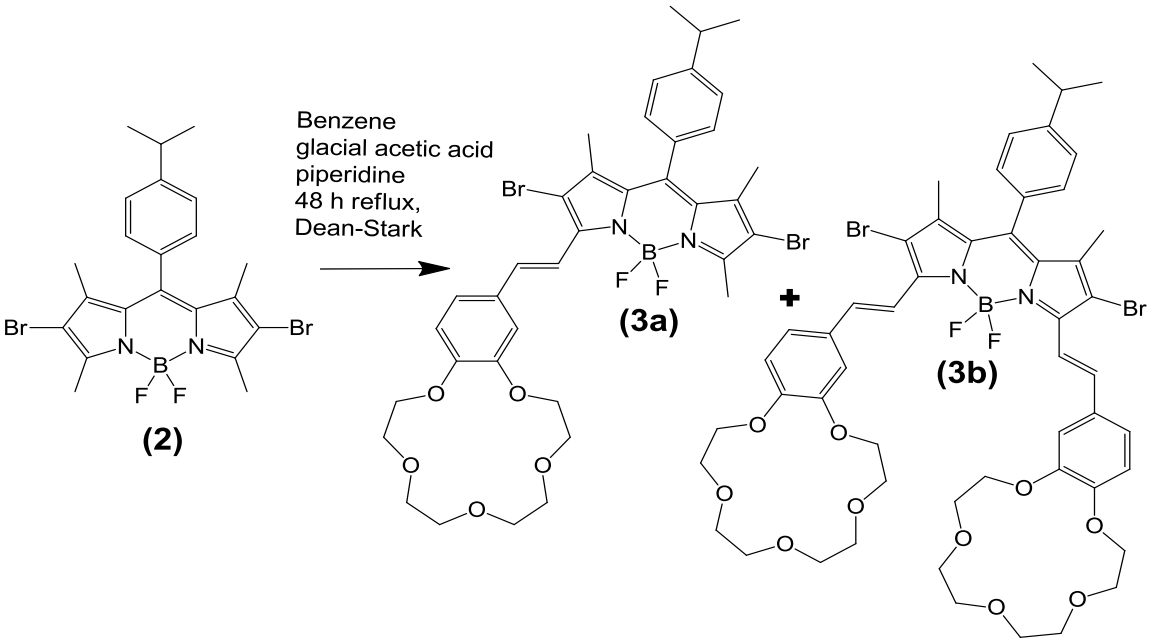

Scheme 8: Knoevenagel condensation of 4-formylbenzo-15-crown-5 and **(2)** resulting in the synthesis of mono-**(3a)** and di-**(3b)** styryl crown ether BODIPY dyes.

2.4.4 4,4'-Difluoro-8-(4-dimethylaminophenyl)-1,3,5,7-tetramethyl-4-bora-3a,4a-diaza-*s*-indacene (4)

(4) was synthesized using the same method as for **(1)**. The only difference is that 4-dimethylaminobenzaldehyde replaces cuminaldehyde as the aldehyde for the condensation reaction.

(4): Eluent: chloroform/hexane (1:3). Obtained: Orange/gold crystals. Yield: (177 mg, 14.2%). FT-IR (cm^{-1}): 3459 (N-H stretch) 2957 (C-H stretch), 2853 (C-H stretch), 2798 (C-H stretch), 1605 (N-H bend), 1460 (C-H bend), 1303, 1186 (C-N stretch), 1150 (C-N stretch), 1048 (C-N stretch), 966, 805, 760, 701, 475. ^{1}H-NMR: (Chloroform-d_1): δ, ppm 6.97–6.99 (2H, m, Ar-H), 6.69–6.72 (2H, m, Ar-H), 5.89(2H, s, py-H), 2.94 (6H, s, -CH_3), 2.47 (6H, s, py-CH_3), 1.41 (6H, s, -CH_3). Calc. for $C_{21}H_{24}BF_2N_3$: Expected: C, 68.5, H, 6.8, N, 11.4; Found: C, 68.5, H, 7.5, N, 10.5. ESI-MS m/z calc: 367.24 amu; Found: 348.1 amu (- $1F^-$).

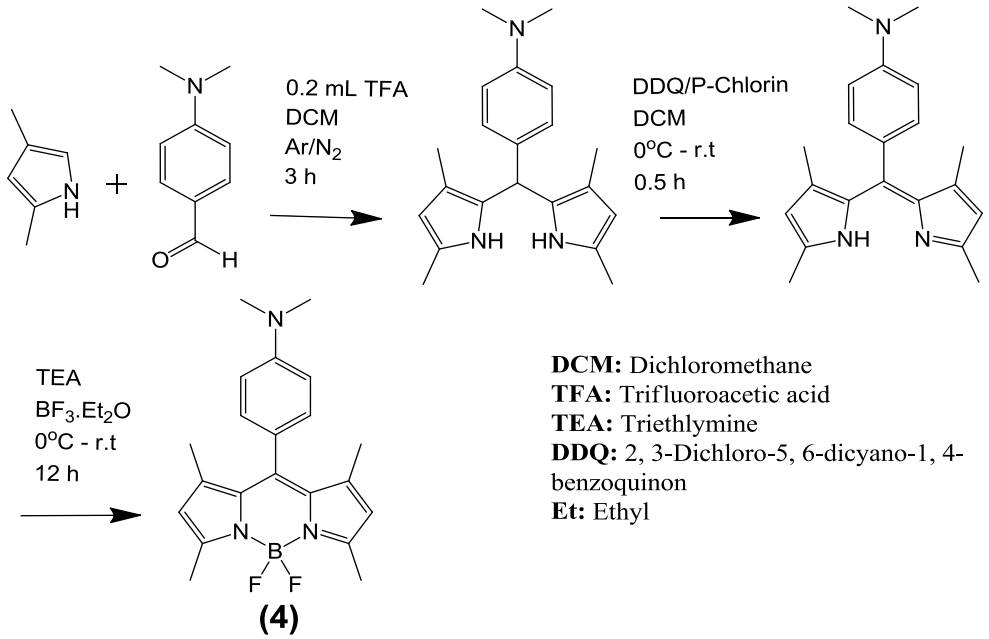

(4)

Scheme 9: Acid catalysed synthesis of 4,4'-difluoro-8-(4-dimethylaminophenyl)-1,3,5,7-tetramethyl-4-bora-3a,4a-diaza-*s*-indacene via the classic "1-pot" method.

2.4.5 4,4'-Difluoro-8-(4-dimethylaminophenyl)-1,3,5,7-tetramethyl-2,6-dibromo-4-bora-3a,4a-diaza-*s*-indacene (5)

BODIPY **(5)** was synthesized following the same method as **(2)** with **(4)** as the BODIPY core.

(5): Eluent: chloroform/hexane (1:3) Obtained: deep red powder. Yield: (70 mg, 97.9%). FT-IR (cm^{-1}): 2959 (C-H stretch), 2920 (C-H stretch), 2851 (C-H stretch), 1600 (N-H bend), 1527, 1309 (C-N aromatic stretch), 1172, 1085 (C-N stretch), 993 (=C-H bend), 793, 758, 715, 585, 530 (C-Br stretch). ^{1}H-NMR: (Chloroform-d_1): δ, ppm 7.23–7.38 (2H, m, Ar-H), 7.06–7.09 (2H, m, Ar-H), 2.83(6H, s, CH_3), 2.53 (6H, s, CH_3), 1.40 (6H, s, -CH_3). ESI-MS m/z calc for $C_{21}H_{23}BF_2Br_2N_3$: 525.05 amu; Found: 525.6 amu.

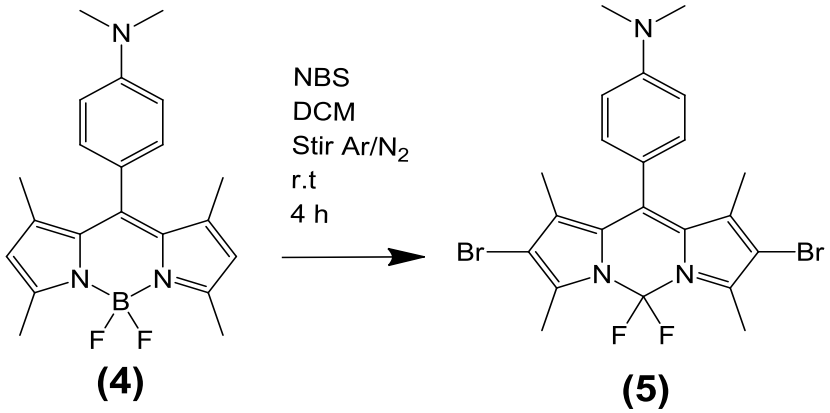

(4) **(5)**

DCM: Dichloromethane
NBS: N-Bromosuccinamide
TEA: Triethlymine
DDQ: 2, 3-Dichloro-5, 6-dicyano-1, 4- benzoquinon
Et: Ethyl

Scheme 10: Synthesis of BODIPY **(5)** via nucleophilic addition of bromine to BODIPY **(4)**.

2.4.6 4,4'-Difluoro-8-(4-dimethylamino)-1,7-tetramethyl-2,6-dibromo-3,5-di-styryl-(4-benzo-15-crown-5)-4-bora-3a,4a-diaza-*s*-indacene (6)

The synthesis of the crown ether BODIPYs **(6a)** and **(6b)** was achieved by the same method as for **(3)**. As before both the mono-**(6a)** and di-**(6b)** crown substituted fractions were isolated.

(6a): Eluent: chloroform/hexane (1:3). Obtained: deep blue ink coloured powder. Yield: (10 mg, 13.1%). FT-IR (cm^{-1}): 3391 (N-H stretch), 2912 (C-H stretch), 2861 (C-H stretch), 1727 (C-H stretch), 1619 (aromatic stretch), 1596 (C-C in ring stretch), 1441, 1352, 1266 (C-O stretch), 1178 (C-N stretch), 1117 (C-N stretch), 983, 852, 764, 589 (C-Br stretch). ^{1}H-NMR: (Chloroform-d_1): δ, ppm 7.95–7.99 (1H, m, Ar-H), 7.41–7.46 (2H, m, Ar-H), 7.07–7.15 (4H, broad m, Ar-H), 4.11–4.17 (2H, m, CH), 4.46–4.49 (4H, m, CH_2 crown ring), 3.30–3.33 (4H, m, CH_2 crown ring), 2.01 (8H, m, CH_2 crown ring), 1.36 (3H, s, CH_3), 1.18 (12H, s, CH_3). ESI-MS m/z calc for $C_{36}H_{40}BF_2Br_2N_3O_5$: 803.34 amu; Found: 804.9 amu (+1H).

(6b): Eluent: chloroform/ethyl acetate (1:1). Obtained: dark green powder. Yield: (21 mg, 19.6%). FT-IR (cm^{-1}): 3434 (N-H stretch), 2920 (C-H stretch), 2857 (C-H stretch), 1733 (C-H stretch), 1594 (N-H bend), 1511, 1266 (C-O stretch), 1172 (C-N stretch), 1097 (C-N stretch), 1015, 934, 660, 524 (C-Br stretch). ^{1}H-NMR: (Chloroform-d_1): δ, ppm 7.95–8.00 (2H, d, Ar-H), 7.43–7.51 (2H, m, Ar-H), 7.07–7.10 (4H, m, Ar-H), 6.81–6.83 (2H, m, Ar-H) 4.12–4.15 (4H, m, CH), 3.85–3.87 (8H, m, CH_2 crown ring),

3.70 (18H, broad m, CH_2 crown ring), 2.84 (6H, m, CH_2 crown ring), 1.44 (6H, s, CH_3), 1.36 (6H, s, CH_3) ESI-MS m/z calc for $C_{51}H_{58}BF_2Br_2N_3O_{10}$: 1081.64 amu; Found: 1083.4 amu (+ 2H).

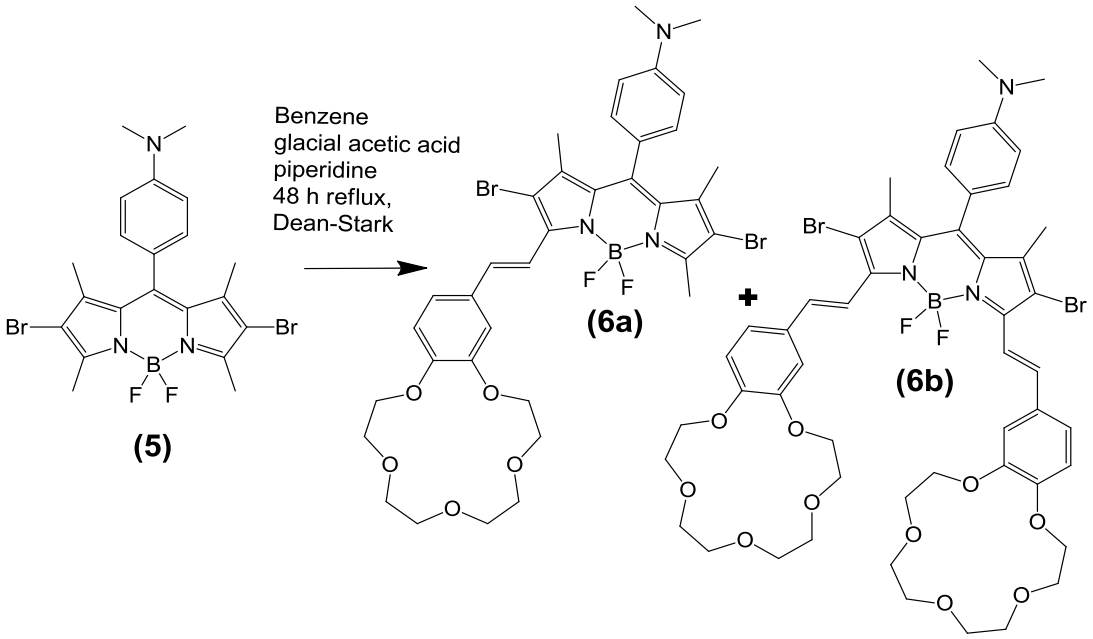

Scheme 11: Knoevenagel condensation of 4-formylbenzo-15-crown-5 and **(5)** resulting in the synthesis of mono-**(6a)** and di-**(6b)** styryl crown ether BODIPY dyes.

2.5 2,3-(4'-Formylbenzo)-1,4,7,10,13-pentaoxacyclopentadeca-2-ene (4-formylbenzo-15-crown-5) (7)

4-Formylbenzo-15-crown-5 was synthesized and isolated according to literature procedures.[117]

3,4 dihydroxybenzaldehyde (13 mmol, 1 mole eq.) was dissolved in Ar purged n-butanol (35 mL) with the subsequent addition of NaOH (28 mmol, 2.2 mole eq) in water (2.5 mL). The solution was stirred under an Ar environment (5 min) after which diethylene glycol bis(2-chloroethyl) ether (13 mmol, 1 mole eq.) was added dropwise using a cannula technique. After the solution was refluxed for 36 h under Ar the

cooled reaction mixture was quenched with HCl (0.16 mL). The crude mixture was filtered and washed repeatedly with MeOH before being evaporated to dryness. The dark residue was continuously extracted by reflux with n-heptane for 3 h and recrystallized in n-heptane to yield white crystals of 4-formylbenzo-15-crown-5.

4-Formylbenzo-15-crown-5: Eluent: n-heptane. Obtained: white crystals. Yield: (255 mg, 6.62%). FT-IR (cm^{-1}): 2928 (O=C-H), 2867 (O=C-H), 1687 (C=O). ^{1}H-NMR: (Chloroform-d_1): δ, ppm 9.83 (1H, s, O=C-H), 7.39–7.45 (2H, m, Ar-H), 6.93–6.95(1H, m, Ar-H), 4.20 (4H, m, crown), 3.93 (4H, m, crown).3.76–3.77 (8H, m, crown). Calc. for $C_{15}H_{20}O_6$: Expected: C, 60.80, H, 6.8, N, 0.0; Found: C, 60.2, H, 6.77, N, 0.02. ESI-MS m/z calc: 296.32; Found: 296.3 amu.

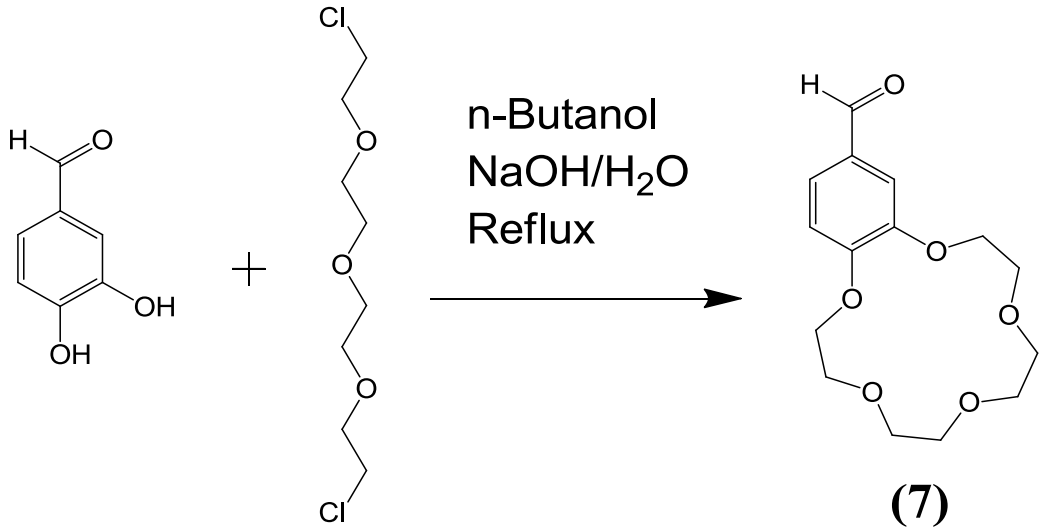

Scheme 12: The ring closure synthesis of 4-formylbenzo-15-crown-5 **(7)**.

2.6 Electrospinning of BODIPY embedded polystyrene nanofibers

Dissolve PS (2.5 g) and the BODIPY dye (2 mg) in 10 ml of DMF: THF (8:2 (v/v)) with vigorous stirring overnight. The solution was drawn up into a large syringe and the

electrospinning settings were adjusted to: voltage: 20 kV, sample distance: 13.5 cm, flow rate: 0.1 mL/h, temperature: 17.7 °C, humidity: 42%.

BODIPY nanofibers: The resulting fibers were collected and observed to be highly fluorescent under UV illumination. Only BODIPYs **(1)**, **(2)**, **(4)** and **(5)** were electrospun into nanofibers.

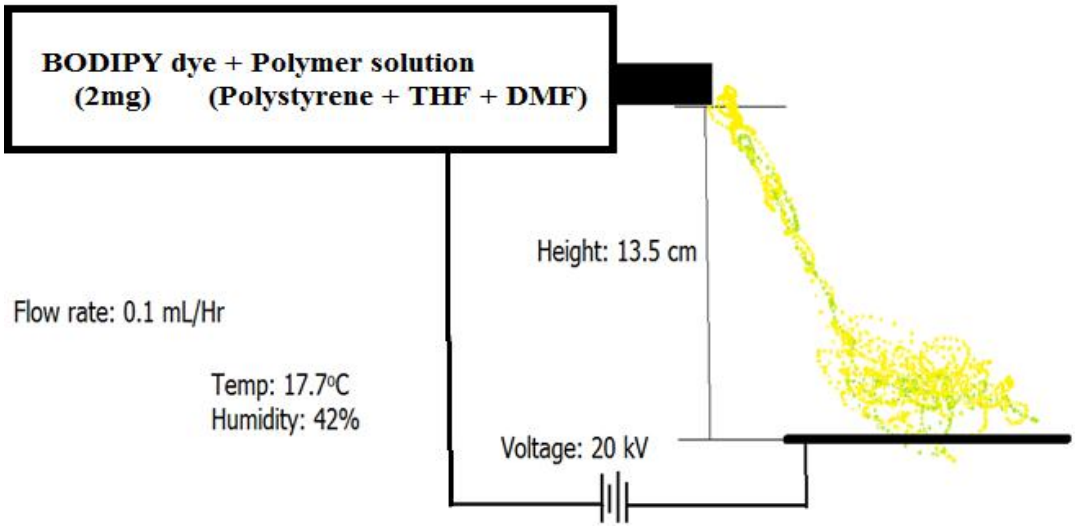

Scheme 13: Electrospinning setup used to produce BODIPY polystyrene nanofibers.

Chapter 3:

Synthesis and Spectroscopic Characterisation of BODIPY Dyes

Introduction:

This chapter seeks to explore the synthesis of two BODIPY dyes and their 2,6-dibrominated analogues.

BODIPY **(1)** has a para-isopropyl substituent on the meso-phenyl group of the BODIPY core and has not been reported to date. BODIPY **(2)** has a para-dimethylamino substituent on the meso-phenyl group of the BODIPY core. BODIPY **(2)** has been reported previously in the literature.[17] Both BODIPY dyes were synthesized by using the classic "one-pot three-step" acid catalysed condensation reaction. These BODIPY dyes were synthesized to be the core molecules for BODIPY dyes with increasingly complex structures. The photophysical properties of these dyes will be investigated in a number of different solvents. BODIPY **(1)** is expected to be highly fluorescent, while BODIPY **(2)** has been reported to be fluorescent only under acid conditions.[17] The next step of this project was to brominate the 2,6-positions of both of these BODIPY dyes. The photophysical properties of these 2,6-dibrominated BODIPY dyes were investigated with a special focus on their ability to generate singlet oxygen.

3.1 1,3,5,7-tetramethyl 8-(4-isopropylphenyl) 4,4-Difluoro-4-bora-3a,4a-diaza-*s*-indacene dye (1)

3.1.1 Synthesis of BODIPY (1)

BODIPY **(1) (Figure 8)** was synthesized for the purpose of filling a gap in the existing literature of BODIPY dyes, as well as to provide a pH insensitive structural analogue with which the photochemical properties of BODIPY **(2)** could be compared. Synthesis of BODIPY **(1)** was achieved via the "classic one-pot 3-step method" as is commonly described in literature.[44] **Scheme 14** highlights the synthetic method employed for the synthesis of BODIPY **(1)**.

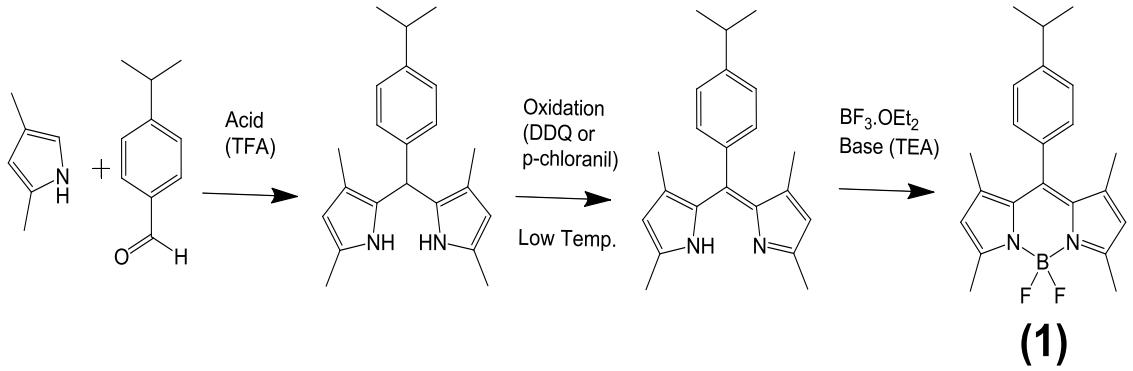

Scheme 14: The acid catalyzed "one-pot 3-step" synthesis of BODIPY **(1).**

The acid catalysed condensation of 2,4-dimethylpyrrole with cuminaldehyde was carried out using trifluoroacetic acid in DCM. The methyl groups on the pyrrole served to sterically block the 2,4-position carbons on the pyrrole in an attempt to reduce unwanted polymerization of the pyrrole unit, thus improving the overall yield of the reaction. Due to the sensitivity of the resulting dipyrromethane, and subsequent dipyrromethene, to both air and light, this entire reaction was carried out under argon

in the dark. The deep red solution containing the dipyrromethane was cooled in an acetone-water slurry and oxidized using *p*-chloranil. Cooling the reaction mixture served a two-fold purpose. Firstly, oxidation by *p*-chloranil is highly exothermic thus cooling of the mixture is required in order to reduce the thermal degradation of the resulting dipyrromethene. Secondly, cooling helped to stabilize the dipyrromethene unit which tends to be rather unstable. Reaction conditions proved to be too harsh when DDQ was used as yields were observed to be lowered significantly. The dipyrromethene was complexed through the addition of $BF_3{\cdot}OEt_2$ under basic conditions. The desired product was easy to identify and isolate using silica chromatography due to its intense yellow colour and intense green fluorescence. This particular BODIPY derivative has not been reported to date.

3.1.2 Structural Analysis of BODIPY (1)

All twenty five protons could be readily identified in the ^{1}H NMR spectroscopy **(Figure 26)**. The two multiplets between 7.31–7.34 and 7.16–7.18 ppm each integrate as two protons and can hence be attributed to the four phenyl protons. The six proton singlet signals at 2.55 and 1.38 ppm, respectively, can be assigned to the twelve methyl protons on the pyrrole core. The doublet signal at 1.28–1.30 ppm integrates to six protons and can be assigned to the six methyl protons on the isopropyl group. Of particular interest are the signals at 5.97 and 2.98 ppm. The broad singlet peak at 5.97 ppm was attributed to the protons at the 2,6-positions of the BODIPY core. This signal should only be present if the 2,6-positions are unsubstituted. The multiplet at 2.98

ppm integrates as a single proton and can be attributed to the isopropyl group providing further evidence for the success of this synthesis.

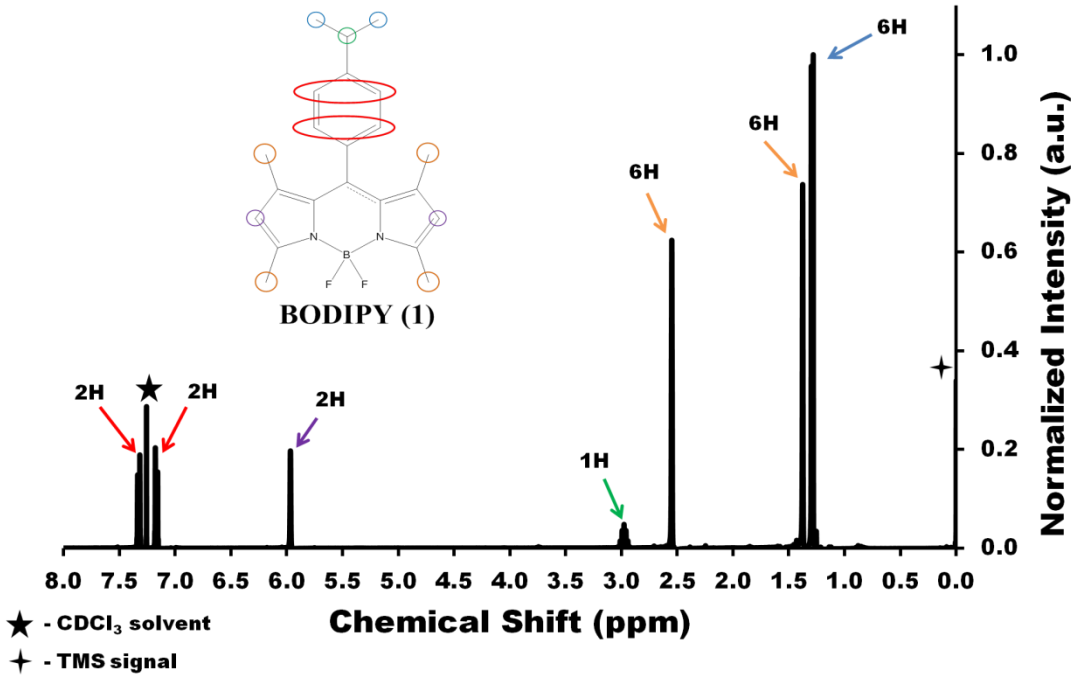

Figure 26: ^{1}H NMR spectrum for BODIPY **(1)** in $CDCl_3$. The stars indicate the solvent and TMS peaks, respectively.

CHNS elemental analysis for this compound was also in good agreement with expected values. Due to the low molecular mass of BODIPY **(1)** (366.26 g.mol^{-1}) ESI-MS had to be used in order to obtain the mass spectrum for this compound with the primary peak expected to appear at ca. 366.26 amu. Despite intense fragmentation the parent peak was observed at 366.2 amu.

FT-IR analysis of BODIPY **(1)** showed peaks that are in good agreement with the vibrations of the BODIPY skeleton that have been reported in literature.[17] The bands observed in the 2800–3000 cm^{-1} region are attributed to the C–H stretch of the terminal methyl groups attached to the BODIPY core. A number of N–C stretch bands, which correspond with the pyrrolic nitrogen atoms, lies in the 1000–1300 cm^{-1} region.

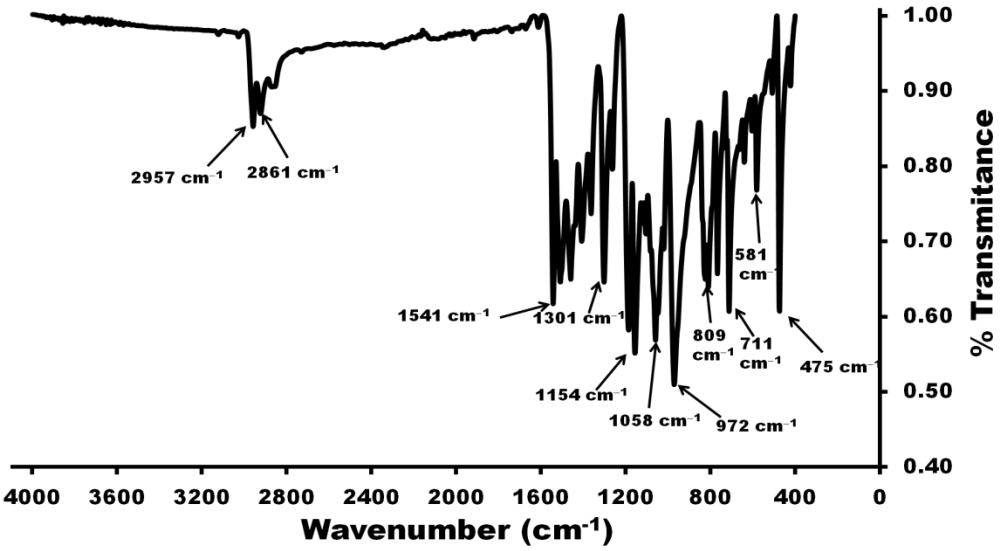

Figure 27: The neat FT-IR spectrum for BODIPY **(1)** highlighting the BODIPY vibrational skeleton.

Small orange crystals of BODIPY **(1)** were obtained after washing and recrystallization from chloroform and cold hexane (1:3 (v/v)). After the initial washing steps cold hexane was used to precipitate out any of the remaining TEA. They appeared to have a golden sheen in ambient light with an intense orange fluorescence under UV irradiation **(Figure 28)**. BODIPY **(1)** is a brilliant yellow colour in solution and displays such intense fluorescence that it can be observed under ambient light conditions **(Figure 28)**.

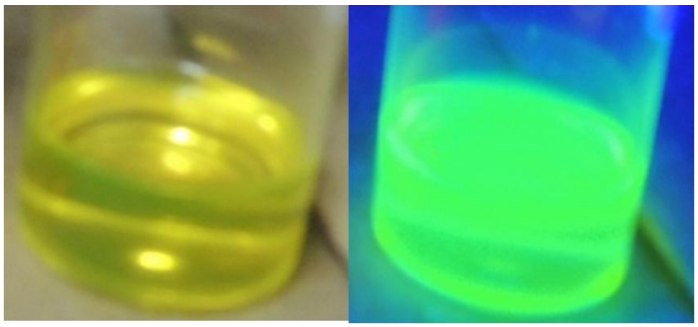

Figure 28: BODIPY **(1)** (in $CHCl_3$) exhibits a striking green emission under UV irradiation. Under close inspection fluorescence can also be observed for the sample under ambient light.

SEM was used to visualize the crystalline structure of the BODIPY dye which had formed into long, rod-shaped crystals **(Figure 29)**.

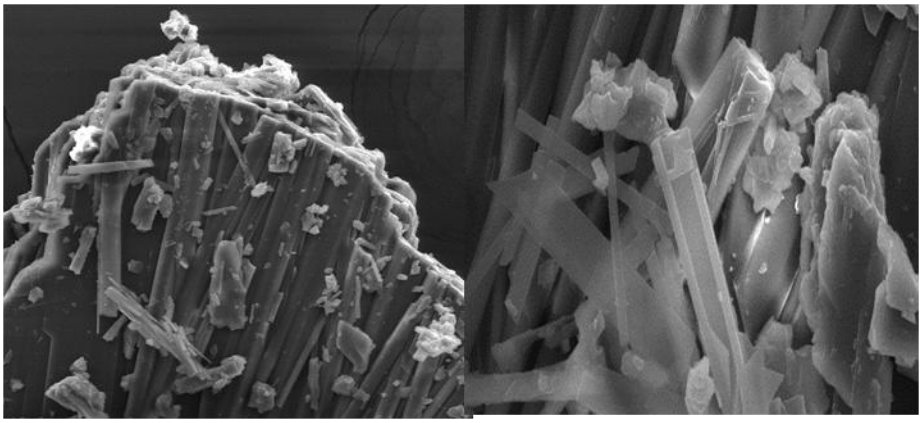

Figure 29: SEM micrograph showing rod-like crystals of BODIPY **(1)**.

3.1.3 Spectroscopic Properties of BODIPY (1)

The electronic absorption spectrum for BODIPY **(1)** is typical of that of a meso-substituted BODIPY with an absorbance maximum at 503 nm in chloroform **(Figure 30)**. BODIPY **(1)** is soluble in a wide range of solvents, and only a slight blue-shift (ca. 4 nm) is observed when the polarity of the solvent is increased. It has been suggested that this blue-shift arises from the polarizability of the solvent as a similar effect has been reported in cyanine-based dyes.[118]

Table 2: Photophysical data for meso (p-isopropylphenyl) substituted BODIPY **(1)**.

Solvent	Absorption (nm)	Emission (nm)	Excitation (nm)	Log ε (M^{-1} cm^{-1})	Φ_F	τ_F (ns)	Stokes Shift (cm^{-1})
Chloroform	503	512	501	5.03	0.91	3.5	350
DMSO	502	512	500	5.04	---	---	389
Ethanol	500	508	498	5.00	---	---	315

Table 2 summarizes the absorption, excitation and emission band maxima values of BODIPY **(1)** in three different solvents. No signs of aggregation could be observed in any of the solvents as would be expected, given the high solubility of BODIPYs. BODIPY **(1)** is highly fluorescent (the band maxima lies at ca. 510 nm) and has an emission spectrum that is typical for a tetra-methyl BODIPY **(Figure 30)**.[4] Intense fluorescence emission was observed in all of the solvents studied and in a similar manner to the trend observed in the absorption spectra; there is a slight blue-shift of the emission maxima with increasing solvent polarity. Small Stokes shifts of approximately 300 cm^{-1} are consistently observed.

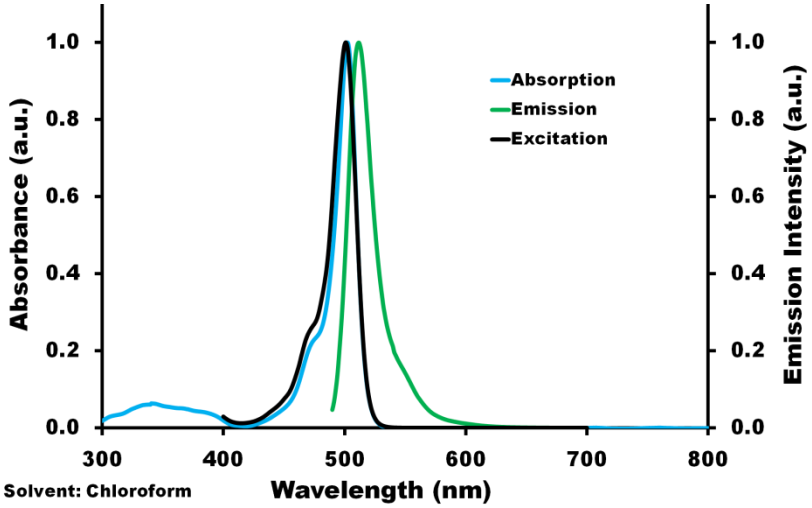

Figure 30: Normalized bands for absorption at 503 nm (blue), emission at 512 nm (green) and excitation at 503 nm (black) in the spectra for BODIPY **(1)** in $CHCl_3$.

Singlet oxygen quantum yields were determined using the comparative method by comparing the rate at which the absorbance of the singlet oxygen trap, DPBF, is decreased in the presence of the BODIPY to that of a known standard. As expected, BODIPY **(1)** did not cause any measurable decrease in DPBF absorption as it is unable to generate singlet oxygen when irradiated. BODIPY **(1)** displays high photostability as

there is no measurable decrease in absorption intensity of a solution containing this BODIPY after repeated prolonged exposure to the beam from the optical parametric oscillator (OPO) of the Ekspla NT 342 B-20-AW laser.

3.2 2,6-dibromo 1,3,5,7-tetramethyl 8-(4-isopropylphenyl) 4,4-Difluoro-4-bora-3a,4a-diaza-*s*-indacene dye (2)

3.2.1 Synthesis of BODIPY (2)

One of the simplest methods for fine-tuning the spectroscopic properties of the BODIPY core is by halogenation. It has long been known that the 2,6-position of a tetramethyl BODIPY dye are the most vulnerable to nucleophilic attack.[67] To this end BODIPY **(1)** was brominated using N-bromosuccinaminde (NBS) to yield the novel compound **(2) (Scheme 15)**.

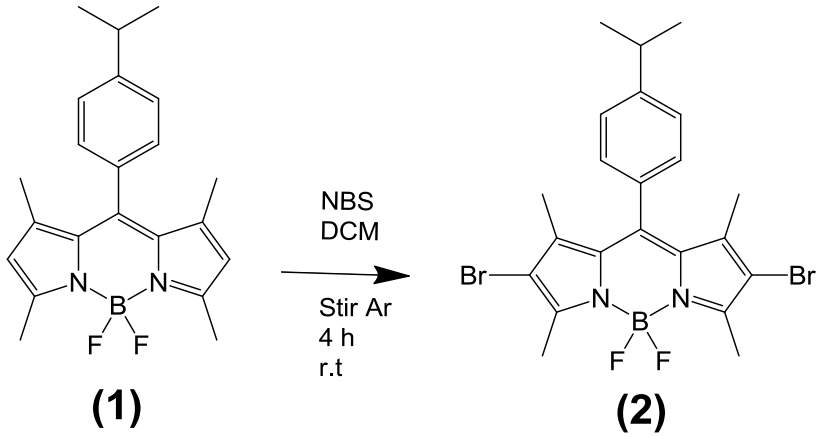

Scheme 15: Synthesis of 2,6-dibrominated BODIPY **(2)** by nucleophilic addition of bromine to BODIPY **(1)**.

The synthesis of **(2)** is straightforward. BODIPY **(1)** and NBS are stirred together in DCM. The reaction should be kept under argon and kept in the dark in order to obtain the best yields. The concentration of BODIPY **(1)** to NBS should be maintained at a 1:1.4 ratio in order to minimize bromination of the meso phenyl group. Duration of the reaction must be relatively short as the NBS reagent is highly reactive and rapidly brominates the 2,6-positions. This can be minimized by carefully monitoring the reaction by TLC. Once the completion of the reaction was confirmed, the mixture was quenched using a solution of sodium thiosulphate in water. The red-pink solution was then separated by silica gel chromatography in 83% yield using ethyl acetate: petroleum ether (1:4 (v/v)) as the eluent.

3.2.2 Structural Analysis of BODIPY (2)

All twenty three protons can be identified in the ^{1}H NMR spectrum. The multiplets that lie between 7.36–7.40 and 7.13–7.17 ppm integrate to two protons each and can be readily assigned to the four phenyl protons. The six proton singlet signals at 2.60 and 1.38 ppm, respectively, can be assigned to the twelve methyl protons on the pyrrole core. The doublet signal seen at 1.30–1.31 ppm integrates to six protons and can be assigned to the six methyl groups on the isopropyl group. The multiplet at 2.98 ppm integrates as one proton and can be attributed to the proton on the isopropyl group. The absence of the two proton signal at 5.97 ppm is particularly noteworthy **(Figure 31)**, since it demonstrates that the synthesis was successful as the hydrogen atoms at the 2,6-positions have been replaced by the bromine atoms.

The predicted atomic mass of 524.05 for BODIPY **(2)** was confirmed by MALDI-TOF mass spectrometry as the primary peak appeared at 525.7 amu (+ 1H).

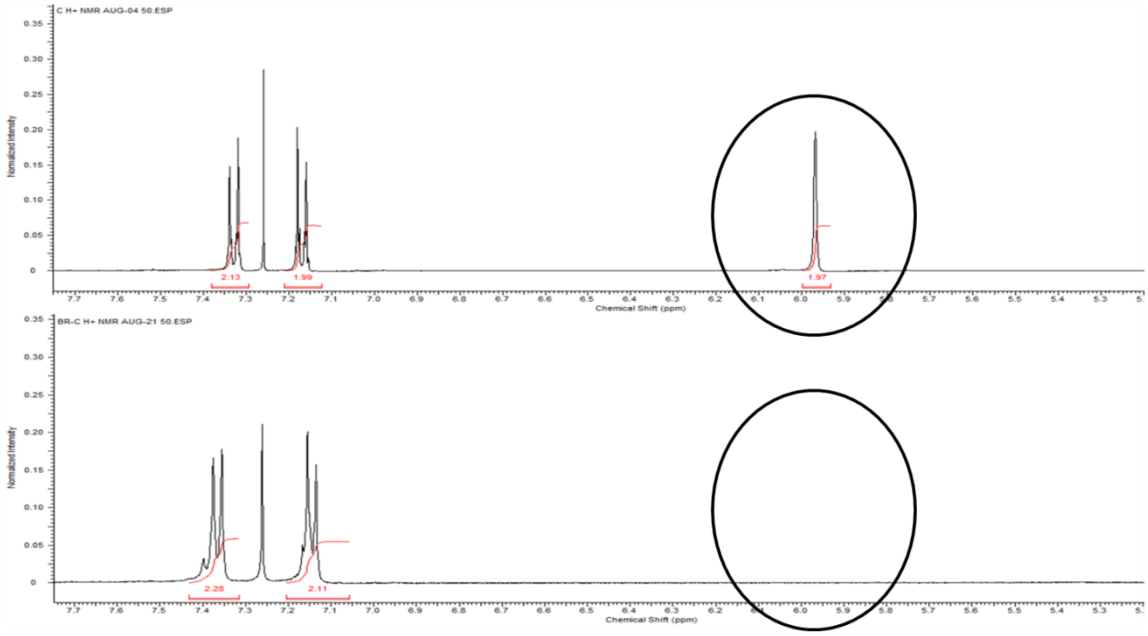

Figure 31: ^{1}H NMR spectra of BODIPY **(1)** top and BODIPY **(2)** bottom highlighting the disappearance of the 2,6-position protons signals at 5.97 ppm.

The FT-IR spectrum for BODIPY **(2)** contains a peak at 530 cm^{-1} which can be attributed to the C–Br stretch associated with the bromination of the 2,6-postions of the BODIPY core. Broadly similar vibrations to that of BODIPY **(1)** are noted as the BODIPY core remains intact after bromination.

A red crystalline powder was obtained after recrystalization of **(2)** in chloroform and hexane (1:3 (v/v)).

BODIPY **(2)** is an orange colour in solution due to a red-shift in its absorption spectrum and possesses a yellow fluorescence that is far weaker than the unbrominated BODIPY **(1) (Figure 32)**.

SEM images reveal that BODIPY **(2)** has distinctly crystalline clefts **(Figure 33).** Slowly evaporating solvent molecules dissolved some of the dye during crystallization which resulted in the tooth-like structures at the top of **a).** in **Figure 33**.

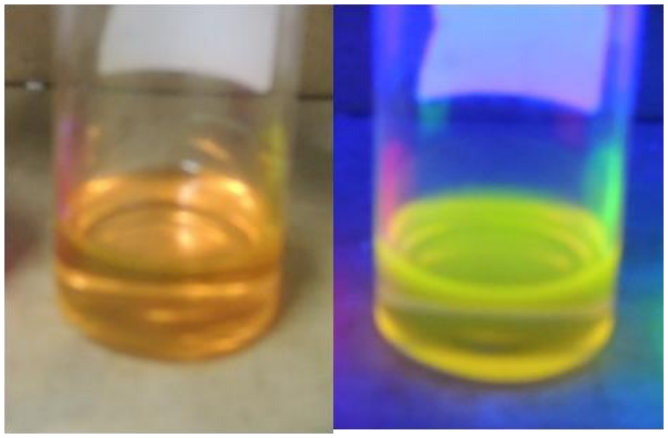

Figure 32: BODIPY **(2)** (in $CHCl_3$) exhibits a much weaker, yellow fluorescence emission under UV irradiation when compared to BODIPY **(1)**.

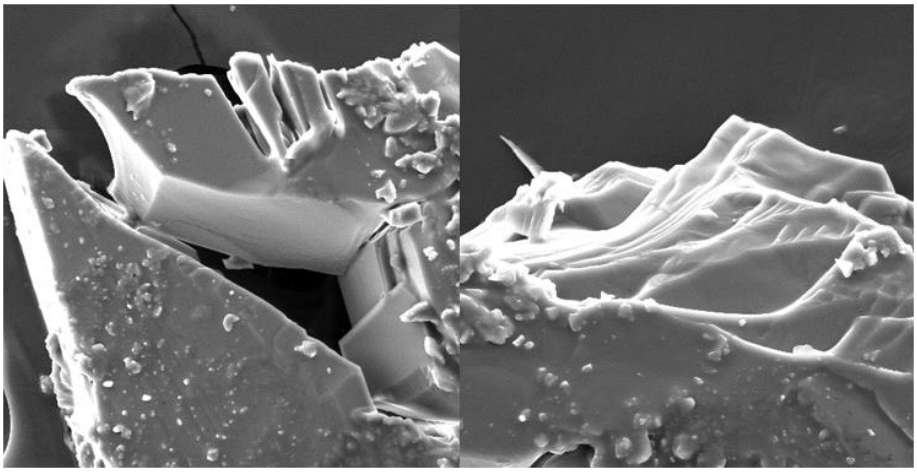

Figure 33: SEM micrograph of BODIPY **(2)** crystals.

3.2.3 Spectroscopic Properties of BODIPY (2)

The electronic absorption and emission spectra for **(2)** are typical for a BODIPY dye (the main bands lie at ca. 530 nm and 540 nm in $CHCl_3$, respectively) with the exception that the absorption maxima is red shifted by ca. 30 nm when compared to that of the parent BODIPY dye **(1)** **(Figure 34)**. This corresponds to a red shift of approximately 15 nm per bromine atom. Attachment of bromine atoms at the 2,6-positions cause a destabilization of the HOMO orbital relative to the LUMO orbital and which decreases the HOMO–LUMO band gap and results in the observed red shift.

Table 3 summarises differences observed in the absorption spectrum data of BODIPY **(2)** in a number of different solvents. The most noteworthy effect of the bromine atoms is the relaxation of the spin-selection rule due to the heavy atom effect, which cause a sharp decrease in the fluorescence quantum yield and an increase in singlet oxygen production. This allows for the synthesis of BODIPYs that could be used for photocatalysis applications or in PDT. Relatively small Stokes shifts of ca. 400 cm^{-1} are observed. BODIPY **(2)** was highly soluble in all of the solvents used and no signs of aggregation were observed. There is a slight blue shift of the main spectral band as the solvent polarity is increased.

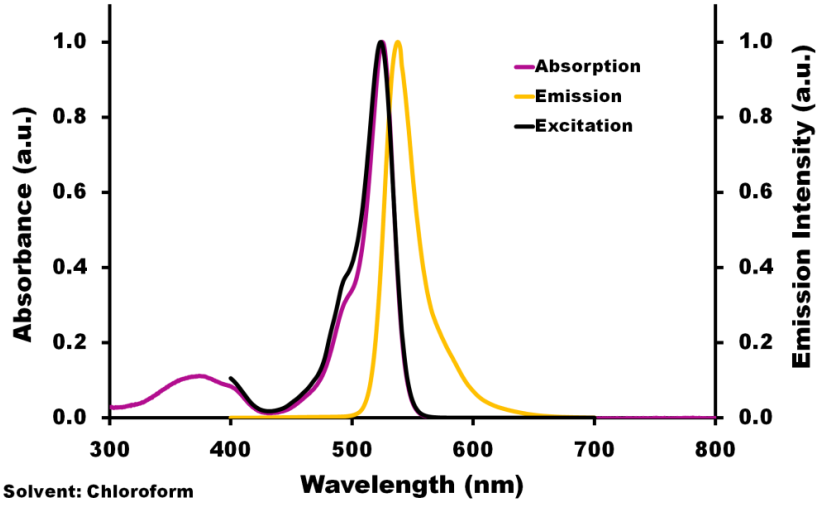

Figure 34: Normalized bands for absorption at 530 nm (purple), emission at 540 nm (yellow) and excitation at 528 nm (black) in the spectra for BODIPY **(2)** in $CHCl_3$.

Table 3: Photophysical data for 2,6-dibrominated BODIPY **(2)**.

Solvent	Abs (nm)	Em (nm)	Ex (nm)	Log ε (M^{-1} cm^{-1})	Φ_F	τ_F (ns)	Stokes Shift (cm^{-1})	Φ_Δ
Chloroform	530	540	528	4.98	0.21	2.0*	349	---
DMSO	527	540	526	5.07	---	---	457	---
Ethanol	525	538	524	5.06	---	---	460	0.80

*Main component of the biexponential fit

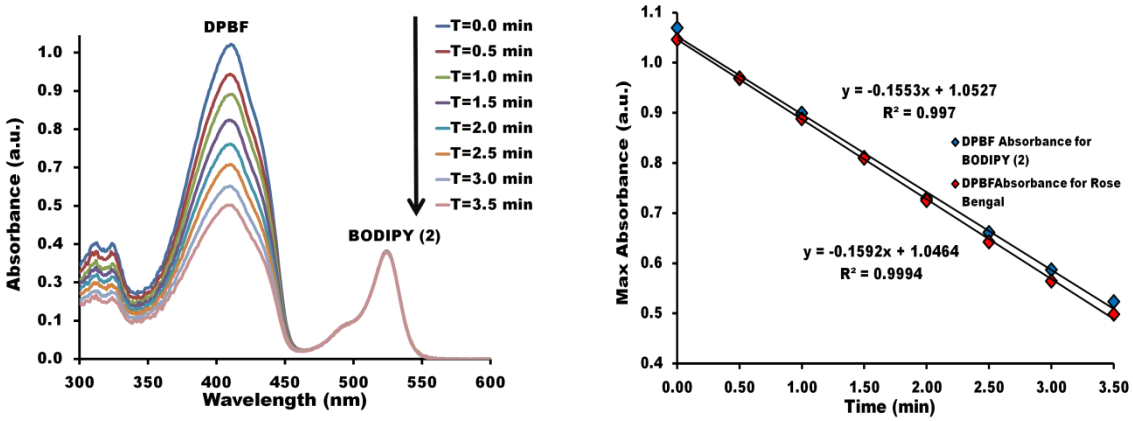

Figure 35: Photocatalytic degradation of DPBF (λ_{max} at 410 nm) in ethanol by BODIPY **(2)** (λ_{max} at 525 nm) at 30 s intervals is indicative of singlet oxygen generation (Left). The Φ_{Δ} value for **(2)** is determined using the comparative method with Rose Bengal (Φ_{Δ} = 0.86) as a standard (right).

3.3 1,3,5,7-tetramethyl 8-(4-dimethylamino phenyl) 4,4-Difluoro-4-bora-3a,4a-diaza-*s*-indacene (4)

3.3.1 Synthesis of BODIPY (4)

BODIPY **(4)** was synthesised following the same method that was described for BODIPY **(1)** with the exception that cuminaldehyde was replaced with 4-dimethylaminobenzaldehyde. The only structural differences between the two BODIPYs are that a nitrogen atom replaces the carbon atom on the para-substituent of the meso-phenyl ring and a lone pair of electrons takes the place of the hydrogen atom that was attached to the carbon at this position. This subtle change imparts a fluorescence response that is dependent on the pH of the solution. BODIPY **(4)** has an intense yellow colour, similar to that of BODIPY **(1)**, but has considerably lower fluorescence emission intensity.

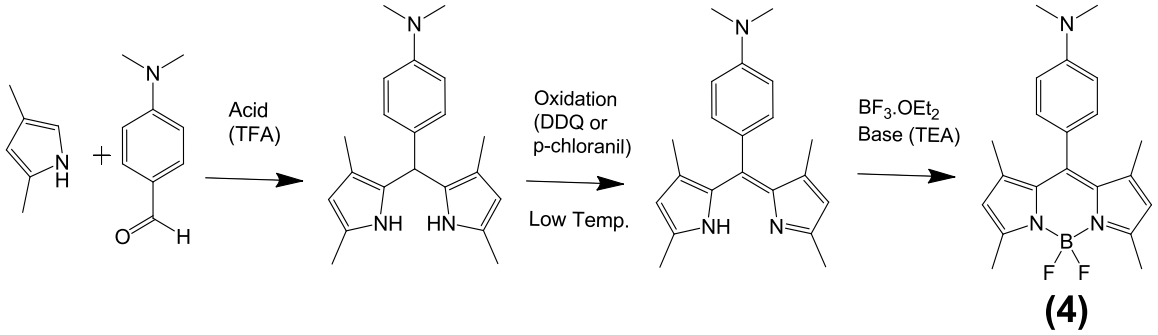

Scheme 16: The acid catalyzed "one-pot 3-step" synthesis of BODIPY **(4).**

3.3.2 Structural Analysis of BODIPY (4)

The signals for all twenty four protons can be identified in the ^{1}H NMR spectrum. The multiplets that lie between 6.97–6.99 and 6.69–6.72 ppm each integrate to two protons can be assigned to the 4 phenyl protons. The six proton signals that lie at 1.41 and 2.47 ppm can be attributed to the twelve methyl protons on the pyrrole core. The singlet signal at 2.94 ppm integrates as six protons and can be assigned to the six methyl protons on the dimethylamino group. Of particular interest is the signal at 5.89 ppm which is attributed to the protons at the 2,6-positions of the BODIPY core. This signal is only present if the 2,6-positions are unsubstituted. The CHNS elemental analysis for this compound showed slightly lower values than expected due to the presence of a water molecule.

As before, the low molecular mass of BODIPY **(4)** (367.24 g.mol^{-1}) warranted the use of ESI-MS to obtain the mass spectrum for this compound. The primary mass fragment is expected to appear at ca. 367.24 amu; however BODIPY **(4)** showed intense fragmentation with the major peak appearing at 348.1 amu. This is consistent with the loss of a fluorine and hydrogen atom from the BODIPY core.

The FT-IR spectrum of BODIPY **(4)** resembles that of BODIPY **(1)**, with the exception of an N-H stretch that lies at 1605 cm^{-1}.

Fine deep orange BODIPY **(4)** crystals were obtained after washing and recrystallization with chloroform and cold hexane (1:3). In a similar manner to what was observed with BODIPY **(1)**, they appeared to have a golden sheen in ambient light with an intense orange fluorescence under UV irradiation **(Figure 36)**.

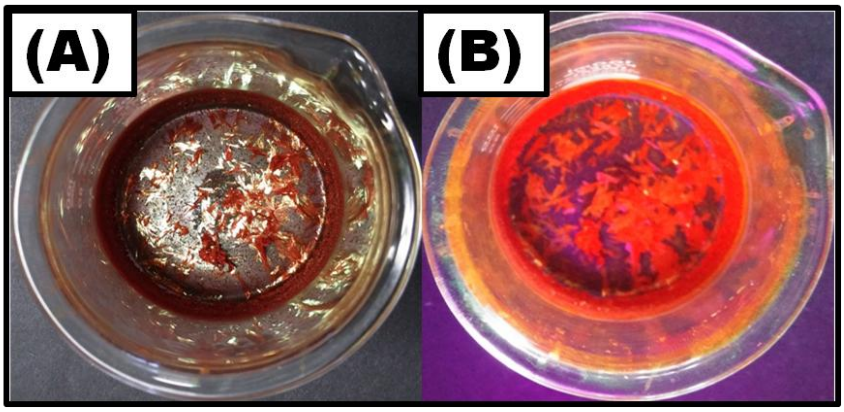

Figure 36: Orange crystals of BODIPY **(4)** in ambient light **(A)** and exhibiting orange solid state fluorescence under UV irradiation **(B)**.

SEM revealed that the crystals of **(4)** appeared to have numerous deep indentations and that there were randomly distributed holes in the BODIPYs crystals **(Figure 37)**. The spherical nature of the holes as well as their variable arrangement could be explained by the evaporation of solvent molecules from the crystal surface. The melting point of this BODIPY was determined to be ca 250°C. Fragmentation of the crystals was observed from ca. 217°C.

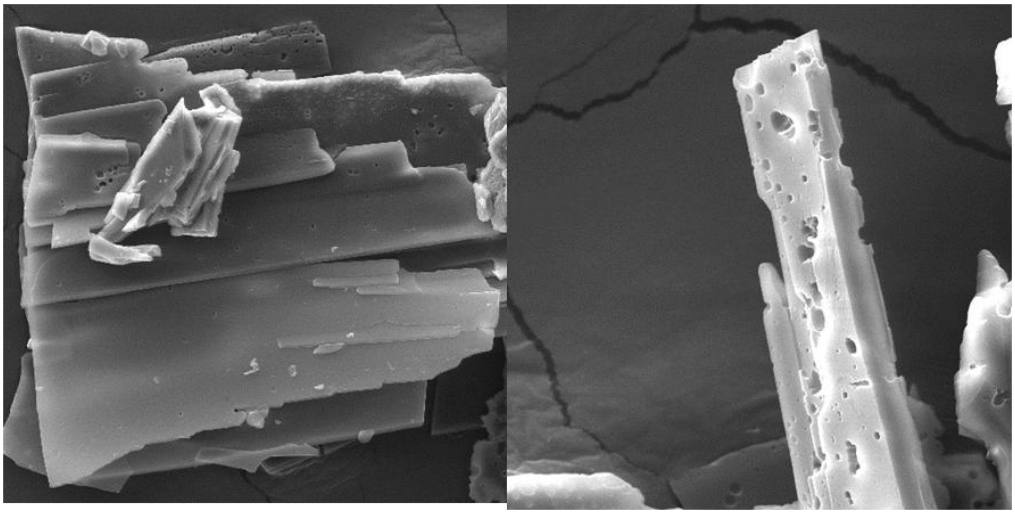

Figure 37: Numerous indentations in the crystal structure can be seen in the SEM micrograph of BODIPY **(4)**.

3.3.3 Spectroscopic properties of BODIPY (4)

The electronic absorption spectrum for BODIPY **(4)** is similar to that reported previously.[17] The main spectral band lies at ca. 503 nm in chloroform **(Figure 39)**. BODIPY **(4)** is soluble in a wide range of solvents and there is a slight blue-shift (ca. 4 nm) of this band when the solvent polarity is increased.

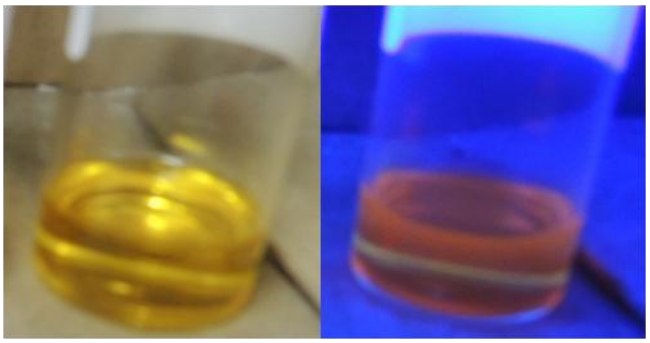

Figure 38: BODIPY **(4)** (in $CHCl_3$) exhibits very weak fluorescence emission under UV irradiation due to quenching by the lone pair of electrons on the nitrogen atom of the amino group. Fluorescence is restored with protonation of the nitrogen atom upon addition of TFA.

The fluorescence emission spectrum of BODIPY **(4)** differs greatly from that of BODIPY **(1)**. The most likely explanation is that the lone pair of electrons from the amino nitrogen quenches fluorescence emission through photon-induced electron transfer (PET) leaving **(4)** with very low emission in solution. It is possible to protonate the dimethylamino-nitrogen atom of BODIPY **(4)** with trifluoroacetic acid and this eliminated the PET process and results in a restoration of green fluorescence at ca. 515 nm. **(Figure 40)**.

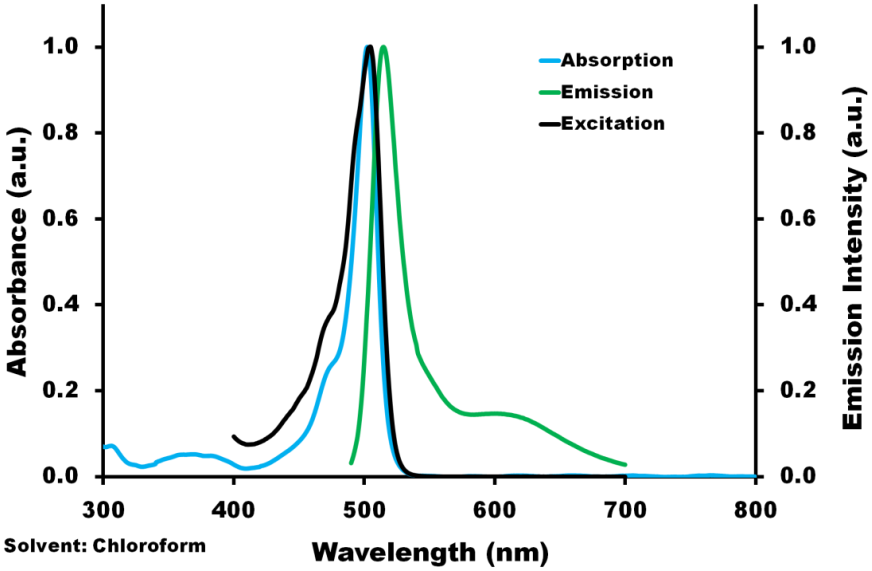

Figure 39: Normalized bands for absorption at 503 nm (blue), emission at 515 nm (green) and excitation at 505nm (black) in the spectra for BODIPY **(4)** in $CHCl_3$**.**

Table 4 summarizes the absorption, excitation and emission values of BODIPY **(4)** in three different solvents in the presence and absence of TFA. While the effect of the nitrogen atom on absorption spectrum is relatively small, the emission spectra for **(4)** is slightly red shifted compared to that of **(1)** with a slightly higher Stokes shift (ca. 500 cm^{-1}). Upon protonation the BODIPY **(4)** absorption and emission spectra in chloroform exhibit red shifts of 4 nm and 6 nm, respectively.

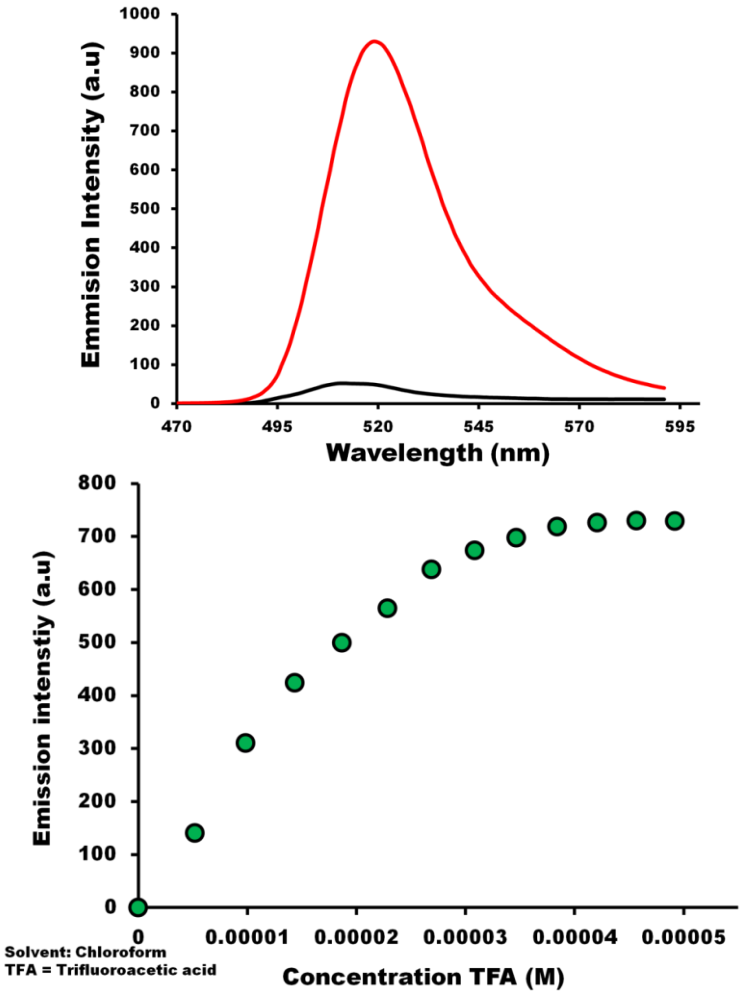

Figure 40: (Top): A demonstration of the "turning-on" of emission intensity of ca. 5 x 10^{-6} M BODIPY **(4)** in $CHCl_3$ after protonation by of 100 µL of TFA. (Bottom): Fluorescence titration of BODIPY **(4)** by addition 10 µL aliquots of TFA.

Table 4: Photophysical data for BODIPY **(4)** in the absence and presence of TFA.

Solvent	Abs (nm)	Em (nm)	Ex (nm)	Log ε (M^{-1} cm^{-1})	Φ_F	τ_F (ns)	Stokes Shift (cm^{-1})
Chloroform	503	515	505	4.92	0.02	n.d	463
Chloroform + TFA	509	521	506	4.85	0.74	---	453
DMSO	501	514	503	4.94	---	---	505
DMSO + TFA	502	516	504	4.80	---	---	541
Ethanol	499	511	501	4.70	---	---	471
Ethanol + TFA	499	514	502	4.76	---	---	585

n.d – not determined

BODIPY **(4)** was also found not to generate any singlet oxygen, even in the presence of TFA, due to low triplet state formation that is inherent with non-halogenated BODIPY dyes.

3.4 2,6-Dibromo 1,3,5,7-tetramethyl 8-(4-dimethylamino) 4,4-difluoro-4-bora-3a,4a-diaza-*s*-indacene dye (5)

3.4.1 Synthesis of BODIPY (5)

(4) was brominated following the same method as for **(2)** to yield BODIPY **(5) (Scheme 17).** The electron donating ability of the dimethylamino group assists in making the meso phenyl carbons less positive. This aids in directing the bromine atoms to the 2,6 positions resulting in a faster reaction time and a higher yield of ca 98%.

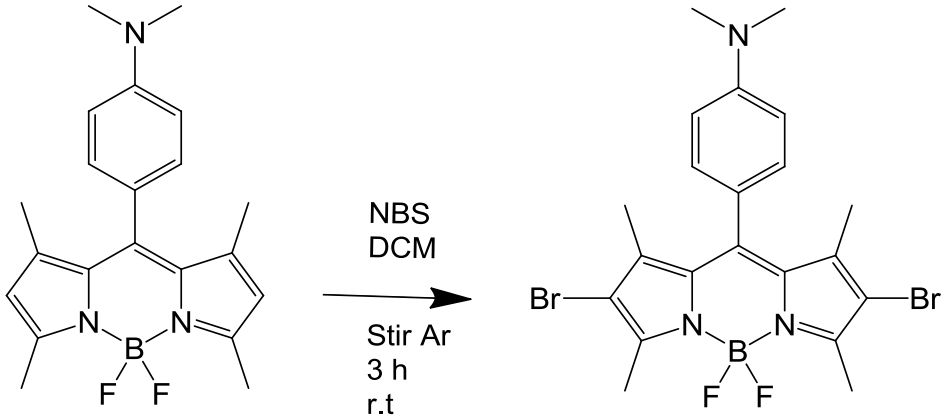

(4) **(5)**

Scheme 17: Synthesis of **(5)** by nucleophilic addition of bromine to BODIPY **(4)**.

3.4.2 Structural Analysis of BODIPY (5)

The ^{1}H NMR revealed two multiplets between 7.06–7.09 and 7.23–7.38 ppm which integrated to two each and were attributed to the 4 phenyl protons. The six proton singlet signals at 1.41 and 2.53 ppm, respectfully, were assigned to the twelve methyl protons on the pyrrole core. The singlet signal observed at 2.83 ppm integrated to six protons corresponds with the six methyl protons on the dimethylamino group. As with **(2)** there is an obvious absence of a proton signal at 5.97 ppm which indicates a successful synthesis as the hydrogen atoms at the 2,6-positions have been replaced by the bromine atoms.

The MADLI-ToF mass spectra confirmed the mass of **(5)** as the primary peak is found at 525.6 amu (+ $1H^{+}$)

The FT-IR spectrum of **(5)** closely resembled that of BODIPY **(4)** with the addition of a C–Br stretch that is observed at 530 cm^{-1}.

A red semi crystalline powder was obtained after recrystalization of **(5)** in chloroform and hexane (1:3 (v/v)). SEM images reveal that **(5)** has both crystalline and amorphous character **(Figure 41)**

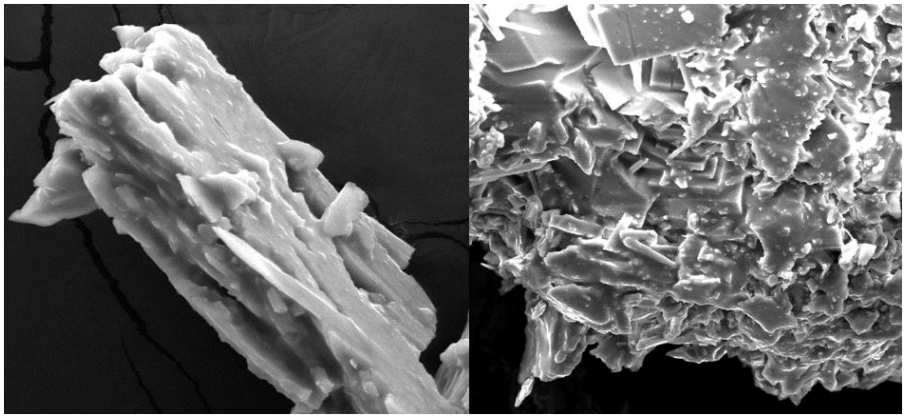

Figure 41: SEM micrograph of BODIPY **(5)** crystals.

3.4.3 Spectroscopic Properties of BODIPY (5)

A red shift of ca. 33 nm can be observed for the band maxima in the absorption and emission spectra of BODIPY **(5)** when compared to that of the BODIPY **(4)** core. **(5)** has an absorption maximum at 533 nm in chloroform **(Figure 43).**

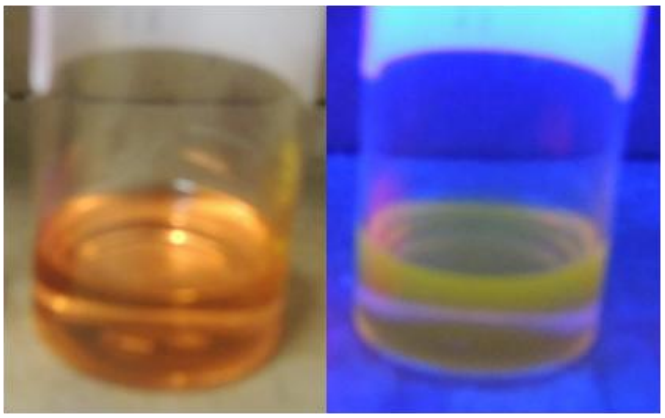

Figure 42: BODIPY **(5)** under ambient (left) and UV (right) light.

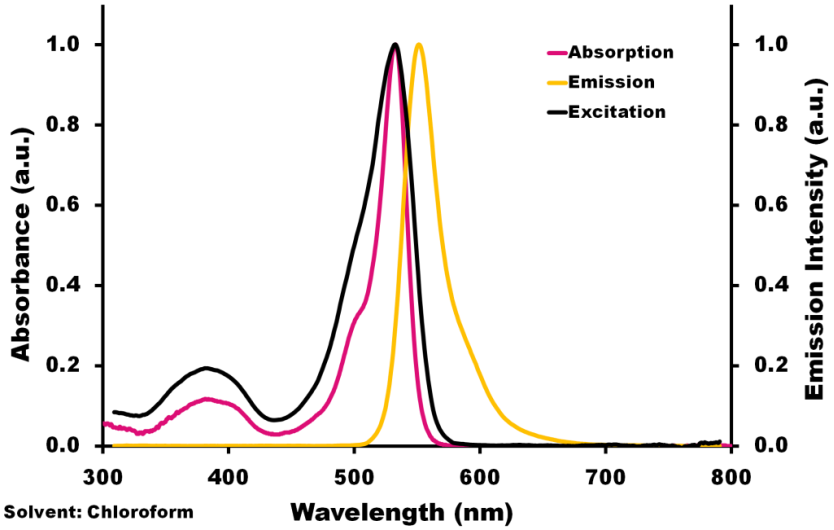

Figure 43: Normalized bands for absorption at 533 nm (purple), emission at 552 nm (yellow) and excitation at 533 nm (black) in the spectra for BODIPY **(5)** in $CHCl_3$.

Table 5 lists the absorbance values of **(5)** in various solvents.

Table 5: Photophysical data for 2,6-dibrominated BODIPY **(5)**.

Solvent	Abs (nm)	Em (nm)	Ex (nm)	Log ε (M^{-1} cm^{-1})	Φ_F	τ_F (ns)	Stokes Shift (cm^{-1})	Φ_Δ
Chloroform	533	552	533	4.70	0.09	n.d	646	---
Ethanol	527	543	---	---	---	---	559	0.82
Ethanol + TFA	528	546	---	---	---	---	624	---

n.d – Not determined.

Concluding remarks:

Two BODIPY dyes, **(1)** and **(4)** were synthesized using the classic "one-pot three-step" acid catalysed condensation reaction and fully characterized using various techniques. The only structural difference between these two BODIPY dyes is that the **(1)** has a *p*-isopropyl substituent on the meso-phenyl group, while **(4)** has a dimethylamino substituent at this position. BODIPY **(1)** possessed many favourable photophysical properties and proved to be highly photostable, but does not generate singlet oxygen upon electronic excitation. BODIPY **(4)** had similar absorption properties to BODIPY **(1)**, but has vastly different fluorescence properties. BODIPY **(4)** was only fluorescent under acidic conditions due to the lone pair of electrons on the dimethylamino nitrogen. This effect was reversible with the addition of a base and allowed BODIPY **(4)** to behave as an "off-on" fluorescence switch. Changing the solvent had very little effect on the photophysical properties of these BODIPY dyes.

Both **(1)** and **(4)** were brominated at the 2,6-positions and fully characterized. This caused a red-shift of the main absorption and emission spectra for each dye. After bromination both BODIPYs **(2)** and **(5)** displayed large singlet oxygen quantum yields and were able to degrade a sample of DPBF in solution. BODIPY **(2)** has a singlet oxygen quantum yield that is similar to that the Rose Bengal and proved to be more

photostable than the standard, suggesting that it may be suitable for use as a standard for Φ_{Δ} measurements.

Chapter 4:

Synthesis and Imaging of BODIPY-Nanofibers

4.1 BODIPY-Polystyrene (BODIPY-PS) Nanofibers:

Two of the major limitations in developing practical applications for BODIPY dyes the application of BODIPY are their poor solubility in water, and the difficulty in recovering the dyes from solution. In order to address these limitations it is advantageous to embed the BODIPY dye within a polymer support, as has been successfully achieved previously with phthalocyanine dyes.[101] BODIPY embedded nanofibers could find use as ion sensor, for example BODIPY **(4)** may be suitable since it is pH sensitive, or in the case of brominated dyes as recyclable singlet oxygen generating photocatalysts. Polystyrene was selected as the polymer support for various BODIPY dyes as it is cheap, relatively safe, chemically inert, and is relatively easy to process into nanofibers. As polystyrene is an aromatic hydrocarbon it may be possible for a π-π interaction to occur between the π-electrons of the benzene groups present on the polymer and those of the BODIPY dye **(Figure 44).** This could result in a stronger dye-polymer interaction and reduce the risk of the dye leeching.

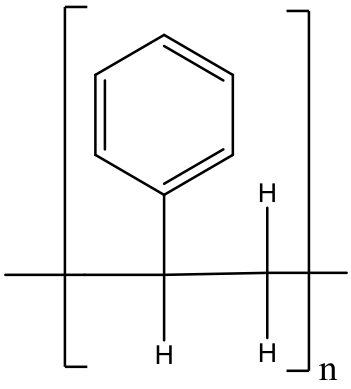

Figure 44: Polystyrene monomer unit.

4.1.1 Synthesis and characterization of PS nanofibers:

Nanofiber morphology is shown to be highly dependent on the viscosity of the polymer solution. A high molecular weight grade of polystyrene, B32, was chosen to reduce the risk of forming of defects, such as beading or branching, that are associated with low viscosity solutions. To further minimize the risk of this it is important that a homogenous polymer mixture is obtained prior to the electrospinning. The polymer solution is prepared by dissolving polystyrene B32 pellets in a mixture of DMF: THF (8:2 (v/v)). The polymer solution is then drawn up into a 20 mL syringe with care, to ensure that no trapped air bubbles are present as these would introduce defects in the resulting nanofibers. The flow rate, and distance between the collector and needle tip were maintained at a constant 0.1 ml/h and 13.5 cm, respectively. The polymer solution was subjected to a series of voltages (10, 15, and 20 kV) in order to determine the optimal set-up conditions **(Scheme 13)**. At low voltage beading was observed and the resulting nanofibers have the largest diameters. The smallest nanofiber diameters are obtained when a potential of 20 kV was employed, making this the ideal voltage for this work. These white PS nanofibers exhibit no fluorescence emission when irradiated with UV light **(Figure 45)**.

4.1.2 Synthesis and characterization of BODIPY-PS nanofibers:

Nanofibers containing BODIPY **(1)** and **(4)** are fabricated by adding 2 mg of BODIPY into respective polymer solutions using the method discussed above. The resulting yellow fibers possess an intense and uniform green fluorescence, which indicates that the

BODIPY dyes are incorporated within the PS nanofibers **(Figure 46)**. There are no observable defects in the BODIPY **(1)**-PS nanofibers; however BODIPY **(4)**-PS nanofibers show intense beading **(Figure 47)**. This could be due to a charge interaction with the dimethylamino nitrogen as the polymer solution passes through the high voltage electric field. Unfortunately, the PS polymer appears to stabilize **(4)** as the BODIPY **(4)**-PS nanofibers are intensely fluorescent. This renders the BODIPY **(4)**-PS nanofibers unusable as a pH sensor material.

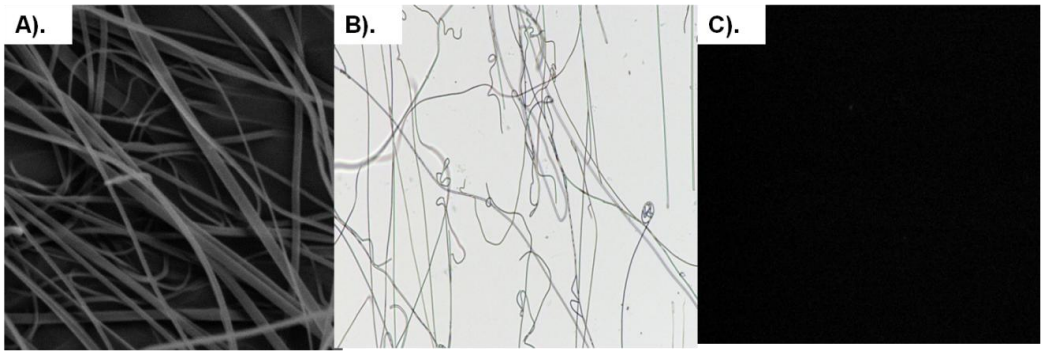

Figure 45: Unfunctionalized PS nanofibers. A) A SEM micrograph showing PS nanofibers. B) PS nanofibers under bright field illumination. C) PS nanofibers under UV irradiation show no fluorescence emission (480–550 nm, wide filter).

Figure 46: **(1)** (left) and **(2)** (right) BODIPY-PS nanofibers in ambient light and under UV irradiation.

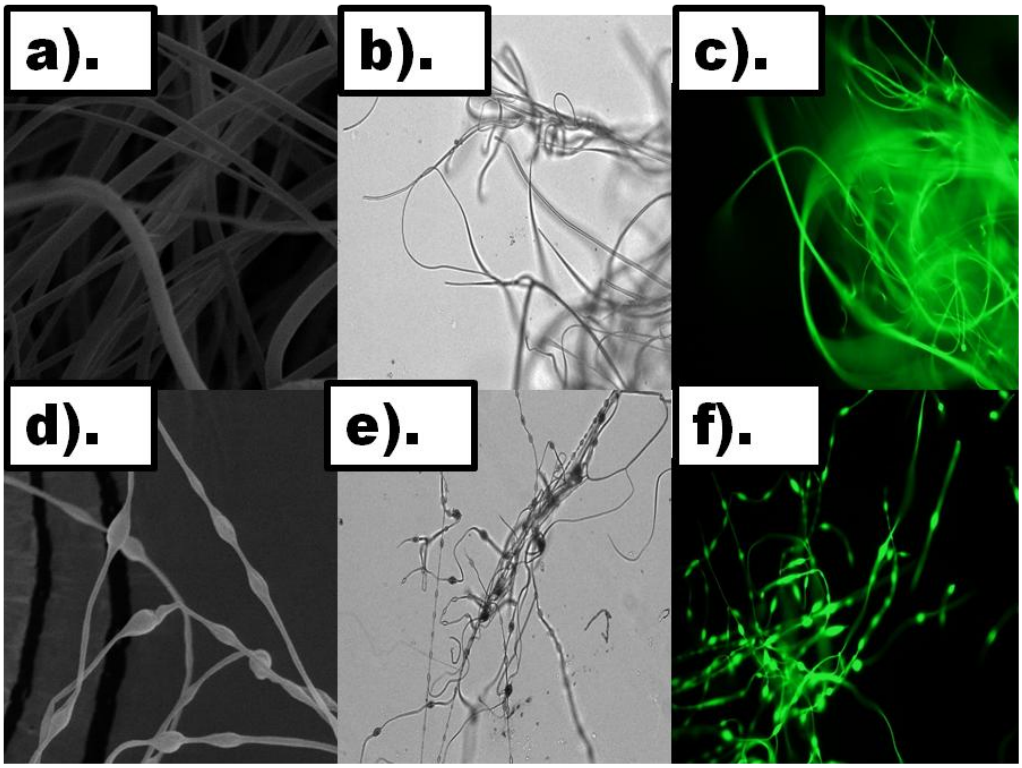

Figure 47: Imaging of BODIPY **(1)**-PS nanofibers (top) and BODIPY **(4)**-PS nanofibers (bottom). a) SEM micrograph of **(1)** embedded nanofibers. b) Bright field illumination of **(1)** embedded nanofibers. c) **(1)** Embedded nanofibers under UV irradiation. d) SEM micrograph of **(4)** embedded nanofibers. e) Bright field illumination of **(4)** embedded nanofibers. f) **(4)** Embedded nanofibers under UV irradiation (480–550 nm, wide filter).

4.1.3 Synthesis and characterization of 2,6-dibrominated BODIPY-PS nanofibers:

Nanofibers containing BODIPY **(2)** and **(5)** are fabricated by adding 2 mg of brominated BODIPY into the respective polymer solutions using the method discussed above. The dibrominated BODIPY-PS nanofibers that were collected are pink and exhibit weak yellow fluorescence when irradiated with UV light **(Figure 46)**. The fluorescence of the **(2)** and **(5)**-PS nanofibers is not as intense as that of their un-brominated forms. Unlike the BODIPY **(4)** nanofibers, **(5)** shows no indications of beading **(Figure 48)**.

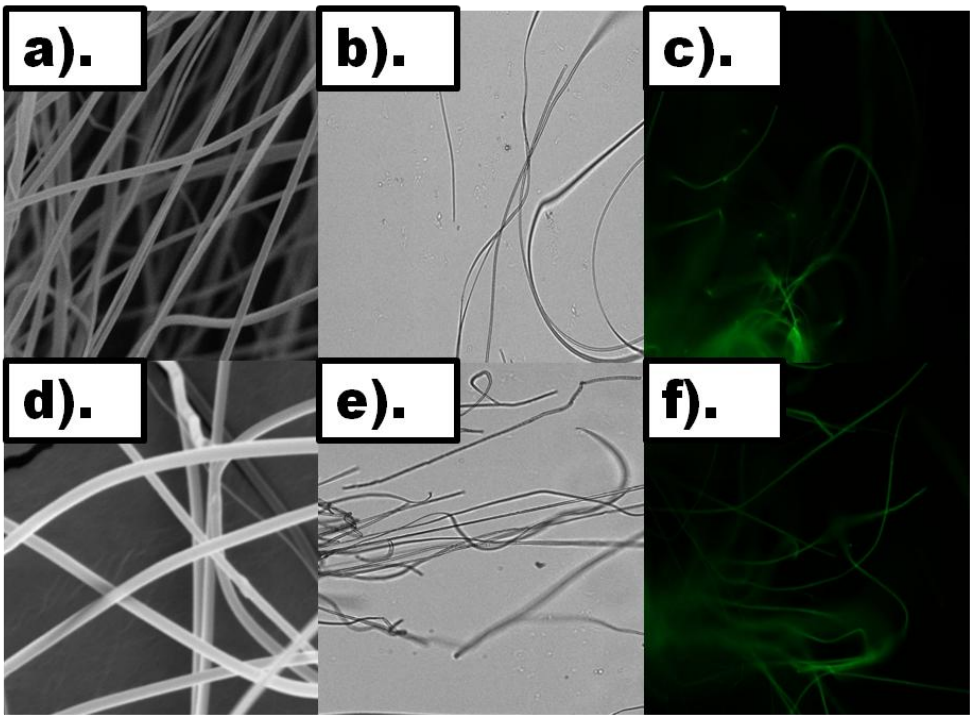

Figure 48: Imaging of BODIPY **(2)**-PS nanofibers (top) and BODIPY **(5)**-PS nanofibers (bottom). a) SEM micrograph of **(2)** embedded nanofibers. b) Bright field illumination of **(2)** embedded nanofibers. c) **(2)** embedded nanofibers under UV irradiation. d) SEM micrograph of **(5)** embedded nanofibers. e) Bright field illumination of **(5)** embedded nanofibers. f) **(5)** Embedded nanofibers under UV irradiation (480–550 nm, wide filter).

Concluding Remarks:

By electrospinning a polymer solution that contained BODIPY dyes it was possible to fabricate highly fluorescent BODIPY embedded polystyrene nanofibers. Polystyrene was chosen due to its many attractive properties and has been successfully used for similar applications involving Pc dyes. The nanofibers that were embedded with BODIPY **(1)** and **(4)** have intense green fluorescence; while the **(2)** and **(5)** embedded nanofibers have weaker yellow fluorescence. To investigate their potential as heterogeneous photocatalysts, 2,6-dibrominated BODIPY embedded nanofibers were irradiated in a solution containing an azo-dye (Tartrazine or Orange-G). It was

expected that the singlet oxygen generated from the brominated BODIPY within the nanofibers should breakdown the azo-dyes in the solution. However, no decease in the concentration of the azo-dyes was observed. This implies that the BODIPY dyes within the nanofibers were unable to generate singlet oxygen, or that the molecular oxygen in the solution could not get close enough to the BODIPY dyes for energy transfer to take place. The singlet oxygen generating capabilities of BODIPY embedded nanofibers clearly requires further in depth research.

Chapter 5:

Synthesis and Spectroscopic Characterisation of Crown Ether-Styryl Substituted BODIPY Dyes

Introduction:

Unsubstituted BODIPYs lack affinity for cations in solution and require ion chelating substituents in order for them to be effective as sensors or molecular switches. Crown ethers have long been known to be effective at chelating various metal cations.[89] To this end 4'-formyl-15-crown-5 was selected for attachment onto the 3,5-positions of the BODIPY core. Several "off-on" fluorescent switches have been developed by appending a crown ether moiety onto a BODIPY dye. However, there are few reports on the effect that these cation complexes have on the photophysical properties of the crown ether-BODIPY dyes, especially with regard to their singlet oxygen generating ability. Four novel crown ether-BODIPY dyes were synthesized from the 2,6-dibrominated analogues of BODIPYs **(1)** and **(4)** using a modified version of the Knoevenagel condensation reaction. The ability of these crown ether-substituted BODIPY dyes to chelate sodium ions, as well as the effects that chelation has on the photophysical properties of these dyes was investigated.

5.1 17-formyl-2,5,8,11,14-pentaoxabicyclo [13.4.0] nonadeca-15,17,19-triene) (4'-formylbenzo-15-crown-5) (7)

5.1.1 Synthesis of 4'-formylbenzo-15-crown-5 (7)

(7) was synthesized according to the method outlined by Castro et al and serves two primary functions **(Scheme 18)**.[117] Firstly, **(7)** is known to preferentially bind to Na^+ ions which allows for the design of a crown ether-substituted styryl-BODIPY as a sensor molecule. Secondly, since the benzo group on **(7)** is aromatic attaching this

molecule to the BODIPY core should extend the aromatic π-conjugation of the BODIPY system resulting in a marked red shift of the main spectral bands.

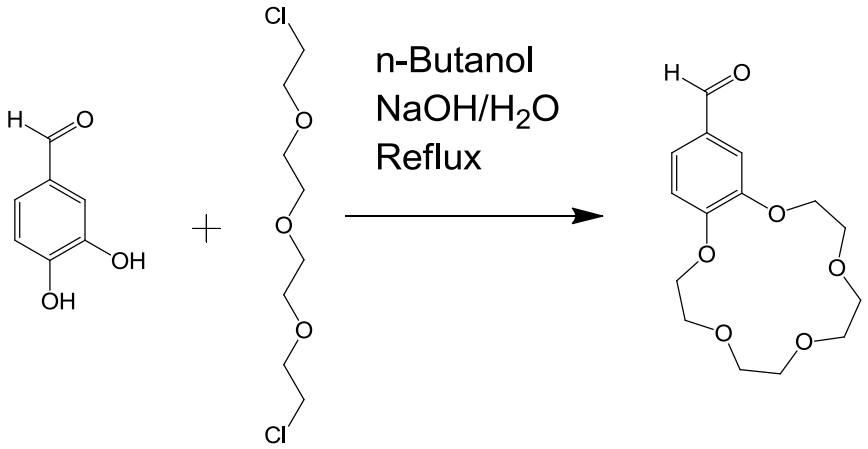

Scheme 18: The ring closure synthesis of 4-formylbenzo-15-crown-5 **(7)**.

A solution of sodium hydroxide was added to a solution of 3,4 dihydroxybenzaldehyde in n-butanol. The benzaldehyde functional group is required to attach the crown ether moiety to BODIPY **(1)**. Both the n-butanol and the reaction vessel were purged with argon to prevent the aldehyde from being oxidized to a carboxylic acid. Diethylene glycol bis (2-chloroethyl) ether is highly reactive, so it was added very slowly using the cannula technique. The reaction vessel was evacuated and filled with argon before refluxing the solution for 36 h. The reaction was quenched with HCl, washed repeatedly with methanol, and vacuum dried until no n-butanol remained. The black residue was then refluxed and recrystallized in n-heptane for 3 h to extract the desired 4'-formylbenzo-15-crown-5 as fine white crystals. A spatula tip of charcoal was added prior to recrystallization to absorb residual n-butanol.

5.1.2 Structural Analysis of 4'-formylbenzo-15-crown-5 (7)

The ^{1}H NMR spectrum of **(7)** contains a single proton singlet at 9.83 ppm which corresponds to the proton of the aldehyde functional group. The two and one proton doublet signals at 7.43–7.45 ppm and 6.93–6.95 ppm, respectively, can be attributed to the protons on the benzene ring. The broad multiplet signal at 4.18–4.22 ppm corresponds to the first four protons on the crown ether ring. The second four protons can be seen as a broad multiplet peak at 3.90–3.95 ppm. The multiplet signal at 3.76–3.77 ppm integrates to eight and can be assigned to the protons on the far end of the crown ether ring. The 4'-formylbenzo-15-crown-5 ^{1}H NMR spectrum matches the spectrum reported in the literature.[117]

The FT-IR spectrum of the 4'-formylbenzo-15-crown-5 almost exactly matches the FT-IR spectrum from Sigma Aldrich.[119] The split peak seen at 2870–2929 cm^{-1} belongs to C–H stretches on the benzene ring and the small peak at 2823 cm^{-1} is attributed to the C–H stretch on the aldehyde. The C=O peak is observed at 1687 cm^{-1}.

White crystals of 4'-formylbenzo-15-crown-5 were obtained after recrystalization in n-heptane. The XRD diffraction pattern shows a low angle (< 50°) and highly crystalline peaks that matches the expected monoclinic crystal structure. SEM imaging confirms the crystalline nature of the crown ether **(Figure 49).**[120]

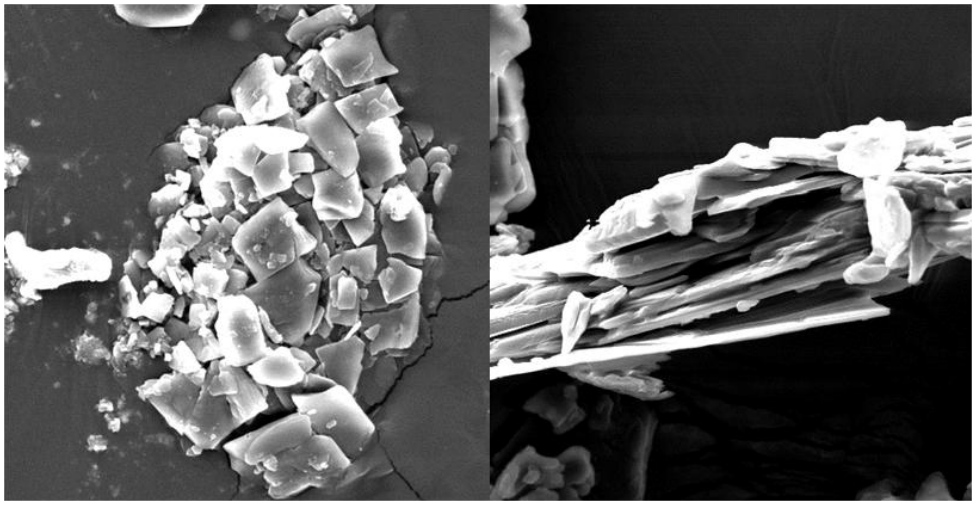

Figure 49: SEM micrograph of 4-formylbenzo-15-crown-5 crystals.

5.1.3 Spectroscopic Properties of 4'-formylbenzo-15-crown-5

4'-Formylbenzo-15-crown-5 has two distinct absorbance peaks at 275 (λ_{max}) and 310 nm **(Figure 50)**. These values are typically of aromatic crown ethers.[89]

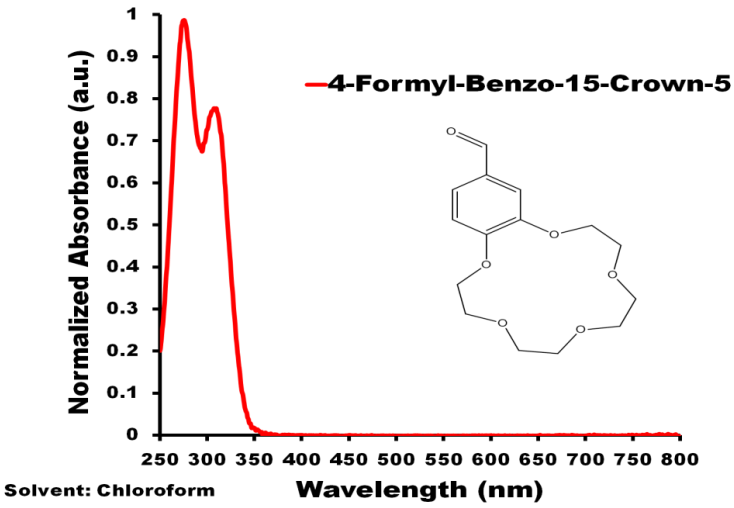

Figure 50: Ground state electronic absorption spectrum of 4-formylbenzo-15-crown-5 in $CHCl_3$.

5.2 4,4'-Difluoro-8-(4-isopropylphenyl)-1,7-dimethyl-2,6-dibromo - 3,5-di-styryl-(4-benzo-15-crown-5)-4-bora-3a,4a-diaza-*s*-indacene (3)

(3) is synthesised using a modified Knoevenagel condensation reaction in order to identify any potential effects that these cation complexes may have on the photophysical properties of the crown ether-BODIPY dyes **(Scheme 1)**. The reaction yielded two distinct fractions, the blue mono-styryl crown ether-BODIPY **(3a)** and the green di-styryl crown ether-BODIPY **(3b)**.

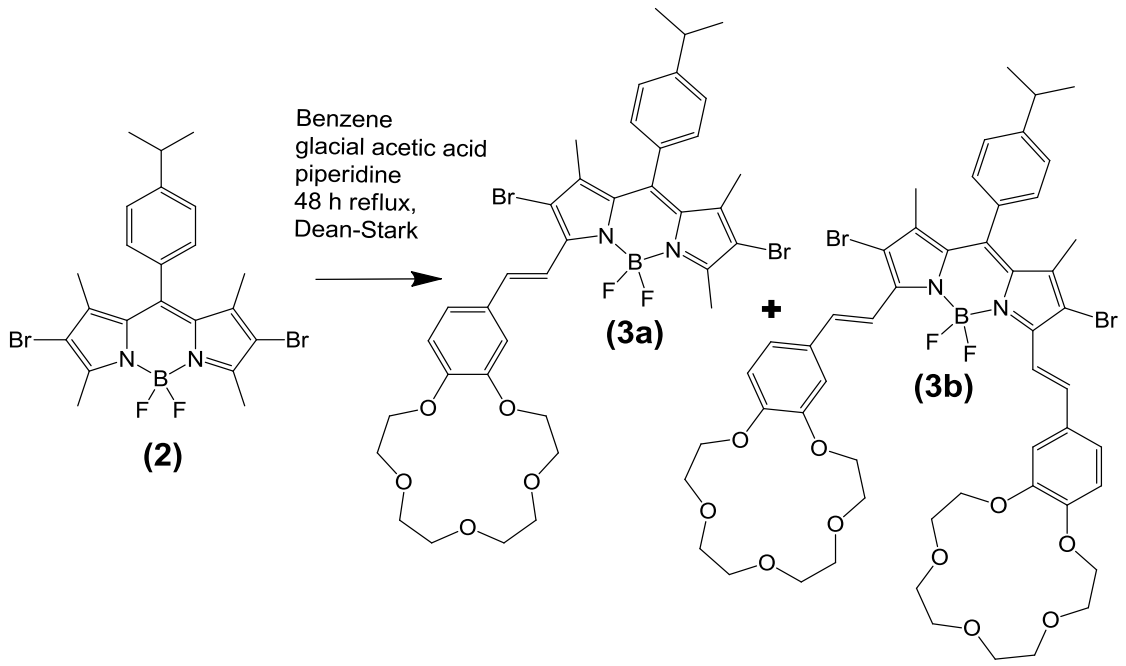

Scheme 19: Knoevenagel condensation of 4'-formylbenzo-15-crown-5 and **(2)** resulting in the synthesis of BODIPY **(3a)** and **(3b)** crown ether-styryl BODIPY dyes.

5.2.1 Synthesis of BODIPY (3)

(2) is dissolved with **(7)** in dry benzene and added with acetic acid to the reaction vessel, which is subsequently evacuated and filled with argon. Water is a by-product of the Knoevenagel condensation reaction and needs to be removed during the reaction so that appreciable yields can be obtained. In order to maximize the removal of water a Dean-Stark trap was used and 4 Å molecular sieves were added into the reaction vessel. Piperidine is added to initiate the condensation reaction and the mixture is refluxed under argon for 48 h. The solution changes colour from orange to deep ink-blue, indicating the formation of mono-styryl-BODIPY. If left for too long the solution begins to turn dark green as more di-styryl-BODIBPY is formed. Therefore, kinetic control of this reaction is essential for maximising its yield of **(3a)**. The reaction is quenched with water and separated by column chromatography to yield **(3a)** ($CHCl_3$:hexane 1:3 (v/v)) and **(3b)** ($CHCl_3$:ethyl acetate 1:1 (v/v)).

Figure 51: BODIPY (3a) displays intense pink emission even under ambient light (left) and BODIPY (3b) (right) under ambient and UV light.

5.2.2 Structural Analysis of BODIPY (3a) and (3b)

*Mono-styryl crown ether-BODIPY **(3a)***

All forty one protons can be identified in the ^{1}H NMR spectrum. Multiplets that lie between 7.07–7.11, 7.29–7.31 and 7.94–7.98 ppm, which integrate to two, four, and one protons respectively can be assigned to the seven phenyl protons (four on the meso phenyl group and the last three on the benzo group of the crown ether). The two proton signal at 4.10–4.18 ppm is assigned to the protons on the styryl bridge between the crown ether and the BODIPY core. The two four proton signals at 3.31–3.33 and 3.46–3.49 ppm, as well as the eight proton double signal at 2.00–2.02 ppm are assigned to the protons on the crown ether ring. The twelve and three proton multiplets at 1.44–1.60 and 1.19–1.35 ppm, respectively, can be assigned to the fifteen methyl protons. The singlet at 2.57 ppm integrates as one proton and can be attributed to the proton on the isopropyl group.

The atomic mass of **(3a)** was determined to be 825.3 amu by MALDI ToF-MS. This differs from the expected value of 802.3 amu by the 23 mass units. This is equivalent to the mass of a single sodium ion, which may have become complexed with the crown ether moiety during synthesis.

FT-IR analysis of **(3a)** shows that the BODIPY skeletal structure remains largely intact as many of the same vibrations from the BODIPY **(1)** core are still observed (see chapter 2). Of particular interest is the appearance of the C-O ester stretch that appears at 1254 cm^{-1} and a large aromatic stretch at 1619 cm^{-1}, which give evidence of a successful bonding between the crown ether moiety and the BODIPY core.

(3a) was purified by column chromatography using a 1:3 (v/v) mixture of $CHCl_3$ and hexane as the eluent to afford a dark blue powder. A solution of **(3a)** is blue in colour and possesses intense pink fluorescence emission **(Figure 51)**.

*Di-styryl crown ether-BODIPY **(3b)***

The multiplets that lie between 7.07–7.13, 7.30–7.32, 7.48–7.60 and 7.94–7.99 ppm, which integrate to two, four, two and two protons respectively, can be assigned to the ten phenyl protons (four on the meso phenyl group and three on each of the crown ether benzo groups). The four proton signal at 4.12–4.16 ppm is assigned to the protons on the styryl bridge between the crown ethers and the BODIPY core. The eight proton multiplet at 3.86–3.87 ppm is assigned to two of the $-CH_2$ groups on each crown ether. The remaining twenty four crown ether protons can be accounted for by the broad signal between 3.57–3.71 ppm. The methyl protons on the BODIPY are identified as the twelve protons signals between 1.19–1.35 ppm. The singlet at 1.98–1.99 ppm integrates as one proton and can be attributed to the proton on the meso–isopropyl group. All fifty nine protons can therefore be identified in the ^1H NMR spectrum of **(3b)**.

Analysis of the mass spectra gave the atomic mass of **(3b)** as 1083 amu (+ $3H^+$).

As with **(3a)**, FT-IR analysis of **(3b)** shows the presence of the C–O ether stretch that appears at 1260 cm^{-1} which provides evidence of a successful bonding between the crown ether moiety and the BODIPY core.

Column chromatography of **(3b)** was carried out using a 1:1 (v/v) mixture of $CHCl_3$ and ethyl acetate to afford a dark green powder. Use of ethyl acetate indicates that the di-

crown ether BODIPY is more polar than the mono-crown ether derivative. This is expected since crowns ethers are known for their ability to enhance amphiphilic character.[93] BODIPY **(3b)** is dark green in solution and has very weak orange fluorescence emission **(Figure 51)**.

5.2.3 Spectroscopic Properties of BODIPY (3a) and (3b)

*Mono-styryl crown ether-BODIPY **(3a)***

The electronic absorption spectrum for **(3a)** is typical of a BODIPY dye spectrum, with the main band maxima at 597 nm in $CHCl_3$ **(Figure 52)**. Appending **(7)** to the 3-position of **(2)** caused the main spectral BODIPY band to shift to the red by approximately 70 nm as is typically observed with when styryl EDGs are added at this position. This red-shift is caused by a destabilization of the HOMO relative to that of the LUMO in such a way as to narrow the HOMO–LUMO band gap. A similar red-shift was also noted for fluorescence emission maxima at 617 nm. A Stokes shift of 543 cm^{-1} is observed for **(3a)**. Absorption by the aromatic crown ether moiety is evident in the weak absorption bands in the 300–400 nm region **(Figure 52)**. BODIPY **(3a)** possesses a high molar extinction coefficient **(Table 6)**. As is evident from **Figure 51 (3a)** has a high quantum yield of 0.57 despite the presence of heavy bromine atoms on the BODIPYs core. The singlet oxygen quantum yield of **(3a)** is determined to be 0.35 in ethanol, which is lower than that of **(2)**. Both of these effects could result from vibrational deactivation of the $S_1 \rightarrow T_1$ state by the crown ether moiety, which would favour higher fluorescence and lower singlet oxygen quantum yields, respectively. **Table 6**

summarizes the photophysical data for **(3a)**. When BODIPY **(3a)** is dissolved in an ethanolic solution containing sodium perchlorate several interesting observations can be made. Firstly, there is a blue-shift (5 nm) and a slight increase in the intensity of the absorption spectrum of the **(3a)** at 588 nm **(Figure 53)**. A blue-shift of 14 nm to 608 nm as well as an increase in the emission intensity is also noted for the emission spectra of **(3a) (Figure 54)**. These effects can be attributed to a stabilization of the BODIPY HOMO orbital and the more rigid structure of the dye structure after chelation with a Na^+ ion.

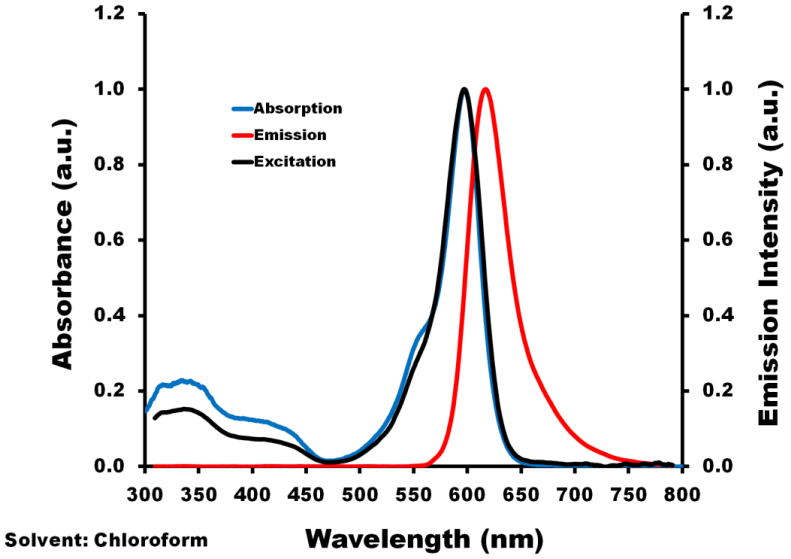

Figure 52: Normalized bands for absorption at 597 nm (blue), emission at 617 nm (red) and excitation at 597 nm (black) in the spectra for BODIPY **(3a)** in $CHCl_3$.

No changes are observed in either spectrum when BODIPY **(2)** is dissolved in the same sodium perchlorate solution. This implies that the effects observed for **(3a)** are indeed caused by the crown-BODIPY interacting with the Na^+ ions in the solution. There is an increase in the singlet oxygen quantum yield from 0.35 to 0.42 for **(3a)** when Na^+ ions are present in the solution **(Figure 55)**. In proof of principle terms, this implies that

(3a), and perhaps more complex crown ether-BODIPY dyes, could be useful as an ion sensors.

Table 6: Photophysical data for mono-styryl crown ether-BODIPY **(3a)**.

Solvent	Absorbance (nm)	Emission (nm)	Excitation (nm)	Log ε (M^{-1} cm^{-1})	Φ_F	τ_F (ns)	Stokes Shift (cm^{-1})	Φ_Δ
Chloroform	597	617	597	4.41	0.57	4.2*	543	---
Ethanol	593	622	---	---	---	---	786	0.35
Ethanol (with Na^+)	588	608	---	---	---	---	559	0.42

*Main component of the biexponential fit.

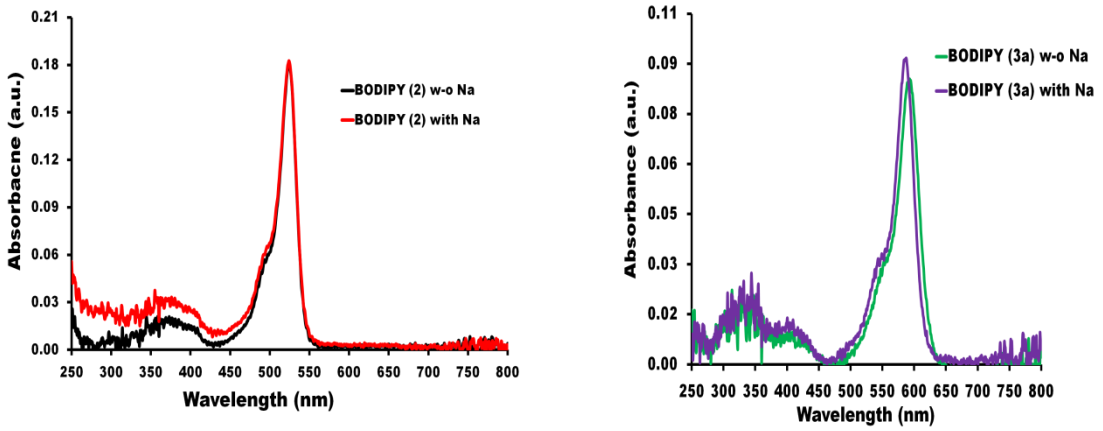

Figure 53: Ground state absorption of BODIPY **(3a)** (right) in the absence and presence of Na^+ in ethanol. BODIPY **(2)** (left) was used as the negative control. Sodium perchlorate was used as the source of Na^+ ions.

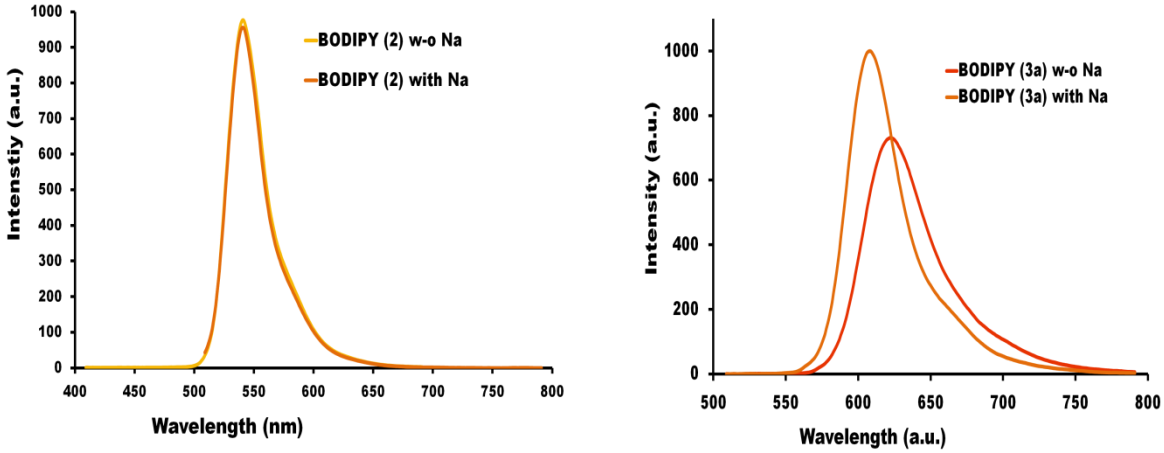

Figure 54: Fluorescence emission spectra for BODIPY **(3a)** (right) in the presence of Na^+ in ethanol. BODIPY **(2)** (left) was used as the negative control. Sodium perchlorate was used as the source of Na^+ ions.

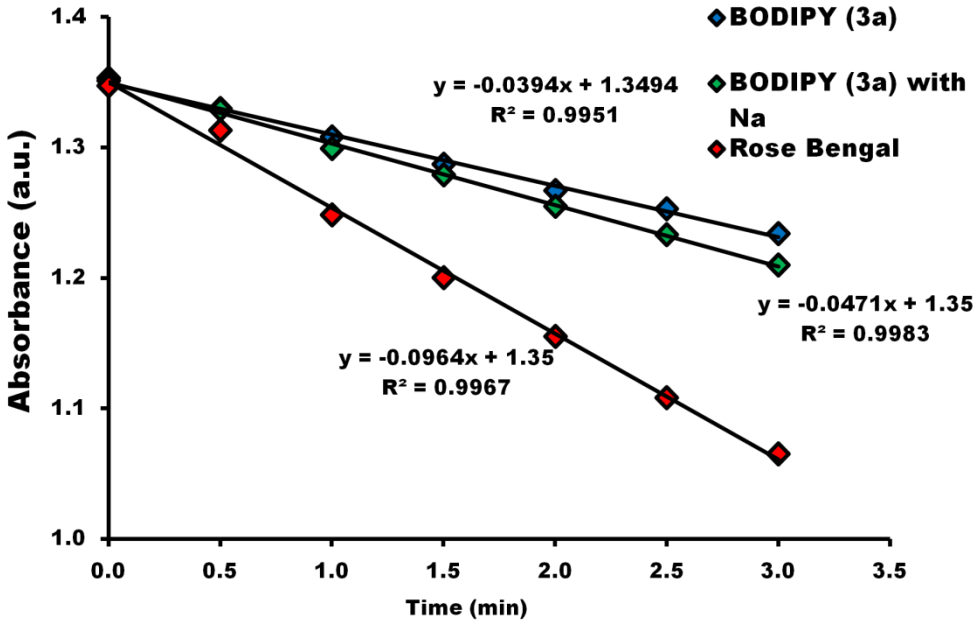

Figure 55: Photocatalytic degradation of DPBF in ethanol by $^1O_2$ generated from Rose Bengal std (red), BODIPY **(3a)** (blue), and **(3a)** in the presence of Na^+ (green). Irradiation at 568 nm in intervals of 30 s.

*Di-styryl crown ether-BODIPY **(3b)***

The electronic absorption spectrum for BODIPY **(3b)** has a number of noteworthy features. The main electronic absorption band lies appears at 670 nm in chloroform **(Figure 56)**. Appending the second crown ether to the 5-position of the BODIPY dye causes the main spectral band to red-shift by a further ca. 70 nm when compared to that of **(3a)** for a total red-shift of 140 nm compared to **(2)**. There is an enhancement of the aromatic crown-ether absorption band in the 300–400 nm region. Unlike the previous BODIPY dyes, the high energy shoulder of **(3b)** at 614 nm is significantly more intense. Another small absorption band appears at around 535 nm and while this is not observed in the spectrum of **(3a)** it may be masked by the main spectral band. The excitation and emission spectra at 672 nm and 696 nm, respectively, for **(3b)** are mirror images. A single emission peak (at 696 nm) was observed even when the

excitation wavelength was adjusted to that of the secondary peaks as would be anticipated based on Kasha's rule. The Φ_F value for **(3b)** is lowered to 0.36 which is to be expected as the styryl bond is flexible and promotes non-radiative fluorescence decay pathways to that seen of **(3a)**. The photophysical data for BODIPY **(3b)** is summarized in **Table 7.**

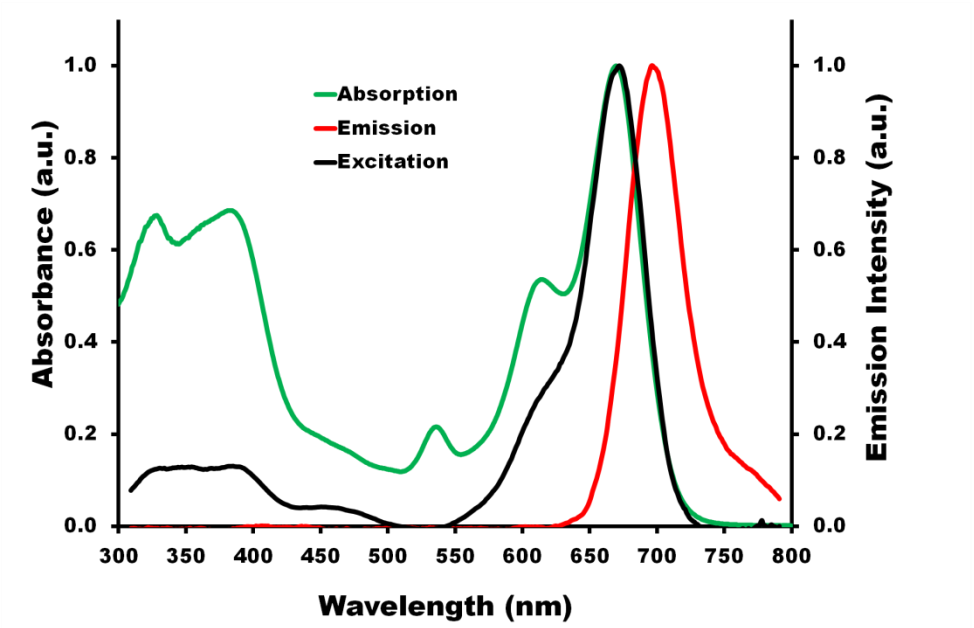

Figure 56: Normalized bands for absorption at 670 nm (green), emission at 696 nm (red) and excitation at 672 nm (black) spectra of BODIPY **(3b)** in $CHCl_3$.

Table 7: Photophysical data for di-styryl crown ether-BODIPY **(3b)**.

Solvent	Absorbance (nm)	Emission (nm)	Excitation (nm)	Log ε (M^{-1} cm^{-1})	Φ_F	τ_F (ns)	Stokes Shift (cm^{-1})	Φ_Δ
Chloroform	670 (614) (535)	696	672	4.53 (4.26) (3.85)	0.36	4.2*	558	---
Ethanol	667	699	---	---	---	---	686	0.28
Ethanol (with Na^+)	656	679	---	---	---	---	516	0.41

*Main component of a biexponential fit.

The singlet oxygen quantum yield of **(3b)** is 0.28 in ethanol and undergoes a 13% increase; to nearly double that of **(3a)** (implying a ca. 7% increase per complexed ion with the addition of Na^+ ions to the solution), to 0.41. As before, both the absorption

and emission bands for **(3b)** undergo a blue-shift (11 and 20nm, respectively) and their intensities increase after complexation of sodium. In this case, there is a doubling of the emission intensity. It is interesting to note that the blue-shift in absorption band maximum that is induced by complexation of **(3b)** with two sodium ions (11 nm) is approximately double that of **(3a)** (5 nm) which implies that there is a 5 nm blue-shift per complexed cation. This strategy could prove useful for improving singlet oxygen generation in high sodium environments, such as in polluted river water or even cancerous tissue.

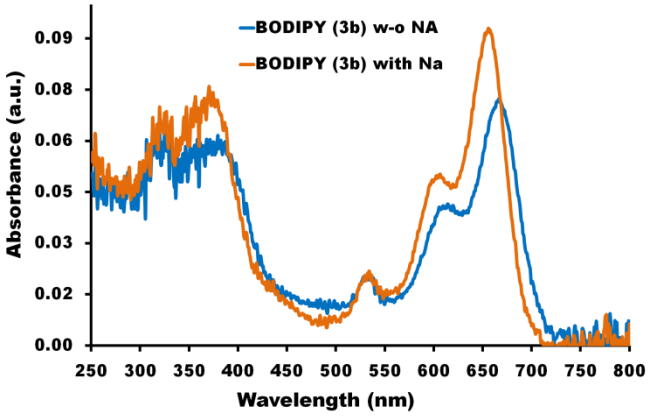

Figure 57: Absorption spectra of BODIPY **(3b)** in the absence (blue) and in the presence of Na^+ (orange) in ethanol. Sodium perchlorate was used as the source of Na^+ ions.

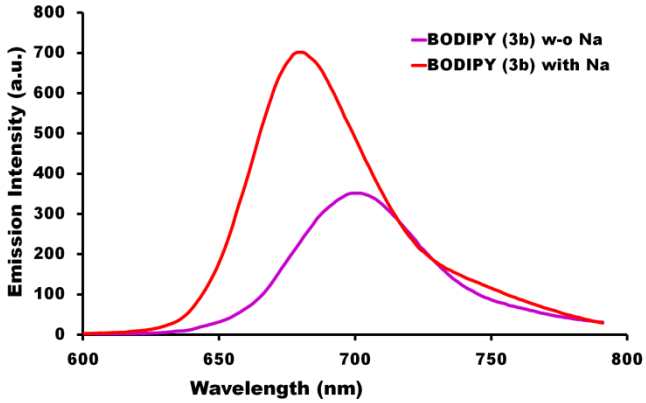

Figure 58: Fluorescence emission spectra for BODIPY **(3b)** in the presence and absence of Na^+ ions in ethanol. Sodium perchlorate was used as the source of Na^+ ions.

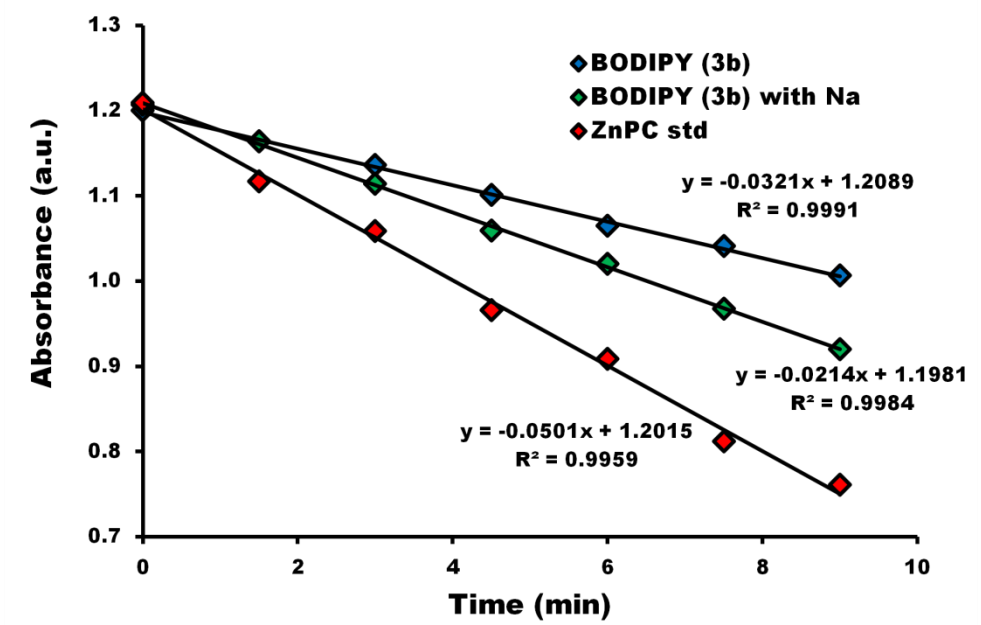

Figure 59: Photocatalytic degradation of DPBF in DMSO by $^1O_2$ generated from ZnPc std (red), BODIPY **(3b)** (blue), and **(3b)** in the presence of Na^+ (green). Irradiation at 667 nm in intervals of 1 min.

5.3 4,4'-Difluoro-8-(4-dimehtylamino)-1,7-dimethyl-2,6-dibromo - 3,5-di-styryl-(4-benzo-15-crown-5)-4-bora-3a,4a-diaza-*s*-indacene (6)

5.3.1 Synthesis of BODIPY (6)

(6a) and **(6b)** were synthesized using the same Knoevenagel condensation reaction method that was used for the synthesis of **(3)**, the only difference being the use of **(5)** as the BODIPY core **(Scheme 20)**. A microwave assisted synthesis method was tested for the preparation of **(6)** in order to improve the reaction time and yield, but this proved unsuccessful. Both the blue mono-substituted crown ether-BODIPY **(6a)** and the green di-substituted crown ether-BODIPY **(6b)** were isolated from the same reaction as two distinct fractions using the same solvent system as for **(3)** **(Figure 60)**.

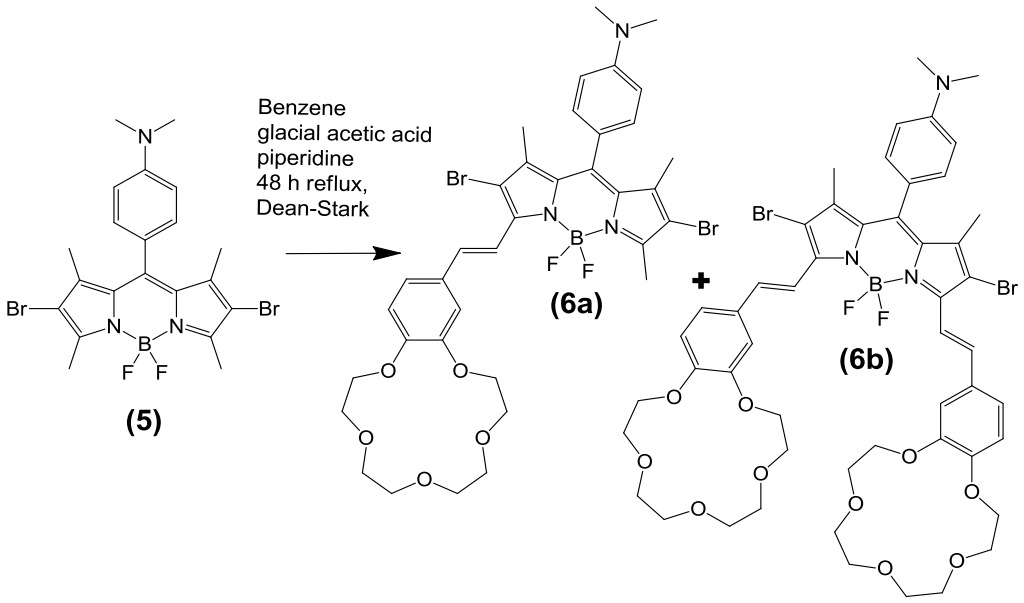

Scheme 20: Knoevenagel condensation of 4-formylbenzo-15-crown-5 and **(2)** resulting in the synthesis of **(6a)** and **(6b)** crown ether-styryl BODIPY dyes.

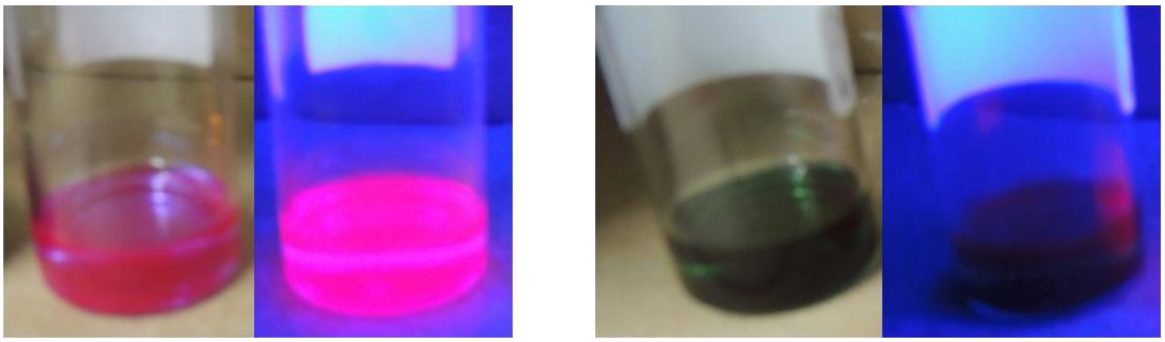

Figure 60: BODIPY **(6a)** is blue in colour and exhibits with bright pink emission even under ambient light (left) and **(6b)** (right) under ambient and UV light.

5.3.2 Structural Analysis of BODIPY (6a) and (6b)

*Mono-styryl crown ether-BODIPY **(6a)***

All forty of protons from the structure of BODIPY **(6a)** can be identified in the ^{1}H NMR spectrum. As before, the seven phenyl protons can be assigned to the multiplet signals seen between 7.07–7.15, 7.41–7.46 and 7.95–7.99 ppm, which integrate to four, two, and one protons respectively. The two proton signal at 4.11–4.17 ppm is

assigned to the protons on styryl bridge between the crown ether and the BODIPY core. The two four proton signals at 3.30–3.33 and 4.46–4.49 ppm, as well as the eight proton signal at 2.01 ppm are assigned to the protons on the crown ether ring. The three and twelve proton signals at 1.36 and 1.18 ppm, respectively, can be assigned to the fifteen methyl protons.

The FT-IR spectrum of BODIPY **(6a)** is very similar to that of **(3a)**, and includes the 1266 cm^{-1} C-O ether stretch and the 1619 cm^{-1} aromatic stretch.

The atomic mass of **(6a)** is found using MADLI ToF mass spectrometry to be 804.9 amu which is in close agreement (+ $1H^{+}$) with the expected value of 803.34 amu.

*Di-styryl crown ether-BODIPY **(6b)***

The multiplets that lie between 6.81–6.83, 7.07–7.10, 7.43–7.51, and 7.95–8.00 ppm, which integrate to two, four, two and two protons respectively, can be assigned to the ten phenyl protons (four on the meso phenyl group and three on the benzo group of each crown ether unit). The four proton signal at 4.12–4.15 ppm is assigned to the protons on styryl bridge between the crown ethers and the BODIPY core. The eight proton multiplet at 3.85–3.87 ppm and the broad twenty four proton signal at 3.70 ppm are assigned to the protons on the crown ether units. Two six proton signals at 1.36 and 1.44 ppm are assigned to the remaining twelve methyl protons, and thus all fifty eight protons are therefore identified in the ^{1}H NMR spectrum of **(6b)**.

The FT-IR spectrum for **(6b)** shows the typical bands of an intact BODIPY core as well as the bands expected from the crown ether moiety.

The atomic mass of the primary **(6b)** fragment is found to be 1083.4 amu, within two amu (+ $2H^+$) of the expected value of 1081.64 amu.

5.3.3 Spectroscopic Properties of BODIPY (6a) and (6b)

*Mono-styryl crown ether-BODIPY **(6a)***

The ground state electronic absorption spectrum for **(6a)** shared the same spectral features as **(3a)**. The absorption maxima for **(6a)** at 602 nm (in $CHCl_3$) is red-shifted by ca. 70 nm when compared to BODIPY **(5)** and slightly red-shifted (by 5 nm) than its **(3a)** counterpart. This gives further evidence that this spectrum is typical of mono-styryl crown ether substituted BODIPY dyes. A Stokes shift of 662 cm^{-1} gives rise to a fluorescence emission maximum at 627 nm for **(6a)**. With a Φ_F value of 0.27, **(6a)** is 30% less fluorescent than **(3a)**. This is due to competition between the PET process of the amino nitrogen, and the flexibility of the crown-ether moiety, which both serve to deactivate the fluorescent state. Addition of TFA to the solution of **(6a)** assists in reducing the PET effects by protonating the amino nitrogen that is at the para-position of the meso-phenyl substituent of the BODIPY dye. **Table 8** summarizes the photophysical data for **(6a)**.

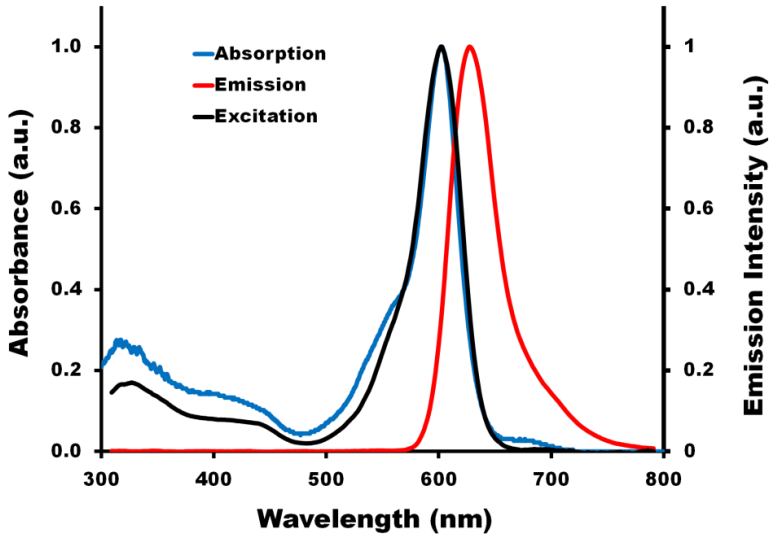

Figure 61: Normalized bands for absorption at 602 nm (blue), emission at 627 nm(red) and excitation at 603 nm (black) in the spectra for BODIPY **(6a)** in $CHCl_3$.

Table 8: Photophysical data for mono-styryl crown ether-BODIPY (6a).

Solvent	Abs (nm)	Em (nm)	Ex (nm)	Log ε (M^{-1} cm^{-1})	Φ_F	τ_F (ns)	Stokes Shift (cm^{-1})	Φ_Δ
Chloroform	602	627	603	4.41	0.27	3.7*	662	---
Ethanol	597	630	---	---	---	---	877	0.45
Ethanol (with TFA)	597	630	---	---	---	---	877	---
Ethanol (with Na^+)	590	615	---	---	---	---	689	0.52
Ethanol (with Na^+ and TFA)	592	618	---	---	---	---	711	0.58

*Main component of the biexponential fit.

Addition of Na^+ to the solution causes the absorption and the emission spectrum maxima of **(6a)** to undergo a blue-shift of 7 nm and 15 nm, respectively. This is coupled by an increase in the absorption intensity of the dye. The increase in absorption and emission intensity is also noted with the addition of TFA; however, TFA alone does not cause a shift in the wavelength maxima as the amino nitrogen is disconnected from the π-system of the BODIPY core. There is a larger blue-shift of the band maximum and an increase in intensity when both sodium and TFA are added to

the solution. **(5)** was used as the control for studying the effects that sodium has on **(6a)**.

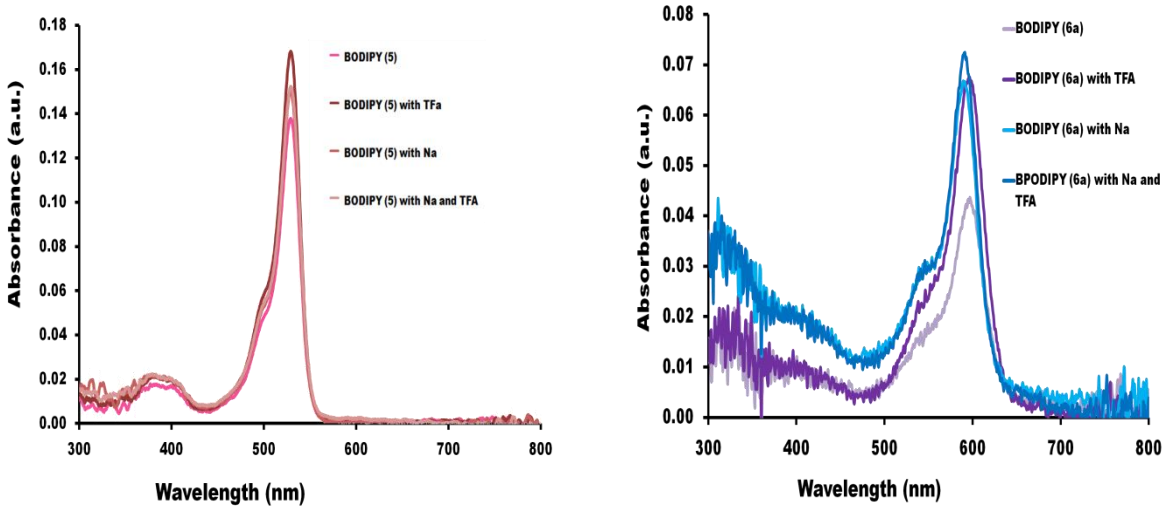

Figure 62: The absorption spectra of BODIPY **(6a)** (right) in the absence and presence of Na^+ and TFA in ethanol. BODIPY **(5)** (left) was used as the negative control. Sodium perchlorate was used as the source of Na^+ ions.

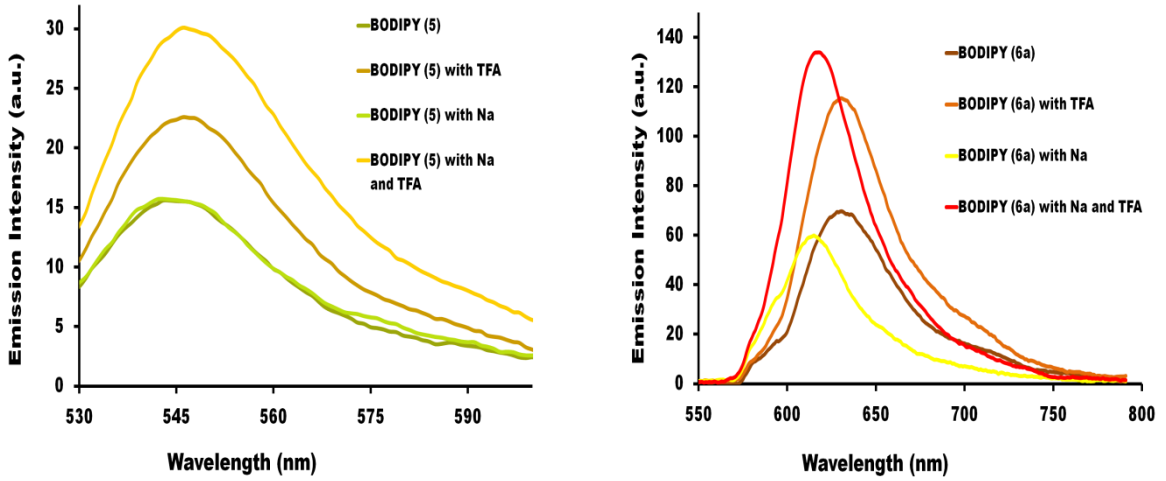

Figure 63: Fluorescence emission spectra for BODIPY **(6a)** (right) in the presence of Na^+ and TFA in ethanol. BODIPY **(5)** (left) was used as the negative control. Sodium perchlorate was used as the source of Na^+ ions.

Adding TFA to BODIPY **(5)** causes an increase in intensity of the absorption and emission intensity, but has no effect on the wavelengths of the band maxima. Any change of wavelength is therefore due to the interaction between Na^+ ions and the

crown-ether moiety. Interestingly Na^+ has a similar effect on the photophysical properties of BODIPY **(5)**, although to a lesser extent. One possibility is that the Na^+ ions are reducing the PET effect by interacting with the lone pair of electrons on the amino nitrogen. **(6a)** has a Φ_Δ value of 0.45 in ethanol, which increases by 7% to 0.52 with the addition of sodium ions to the solution. A further 6% (Φ_Δ value of 0.58) increase is observed once TFA is added to the solution.

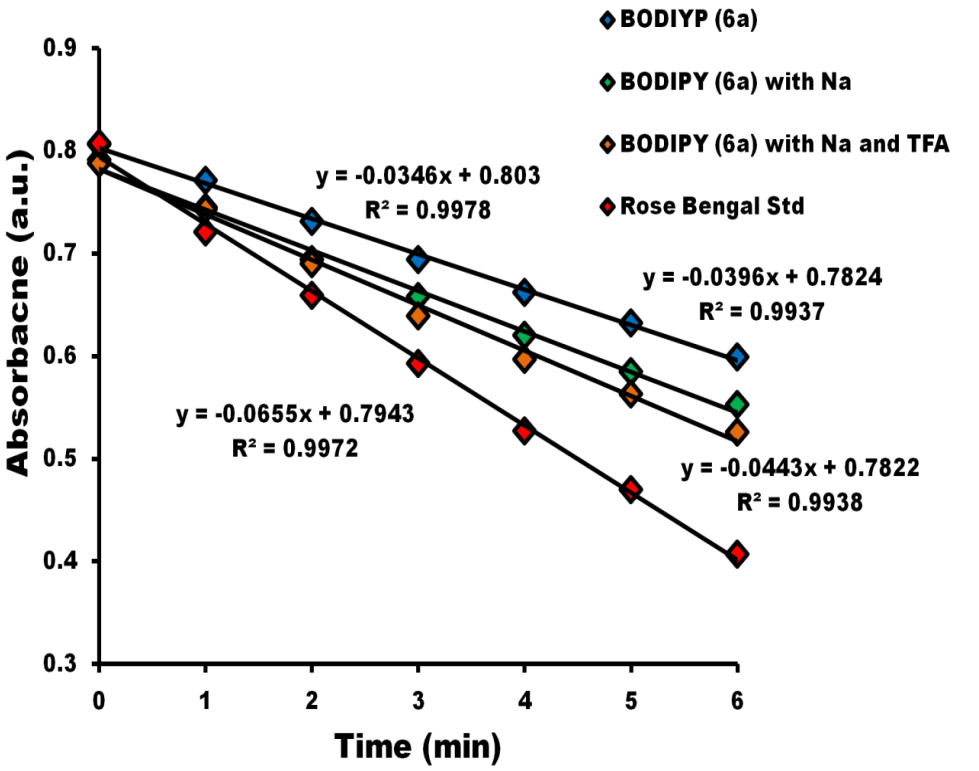

Figure 64: Photocatalytic degradation of DPBF in ethanol by $^1O_2$ generated from Rose Bengal (red), BODIPY **(6a)** (blue), **(6a)** in the presence of Na^+ (green) and **(6a)** in the presence of Na^+ and TFA (orange). Irradiation at 570 nm in intervals of 1 min.

*Di-styryl crown ether-BODIPY **(6b)***

The absorption maxima for BODIPY **(6b)** lies at 676 nm in $CHCl_3$ with a shoulder of intensity on the high energy side of the band at 622 nm **(Table 9)**. The red-shifts seen for the main spectral bands of **(6b)** are consistent with those observed for **(3b)**. One

major difference between the spectra of **(6b)** and **(3b)** is the absence of the small peak at 535 nm. Absorption bands associated with the crown ether ring can be seen in the 300–400 nm region. The main spectral band in the emission spectrum for **(6b)** at 706 nm has a Stokes shift of 629 cm^{-1} compared to the absorption spectra. The Φ_F value for **(6b)** is 0.19 due to the combined quenching effects of the two crown ether-styryl groups and PET effects.

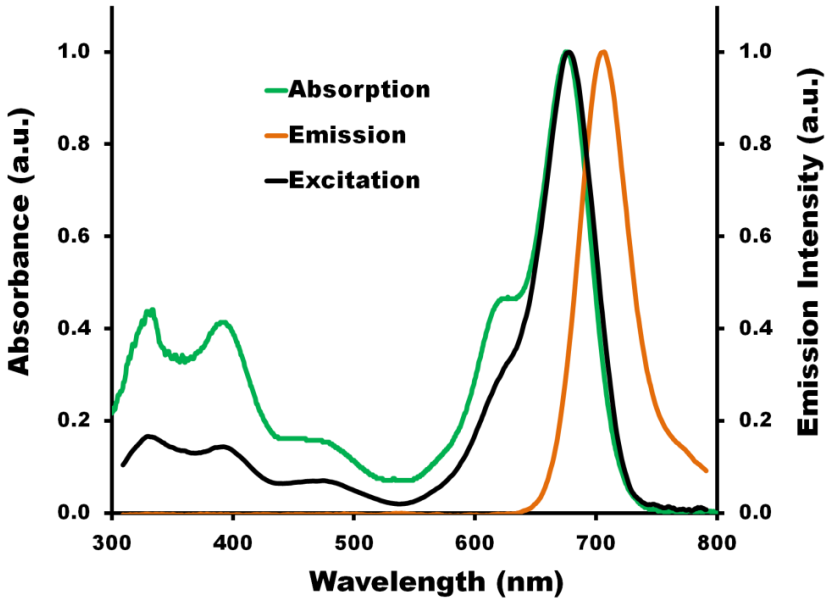

Figure 65: Normalized bands for absorption at 676 nm (green), emission at 706 nm (orange) and excitation at 678 nm (black) in the spectra for BODIPY **(6b)** in $CHCl_3$.

Table 9: Photophysical data for di-styryl crown ether-BODIPY BODIPY **(6b)**.

Solvent	Abs (nm)	Em (nm)	Ex (nm)	Log ε (M^{-1} cm^{-1})	Φ_F	τ_F (ns)	Stokes Shift (cm^{-1})	Φ_Δ
Chloroform	676	706	678	4.86	0.19	4.3*	629	---
Ethanol	673	708	---	---	---	---	735	0.39
Ethanol (with TFA)	676	706	---	---	---	---	629	---
Ethanol (with Na^+)	658	688	---	---	---	---	663	0.29
Ethanol (with Na^+ and TFA)	660	693	---	---	---	---	722	---

*Main component of a biexponential fit.

The addition of TFA causes the maximum absorption band to red-shift by 3 nm, but does not alter the wavelength maximum of the emission spectrum. The addition of sodium ions, however, causes the main spectral bands in the absorption and emission spectra of **(6b)** to blue-shift by 18 nm to 658 and 688 nm, respectively. In this case, there is a slight decrease in the intensity of both bands after complexation with sodium. As before, blue-shifts of the main spectral bands are only observed after the addition of Na^+ ions to the solution.

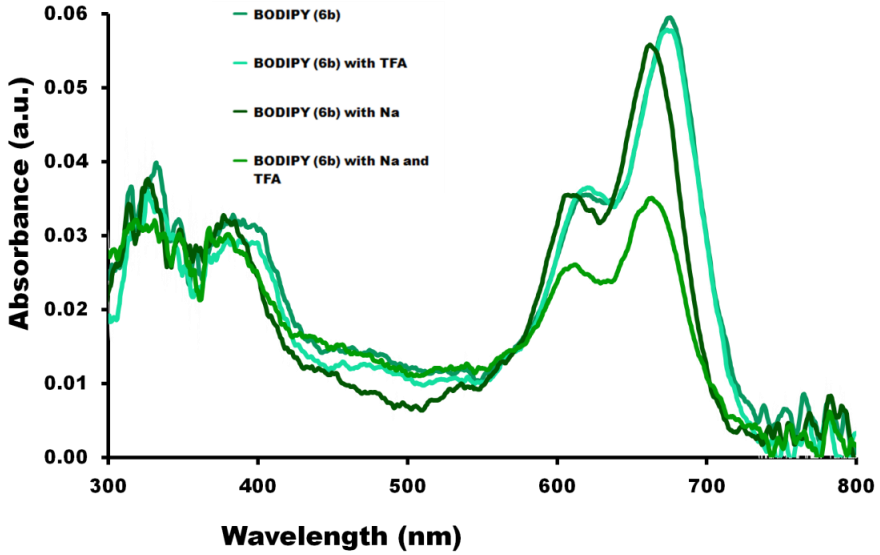

Figure 66: The absorption spectra of BODIPY **(6b)** in the absence and presence of Na^+ and TFA in ethanol. Sodium perchlorate was used as the source of Na^+ ions.

The Φ_Δ value of 0.29 for **(6b)** in the presence of sodium is 10% less than that of **(6b)** when no sodium was present.

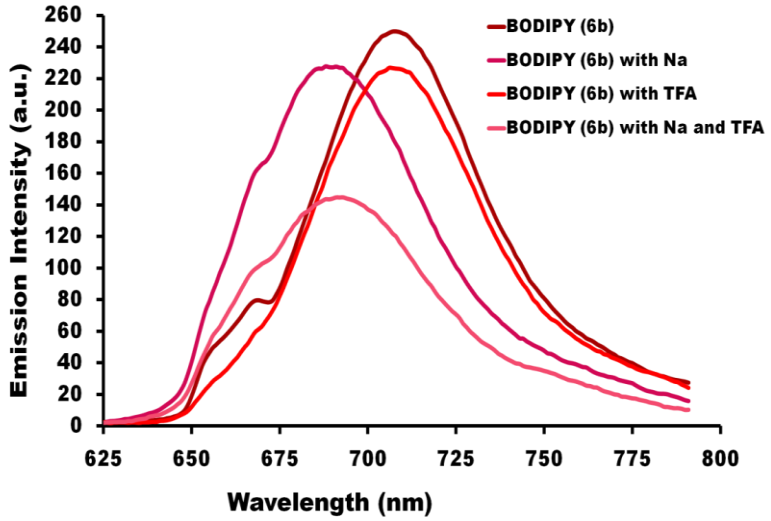

Figure 67: Fluorescence emission spectra for BODIPY **(6b)** in the presence of Na^+ and TFA in ethanol. Sodium perchlorate was used as the source of Na^+ ions.

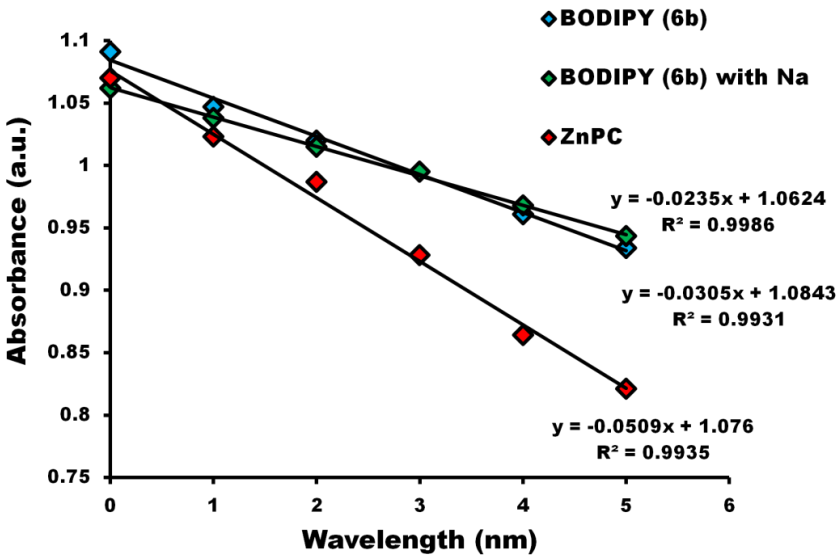

Figure 68: Photocatalytic degradation of DPBF in DMSO by $^1O_2$ generated from ZnPc (red), BODIPY **(6b)** (blue), and **(6b)** in the presence of Na^+ (green). Irradiation at 663 nm in intervals of 1 min.

Concluding remarks:

4'-Formylbenzo-15-crown-5 was successfully synthesized and fully characterized.

Four novel crown ether-BODIPY dyes (mono- and di-styryl analogues of both BODIPY **(2)** and **(5)**) were synthesized from 4'-formylbenzo-15-crown-5 using a modified version of the Knoevenagel condensation reaction. The crown ether moieties were attached via styryl bonds at the 3 or 5-position of the BODIPY core and this has several significant effects on the photophysical properties of the BODIPY dyes. The main band maxima in the crown ether-BODIPY absorption and emission spectra undergo a red-shift of approximately 70 nm for each styryl group that is attached to the BODIPY core. Sodium ions have no effect on the electronic spectra of BODIPYs that lack a crown ether moiety, but can cause the absorption and emission spectra for crown ether-BODIPY dyes to blue-shift and become slightly more intense. The addition of the flexible crown ether groups to the BOIDPY core causes a decrease in fluorescence quantum yield as well as a decrease in singlet oxygen quantum yield. The singlet oxygen quantum yields are lower for the crown ether-BOIDPYs than for the dibrominated BODIPYs, but can be improved slightly when the crown ether moieties complex sodium ions. These effects are approximately doubled when a di-styryl crown ether-BODIPY complexes with a second sodium ion.

Chapter 6:

Molecular Modelling of BODIPY Dyes

6.1 Geometry Optimizations and TD-DFT calculations

The density functional theory (DFT) method was used to carry out geometry optimizations with the Becke, three-parameter, Lee-Yang-Parr (B3LYP) functional of the Gaussian09 program package, and SDD basis sets The SDD basis set is the Gaussian09 default basis set. While it is not particularly well suited to handling a specific range of atoms it offers reasonable approximations for all atoms, including the heavy bromine and iodine atoms that were used in this study. The calculations were performed at the Centre for High Performance Computing (CHPC).[115] While the B3LYP functional has been used extensively for structural analysis it has a tendency to greatly underestimate long-range charge transfer excitation, which are frequently encountered with BODIPY dyes.[57,119] TD-DFT calculations were carried out on the B3LYP optimized geometries using the Coulomb-attenuated B3LYP (CAM-B3LYP) functional in order to determine the electronic absorption properties of selected BODIPY dyes. The CAM-B3LYP functional is better suited to handling transitions with charge transfer character as it combines elements of the hybrid B3LYP functional with increasing fractions of Hartree-Fock (HF) exchange parameters, resulting in a functional with improved long-range capabilities.[121] This proved to be sufficiently accurate for the determination of the main spectral trends and structural property relationships of a series of structurally related BODIPY dyes.

6.1.1 Molecular Modelling for BODIPY dyes: (1), (2), (4), (5)

The TD-DFT calculations predict that the lowest lying $S_0 \rightarrow S_1$ transition is almost entirely associated with the HOMO → LUMO one-electron transition **(Table 10)**. BODIPYs possess C_{2v} symmetry as a result of the rigid plane conformation adopted by the dipyrromethane ligand after complexation with a boron atom **(Figure 69)**. This results in HOMO and LUMO MOs that are well separated from other MOs as seen in **Figure 70**. Changing the para-substituent at the meso-phenyl of the BODIPY appears to cause no change in the HOMO–LUMO band gap of the BODIPY MOs which is consistent with experimental observations. This can be rationalized as the meso-phenyl substituent is forced out of plane by the methyl groups at the 1,7-positions, which results in a poor conjugation with the BODIPYs π-system. The nodal patterns of HOMO−1 for BODIPYs **(4)** and **(5)** are similar to those of the HOMO of the other BODIPY dyes. The calculations for BODIPY **(4)** predict that the HOMO and HOMO−1 MOs are near degenerate, and that the main transition occurs between the HOMO−1 and LUMO orbitals **(Figure 70)**. This suggests that an intermolecular charge transfer (ICT) process can occur between the electron donating amino nitrogen atom and the BODIPY core, which would quench the fluorescence. This explains the low fluorescence quantum yield observed for BODIPY **(4)**. There is a marked lifting of degeneracy of the HOMO MOs upon protonation of the para-substituent of BODIPY **(4)** and a restoration of the HOMO–LUMO main transition. In this case, the lone pair of electrons on the amino nitrogen atom are no longer able to undergo ICT and cannot quench the BODIPYs fluorescence. This also explains the “off-on” effect observed in

the fluorescence with the protonation of BODIPY **(4) (Figure 40)**. The same effect is also observed in the calculations for BODPY **(5)**.

A red-shift of the main band maxima in the electronic absorption and emission spectra of BODIPY dyes is observed when a structural alterations change the energies of the two frontier orbitals in such a way that there is a narrowing of the HOMO−LUMO band gap. When bromine atoms are added at the 2,6-positions they cause a destabilization of the HOMO orbital relative to the LUMO orbital. This causes a narrowing of the HOMO−LUMO gap and results in the ca 30 nm red-shift observed in the electronic absorption and emission spectra for the brominated BODIPY dyes. This occurs as the LUMO possesses a nodal plane at the 2,6-position, while there is MO coefficient at these positions in the HOMO.

The calculations for the 2,6-dibrominated BODIPYs indicate the presence of a second less intense absorption band that is blue-shifted compared to the main absorption band. This HOMO−2 → LUMO one-electron transition can be observed in the experimental spectra of the dibrominated BODIPY in the 320–420 nm region **(Figure 73)**.

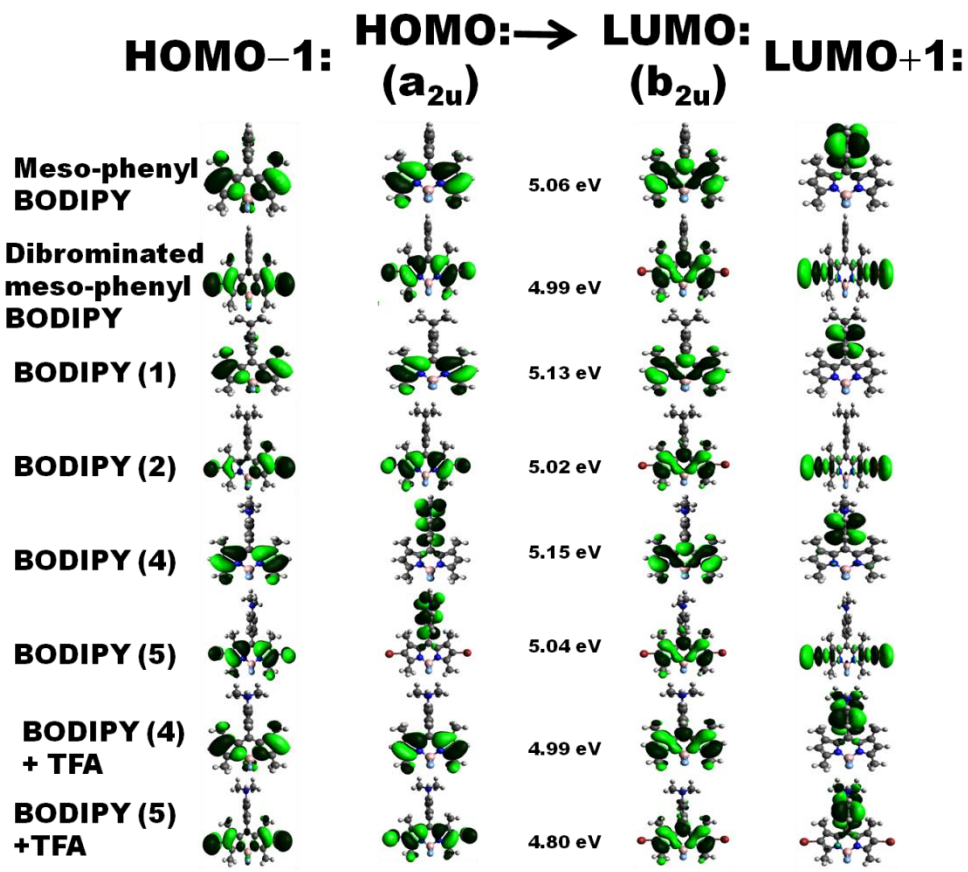

Figure 69: Nodal patterns and MO energies of the four frontier π-MO for meso-substituted BODIPYs **(1)** and **(4)** and their 2,6-dibrominated analogues **(2)** and **(5)**. MO energies of selected BODIPY dyes at an isosurface value of 0.04 a.u. HOMO-LUMO gap energies are highlighted for the main electronic transition ($a_{2u} \rightarrow b_{2u}$). The positions and relative magnitudes of MO coefficients can provide insight into the effects of structural changes on the photophysical properties of studied BODIPY dyes.

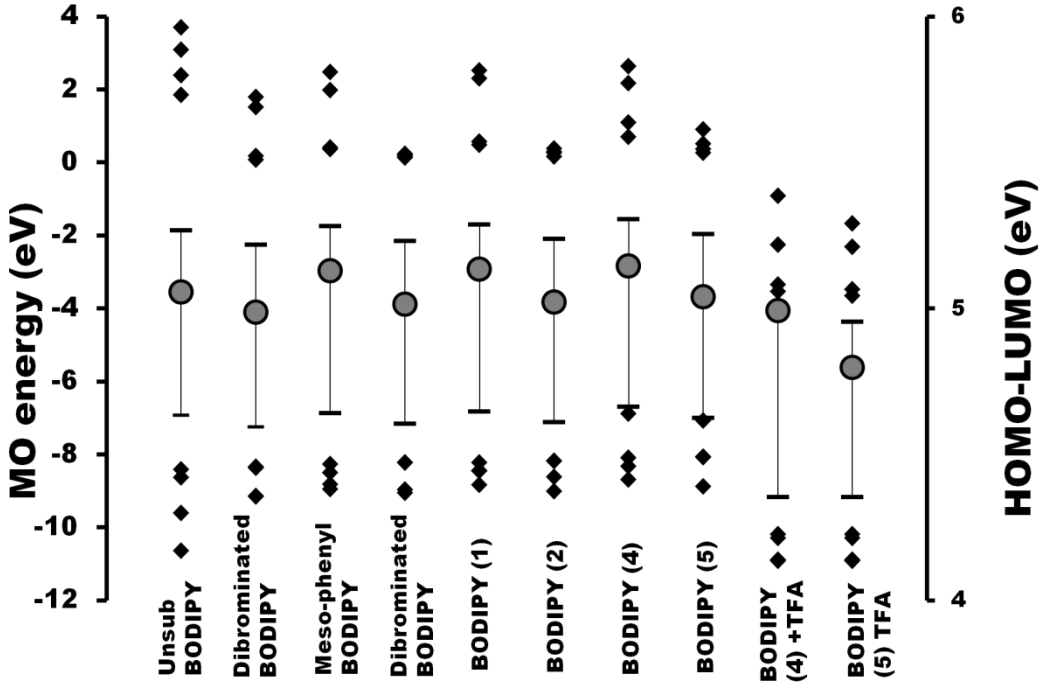

Figure 70: The frontier MO energies and HOMO-LUMO gaps for of meso-substituted BODIPYs **(1)** and **(4)** and their 2,6-dibrominated analogues **(2)** and **(5)** using the CAM-B3LYP functional with SDD basis sets. Dashes represent the HOMO and LUMO MO; diamonds represent the HOMO−1 to HOMO−4 and LUMO−1 to LUMO−4 π-MOs; circles represent the HOMO−LUMO band gap energy for selected BODIPY analogues.

Table 10: TD-DFT calculation of electronic excitation energy, oscilator strengths and wave functions for meso-substituted BODIPY dyes **(1)** and **(4)** BODIPY dyes and their 2,6-dibrominated **(2)** and **(5)** analogues calculated by using the CAM-B3LYP functional with SDD basis set.

BODIPIY	#[a]	E (eV)[b]	λ[c]	*f*[d]	Wavefunction[e]
Unsubstituted BODIPY	S1	2.99	414	0.59	H → L (97%), H−1 → L (3%), …
	S2	3.85	322	0.084	H−1 → L (96%), H → L (3%), …
	S3	4.11	301	0.066	H−2 → L (98%), …
	S4	5.52	225	0.15	H−3 → L (95%), H → L+1 (2%), …
Dibrominated BODIPY	S1	2.89	429	0.72	H → L (96%), …
	S2	3.72	333	0.21	H−2 → L (93%), H → L (2%), …
	S3	3.83	324	0.06	H−1 → L (90%), H−5 → L (8%), …
	S4	4.61	269	0.00	H → L+1 (56%), H−1 → L+2 (26%), H−2 → L+1 (13%), …
Meso-phenyl BODIPY	S1	3.02	410	0.55	H → L (96%), H−1 → L (3%), …
	S2	3.84	323	0.075	H−1 → L (96%), H → L (3%), …
	S3	4.13	300	0.056	H−2 → L (98%), …
	S4	4.54	273	0.000	H−3 → L (96%), …
Dibrominated meso-phenyl BODIPY	S1	2.89	430	0.68	H → L (97%), …
	S2	3.68	337	0.15	H−2 → L (94%), …
	S3	3.83	324	0.072	H−1 → L (90%), …

	S4	4.34	286	0.001	H–3 → L (63%), H–5 → L (34%), …
BODIPY **(1)**	S1	3.02	410	0.54	H → L (96%), H–1 → L (2%), …
	S2	3.84	323	0.072	H–1 → L (96%), H → L (3%), …
	S3	4.13	300	0.057	H–3 → L (98%), …
	S4	4.30	289	0.000	H–2 → L (96%), …
BODIPY **(2)**	S1	2.89	429	0.67	H → L (97%), …
	S2	3.69	336	0.14	H–2 → L (78%), H–1 → L (16%), …
	S3	3.84	323	0.082	H–1 → L (75%), H–2 → L (16%), …
	S4	4.08	304	0.011	H–3 → L (95%), …
BODIPY **(4)**	S1	3.03	410	0.54	H → L (97%), H–2 → L (2%), …
	S2	3.27	380	0.001	H–1 → L (95%), H–5 → L (4%), …
	S3	3.85	322	0.072	H–2 → L (96%), H → L (3%), …
	S4	4.15	299	0.055	H–3 → L (98%), …
BODIPY **(5)**	S1	2.90	427	0.67	H → L (97%), …
	S2	3.05	406	0.093	H–1 → L (95%), …
	S3	3.70	335	0.14	H–2 → L (94%), …
	S4	3.87	321	0.070	H–3 → L (90%), …
BODIPY **(4)** + TFA	S1	2.96	420	0.55	H → L (97%), H–1 → L (2%), …
	S2	3.42	362	0.001	H → L+1 (97%), …
	S3	3.67	338	0.017	H → L+2 (98%), …
	S4	3.77	329	0.069	H–1 → L (97%), H → L (3%), …
BODIPY **(5)** + TFA	S1	2.76	449	0.67	H → L (97%), …
	S2	3.53	351	0.021	H → L+1 (61%), H–2 → L (33%), …
	S3	3.58	346	0.15	H–2 → L (61%), H → L+1 (32%), H–2 →L+1 (3%), …
	S4	3.64	340	0.068	H–1 → L (90%), H–5 → L (8%), …

a - Excited state number assinged in increasing energy in the TD-DFT calculations. b – Calculated band energies in eV. c – Calculated wavelengths in nm. d – Calculated oscilator strengths e – Wavefunctions of MOs involved in transition, and their respective contributions, based on eigenvectors predicted by TD-DFT. H and L refer to the HOMO and LUMO, respectively.

6.1.2 Molecular Modelling for Crown ether-BODIPY dyes (3) and (6)

Although there are no nodal planes at the 3,5-postions in ether the HOMO or LUMO, the MO coefficients at the HOMO and LUMO are unevenly distributed.[58] A larger MO coefficient on the HOMO suggests that any structural alterations at this position should result in a greater effect on the HOMO than on the LUMO and can thus result

in a change in magnitude of the HOMO–LUMO band gap. The addition of styryl crown ether moieties at the 3 and/or 5-positions can extend the π-system of the BODIPY core and destabilize the HOMO to a greater extent than the LUMO, and this results in a ca. 70 nm red-shift of the main absorption and emission spectral bands. This red-shift is enhanced by a further 70 nm with the addition of a second styryl crown ether moiety. The HOMO–LUMO one-electron transitions remain the dominate transition for the crown ether styryl BODIPY dyes where the most intense predicted band is concerned. Another effect of having a larger MO coefficient on the HOMO than in the LUMO for these BODIPYs is that any structural modification of the styryl groups is likely to cause a shift in the wavelength of the main bands in the absorption and emission spectra, which is what was observed upon complexation of the crown ether moieties with a sodium ion.

Minor one-electron transitions are also calculated for HOMO−1 → LUMO; HOMO−2 → LUMO; and HOMO−3 → LUMO transitions **(Table 11).** These transitions are primarily associated with the styryl substituents and result in the weak absorption bands observed over the 300–450 nm region in both mono and di-styryl crown ether BODIPYs.[58]

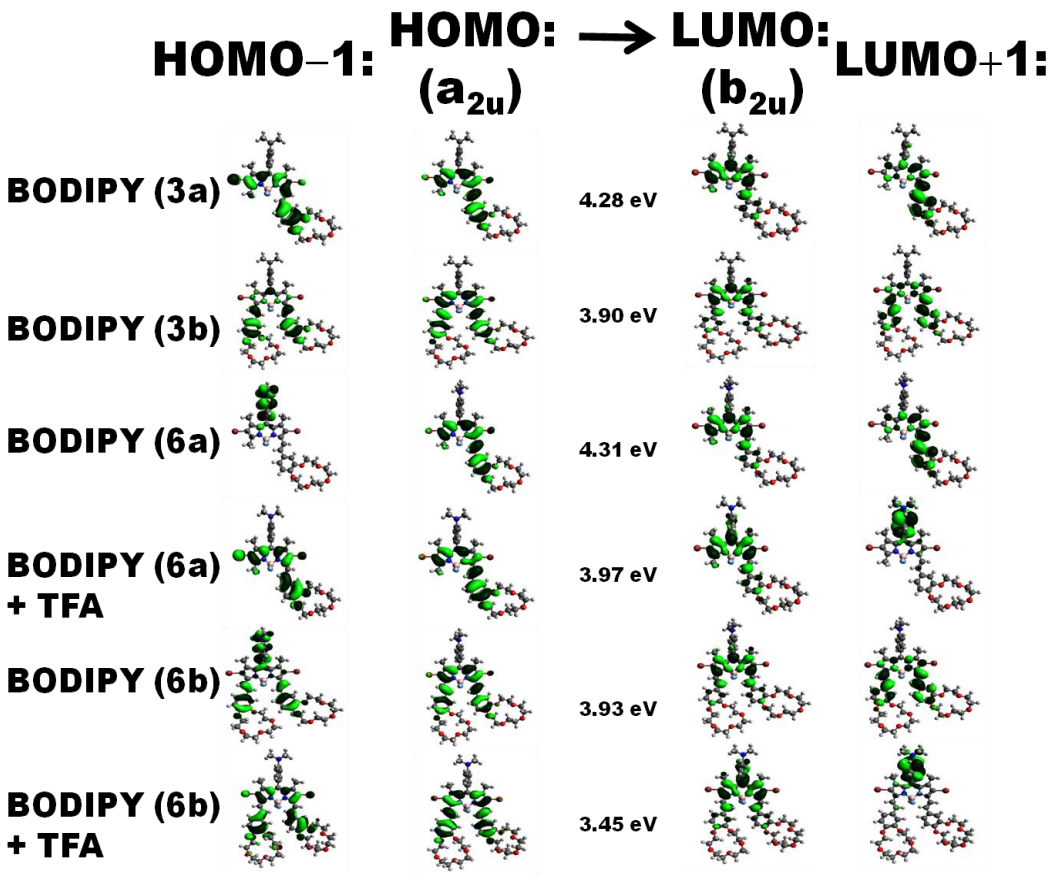

Figure 71: Nodal patterns and MO energies of the four frontier π-MO for crown ether-BODIPY dyes **(3a)**, **(3b)**, **(6a)** and **(6b)**. MO energies of selected BODIPY dyes at an isosurface value of 0.04 a.u. HOMO−LUMO gap energies are highlighted for the main electronic transition ($a_{2u} \rightarrow b_{2u}$). The positions and relative magnitudes of MO coefficients can provide insight into the potential effects of structural changes on the photophysical properties of studied BODIPY dyes.

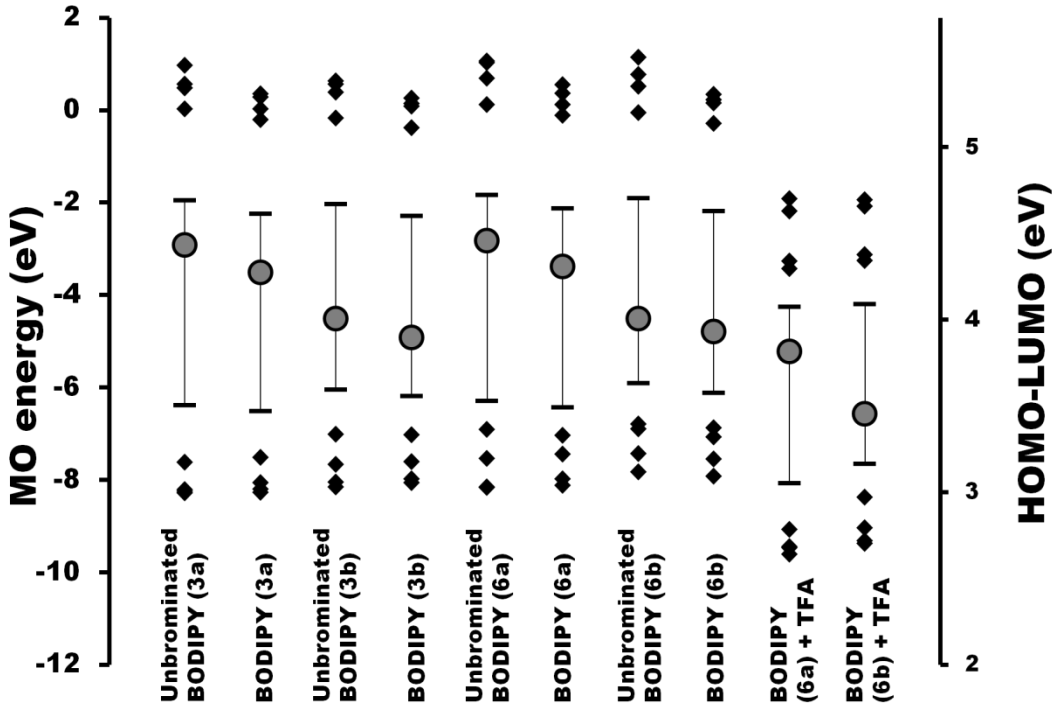

Figure 72: The frontier MO energies and HOMO–LUMO gaps for a select range of Crown ether-BODIPY dyes **(3a)**, **(3b)**, **(6a)** and **(6b)** using the CAM-B3LYP functional with the SDD basis set. Dashes represent the HOMO and LUMO MO; diamonds represent the HOMO–1 to HOMO–4 and LUMO–1 to LUMO–4 π-MOs; circles represent the HOMO–LUMO band gap energy for selected BODIPY analogues.

Table 11: TD-DFT calculation of electronic excitation energy, oscilator strengths and wave functions crown ether-BODIPY dyes **(3a)** and **(3b)** and their 2,6-dibrominated analogues **(6a)**, **(6b)** calculated by using the CAM-B3LYP functional with SDD basis set.

BODIPIY	#[a]	E (eV)[b]	λ[c]	*f*[d]	Wavefunction[e]
Unbrominated BODIPY **(3a)**	S1	2.53	491	0.93	H → L (96%), …
	S2	3.73	332	0.14	H–1 → L (84%), H–4 → L (9%), …
	S3	3.92	317	0.30	H–1 → L (73%), H–4 → L (11%), H–2 → L (3%), …
	S4	4.08	304	0.16	H–7 → L (90%), H–1 → L (7%), …
BODIPY **(3a)**	S1	2.41	515	1.0	H → L (94%), H–1 → L (4%), …
	S2	3.45	360	0.27	H–1 → L (53%), H–2 → L (24%), H–4 → L (10%), H → L (2%), …
	S3	3.73	332	0.16	H–2 → L (34%), H–1 → L (30%), H–3 → L (22%), …
	S4	3.81	325	0.14	H–4 → L (80%), H–1 → L (5%), H–2 → L (4%), H–3 → L (3%), …
Unbrominated BODIPY **(3b)**	S1	2.14	579	0.58	H → L (96%), …
	S2	3.35	360	0.97	H–1 → L (92%), …
	S3	3.72	334	0.025	H–6 → L (90%), H–2 → L (3%), …
	S4	4.02	308	0.11	H → L+1 (13%), …
BODIPY **(3b)**	S1	2.05	605	0.60	H → L (96%), …
	S2	3.17	392	0.98	H–1 → L (93%), …
	S3	3.48	357	0.004	H–4 → L (41%), H–2 → L (31%), H–6 → L (11%), H–5 → L (7%), H–3 → L (2%), …

	S4	3.77	329	0.049	H−5 → L (42%), H−6 → L (36%), H−3 → L (6%), …
Unbrominated BODIPY **(6a)**	S1	2.54	489	0.93	H → L (96%), …
	S2	3.16	393	0.002	H−1 → L (93%), …
	S3	3.74	331	0.14	H−4 → L (56%), H−3 → L (30%), H−2 → L (6%), …
	S4	3.94	315	0.33	H−2 → L (74%), H−3 → L (9%), H−7 → L (7%), …
BODIPY **(6a)**	S1	2.42	511	1.0	H → L (94%), H−2 → L (3%), …
	S2	22.99	414	0.098	H−1 → L (94%), …
	S3	3.49	356	0.23	H−2 → L (48%), H−3 → L (29%), H−5 → L (10%), H−4 → L (4%), H → L (2%), …
	S4	3.76	330	0.16	H−3 → L (36%), H−2 → L (33%), H−4 → L (19%), …
Unbrominated BODIPY **(6a)** + TFA	S1	2.29	542	1.1	H → L (94%), H−1 → L (4%), …
	S2	3.00	420	0.001	H → L+1 (83%), H−1 → L+1 (14%), …
	S3	3.19	389	0.029	H → L+2 (84%), H−1 → L+2 (13%), …
	S4	3.36	369	0.28	H−1 → L (84%), H → L (4%), …
BODIPY **(6a)** + TFA	S1	2.16	574	1.1	H → L (93%), H−1 → L (5%), …
	S2	3.06	406	0.039	H → L+1 (82%), H−1 → L+1 (12%), …
	S3	3.13	397	0.26	H−1 → L (78%), H → L (4%), H−4 → L (4%), …
	S4	3.28	378	0.027	H → L+2 (85%), H−1 → L+2 (12%), …
Unbrominated BODIPY **(6b)**	S1	2.13	582	0.54	H → L (96%), …
	S2	3.11	399	0.24	H−1 → L (65%), H−2 → L (29%), …
	S3	3.35	370	0.78	H−2 → L (64%), H−1 → L (28%), …
	S4	3.72	334	0.020	H−6 → L (88%), H−3 → L (5%), …
BODIPY **(6b)**	S1	2.07	599	0.59	H → L (96%), …
	S2	2.93	424	0.49	H−1 → L (75%), H−2 → L (19%), …
	S3	3.26	381	0.60	H−2 → L (74%), H−1 → L (19%), …
	S4	3.50	355	0.005	H−5 → L (46%), H−3 → L (28%), H−7 → L (9%), H−4 → L (6%), …
Unbrominated BODIPY **(6b)** + TFA	S1	1.87	662	0.54	H → L (95%), …
	S2	2.73	454	0.008	H → L+1 (89%), H−2 → L+1 (6%), …
	S3	2.85	422	0.82	H−1 → L (93%), …
	S4	2.94	367	0.15	H → L+2 (90%), H−2 → L+2 (5%), …
BODIPY **(6b)** + TFA	S1	1.79	693	0.59	H → L (95%), …
	S2	2.75	451	0.90	H−1 → L (94%), …
	S3	2.85	436	0.024	H → L+1 (88%), H−2 → L+1 (5%), …
	S4	3.04	408	0.12	H → L+2 (90%), H−2 → L+2 (5%), …

a - Excited state number assinged in increasing energy in the TD-DFT calculations. b – Calculated band energies in eV. c – Calculated wavelengths in nm. d – Calculated oscilator strengths d – Wavefunction of MOs involved in transition, and their respective contributions, based on eigenvectors predicted by TD-DFT. H and L refer to the HOMO and LUMO, respectively.

6.1.3 Comparison between predicted model and real spectra for BODIPYs (1), (2), (3a) and (3b)

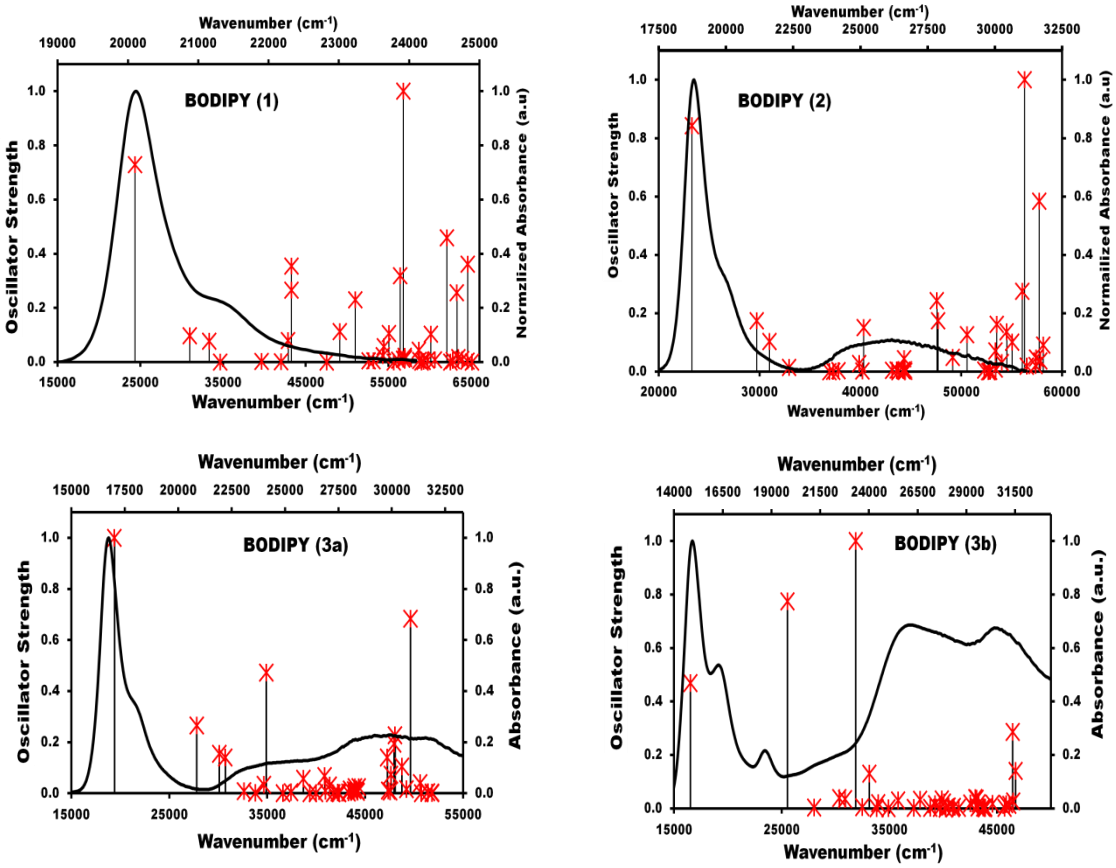

Figure 73: TD-DFT calculated oscillator strengths of the first forty excited states overlaid with the experimental electronic absorption spectra on the secondary axis for selected BODIPY dye analogues. BODIPY absorption spectra are recorded in $CHCl_3$. (Top left) BODIPY **(1)**. (Top right) BODIPY **(2)**. (Bottom left) BODIPY **(3a)**. (Bottom right) BODIPY **(3b)**.

6.1.4 Concluding remarks

TD-DFT calculations are a useful tool for establishing trends in the energy of BODIPY molecular orbitals. Studying these trends can provide insight into the photophysical properties of BODIPY dyes that allows for the rationalization of spectral shifts; the morphology of absorption bands; as well as offering possible explanations for observed fluorescence behaviour of BODIPY dyes that are caused by structural

modifications of the BODIPY core. Careful use of molecular modelling could assist in the rational design of BODIPY dye molecules for sensor applications. The modelling data show that complexation between a metal ion and a styryl crown ether moiety at the BODIPYs 3,5-position could result in a small, but measurable change in the absorption spectrum of the complex. There is a satisfactory match between the trends in the BODIPY calculations and the experimental electronic absorption spectra **(Figure 73)**.

Chapter 7:

Conclusions, Limitations and Future Work

7.1 Conclusions

Two BODIPY dyes (including the novel *meso*-(*p*-isopropylphenyl) substituted BODIPY **(1)**) with different para-substituents on the meso-phenyl functional group were synthesized using the acid catalysed condensation reaction and were fully characterized. **(1)** displays highly favourable photophysical properties. Interestingly, **(2)** demonstrated "off-on" fluorescence emission when protonated by TFA. This effect was no longer observed when **(2)** was electrospun into PS nanofibers as its fluorescence properties remained "on" even in the absence of TFA. Subsequently, BODIPY dyes **(1)** and **(2)** were synthesised to serve as the core for increasingly complex BODIPY dyes.

In order to enhance the rate of ISC, and thus enable the BODIPY dyes to generate singlet oxygen, bromine atoms were attached at the 2,6-positions to form BODIPYs **(2)** and **(5).** Due to the heavy atom effect a marked decrease in fluorescence quantum yield which was accompanied by an increase in singlet oxygen quantum generation. The brominated BODIPY dyes are highly photostable during experiments with intense ns pulsed laser beams and this makes them good candidates for singlet oxygen applications. These BODIPYs were electrospun into PS nanofibers where they were to be used for the photodegradation of azo-dyes such as tartrazine and Orange-G. Once the BODIPYs were embedded in the nanofibers, however, no singlet oxygen generation could be detected.

Four novel crown ether styryl-BODIPY dyes were synthesized from the two brominated BODIPY dyes. These compounds exhibit moderately high fluorescence and singlet oxygen quantum yields. When the crown ether moieties complex sodium ions in

solution they are accompanied by a slight blue-shift of the band maxima in the absorption and emission spectra. An increase in the singlet oxygen quantum yield was also observed for **(3a)** and **(3b)**.

7.2 Limitations

- Most of the environmental contaminants of interest (such as azo-dyes) are found in aqueous media. Using BODIPYs dyes to degrade such pollutants could be problematic as none of the BODIPY dyes synthesized in this study are soluble in water. The use of a solid nanofibers support was explored in this work as it offers the potential to recycle the BODIPY photocatalyst. It may also be possible to solve this problem by adding water solubilising groups to the BODIPY dyes.
- Despite the favourable properties of polystyrene for fabricating nanofibers such as chemical inertness; transparency; and low cost, it is unfortunately hydrophobic. This means that the distance between the solution and the BODIPY inside the fiber is too great to allow transfer of the singlet excited state energy. Polymers other than polystryrene should therefore be explored for the fabrication of BODIPY embedded nanofibers.
- 4'-formylbenzo-15-crown-5 is not particularly selective as it is able to bind both Na^+ and K^+ ions. While it is sufficient for proof of principle, an aza- or thiaaza-crown ether moiety would be better suited for studying the effects that complexation of ions with greater environmental impact have on the photophysical properties of a crown ether BODIPY dye.

- Sodium is a light metal which means that the ability for sodium to improve the singlet oxygen quantum yield by the heavy atom effect is severely limited. The ability to chelate heavier atoms, such as Hg^{2+} or Ag^{+}, could prove more efficient at enhancing the singlet oxygen quantum yield.

7.3 Future Work

TD-DFT calculations should include complexes of crown ether BODIPY dyes in order to gain further insight into the effect that chelation of a metal ion has on the photophysical properties of these BODIPY dyes.

Replacing the 2,6-position bromine atoms with iodine atoms could further improve the singlet oxygen quantum yields of BODIPY dyes.

Hydrophilic polymers, such as chitosan, should be explored as alternative materials for the fabrication of BODIPY embedded nanofibers.

Further studies on the photodegradation of azo-dyes could prove useful for comparing the photocatalytic ability of BODIPY dyes in solution and those embedded in nanofibers.

It would be of great interest to compare the photophysical properties of crown ether BODIPY dye complexes that contain heavier ions, such as Ag^{+} and Hg^{2+}. This would enable BODIPY dyes to act as ion sensor molecules for environmentally significant ions as well as offering a potentially viable method for improving the singlet oxygen quantum yield of such molecules due to the heavy atom effect.

References

1 A. Treibs and F.-H. Kreuzer, *Justus Liebigs Ann. Chem.*, 1968, **718**, 208–223.

2 F. J. Monsma, C. Barton, H. C. Kang, D. L. Brassard, R. P. Haugland and D. R. Sibley, *J. Neurochem.*, 1989, **52**, 1641–4.

3 G. Ulrich, R. Ziessel and A. Harriman, *Angew. Chem. Int. Ed.*, 2008, **47**, 1184–1201.

4 B. Hinkeldey, A. Schmitt and G. Jung, *ChemPhysChem*, 2008, **9**, 2019–2027.

5 J. Bañuelos, V. Martín, C. F. A. Gómez-Durán, I. J. A. Córdoba, E. Peña-Cabrera, I. García-Moreno, Á. Costela, M. E. Pérez-Ojeda, T. Arbeloa and Í. L. Arbeloa, *Chem. Eur. J.*, 2011, **17**, 7261–7270.

6 M. E. Pérez-Ojeda, C. Thivierge, V. Martín, Á. Costela, K. Burgess and I. García-Moreno, *Opt. Mater. Express*, 2011, **1**, 243.

7 M. Benstead, G. H. Mehl and R. W. Boyle, *Tetrahedron*, 2011, **67**, 3573–3601.

8 A. Harriman, G. Izzet and R. Ziessel, *J. Am. Chem. Soc.*, 2006, **128**, 10868–10875.

9 T. K. Khan, M. Bröring, S. Mathur and M. Ravikanth, *Coord. Chem. Rev.*, 2013, **257**, 2348–2387.

10 S. L. Niu, C. Massif, G. Ulrich, P. Y. Renard, A. Romieu and R. Ziessel, *Chem. Eur. J.*, 2012, **18**, 7229–7242.

11 A. Poirel, P. Retailleau, A. De Nicola and R. Ziessel, *Chem. - A Eur. J.*, 2014, **20**, 1252–1257.

12 S. Zhu, J. Zhang, J. Janjanam, J. Bi, G. Vegesna, A. Tiwari, F. T. Luo, J. Wei and H. Liu, *Anal. Chim. Acta*, 2013, **758**, 138–144.

13 Y. Ni, L. Zeng, N. Y. Kang, K. W. Huang, L. Wang, Z. Zeng, Y. T. Chang and J. Wu, *Chem. Eur. J.*, 2014, **20**, 2301–2310.

14 R. D. Moriarty, A. Martin, K. Adamson, E. O'Reilly, P. Mollard, R. J. Forster and T. E.

Keyes, *J. Microsc.*, 2014, **253**, 204–218.

15 M. Baruah, W. Qin, N. Basari and W. M. De Borggraeve, *Synthesis*, 1–26.

16 Y.-H. Yu, Z. Shen, H.-Y. Xu, Y.-W. Wang, T. Okujima, N. Ono, Y.-Z. Li and X.-Z. You, *J. Mol. Struct.*, 2007, **827**, 130–136.

17 S. Hoogendoorn, A. E. M. Blom, L. I. Willems, G. A. Van Der Marel and H. S. Overkleeft, *Org. Lett.*, 2011, **13**, 5656–5659.

18 M. J. Culzoni, M. de la Peña, A Machuca, H. C. Goicoechea, R. Brasca and R. Babiano, *Talanta*, 2013, **117**, 288–96.

19 J. Wang, Y. Xie, Z. Wang and Q. Song, *Sens. Actuators, B.*, 2014, **194**, 149–155.

20 D. Wang, Y. Shiraishi and T. Hirai, *Tetrahedron Lett.*, 2010, **51**, 2545–2549.

21 Z. Ekmekci, M. D. Yilmaz and E. U. Akkaya, *Org. Lett.*, 2008, **10**, 461–464.

22 M. Işik, R. Guliyev, S. Kolemen, Y. Altay, B. Senturk, T. Tekinay and E. U. Akkaya, *Org. Lett.*, 2014, **16**, 3260–3263.

23 T. Yogo, Y. Urano, Y. Ishitsuka, F. Maniwa and T. Nagano, *J. Am. Chem. Soc.*, 2005, **127**, 12162–12163.

24 A. Gorman, J. Killoran, C. Shea, T. Kenna, W. M. Gallagher and D. F. Shea, *J. Am. Chem. Soc.*, 2004, **126**, 10619–10631.

25 W. M. Gallagher, L. T. Allen, C. O. Shea, T. Kenna, M. Hall, A. Gorman, J. Killoran and D. F. Shea, 2005, **06**, 1702–1710.

26 H. He, P. C. Lo, S. L. Yeung, W. P. Fong and D. K. Ng, *Chem Commun*, 2011, **47**, 4748–4750.

27 X. Cui, C. Zhang, K. Xu and J. Zhao, *J. Mater. Chem. C*, 2015, **3**, 8735–8759.

28 A. C. Benniston and G. Copley, *Phys. Chem. Chem. Phys.*, 2009, **11**, 4124–4131.

29 Y. W. Wang, A. B. Descalzo, Z. Shen, X. Z. You and K. Rurack, *Chem. Eur. J.*, 2010, **16**, 2887–2903.

30 S. K. S. L. J. Kim, *Chem. Soc. Rev.*, 2010, **39**, 3784–3809.

31 Y. Ni and J. Wu, *Org. Biomol. Chem.*, 2014, **12**, 3774.

32 N. Boens, V. Leen and W. Dehaen, *Chem. Soc. Rev.*, 2012, **41**, 1130–1172.

33 Y. Kubota, J. Uehara, K. Funabiki, M. Ebihara and M. Matsui, *Tetrahedron Lett.*, 2010, **51**, 6195–6198.

34 Z. Dost, S. Atilgan and E. U. Akkaya, *Tetrahedron*, 2006, **62**, 8484–8488.

35 A. Loudet and K. Burgess, *Chem. Rev.*, 2007, **107**, 4891–4932.

36 K. Tram, H. Yan, H. A. Jenkins, S. Vassiliev and D. Bruce, *Dye. Pigm.*, 2009, **82**, 392–395.

37 W. Qin, T. Rohand, W. Dehaen, J. N. Clifford, K. Driesen, D. Beljonne, B. Van Averbeke, M. Der Van Auweraer and N. Boens, *J. Phys. Chem. A*, 2007, **111**, 8588–8597.

38 A. Kamkaew, S. H. Lim, H. B. Lee, L. V. Kiew, L. Y. Chung and K. Burgess, *Chem. Soc. Rev.*, 2013, **42**, 77–88.

39 V. Lakshmi and M. Ravikanth, *Dalton. Trans.*, 2012, **41**, 5903.

40 S. L. Niu, G. Ulrich, P. Retailleau, J. Harrowfield and R. Ziessel, *Tetrahedron Lett.*, 2009, **50**, 3840–3844.

41 S. L. Niu, C. Massif, G. Ulrich, R. Ziessel, P.-Y. Renard and A. Romieu, *Org. Biomol. Chem.*, 2011, **9**, 66–69.

42 J. Xu, Q. Li, Y. Yue, Y. Guo and S. Shao, *Biosens. Bioelectron.*, 2014, **56**, 58–63.

43 S. L. Niu, G. Ulrich, R. Ziessel, A. Kiss, P. Y. Renard and A. Romieu, *Org. Lett.*, 2009, **11**, 2049–2052.

44 A. Schmitt, B. Hinkeldey, M. Wild and G. Jung, *J Fluoresc*., 2009, **19**, 755-758

45 T. E. Wood and A. Thompson, *Chem. Rev.*, 2007, **107**, 1831–1861.

46 B. J. Littler, M. Miller, C. H. Hung, R. W. Wagner, D. F. O'Shea, P. D. Boyle and J. S. Lindsey, *J. Org. Chem.*, 1999, **64**, 1391–1396.

47 M. Zhang, E. Hao, Y. Xu, S. Zhang, H. Zhu, Q. Wang, C. Yu and L. Jiao, *RSC Adv.*, 2012, **2**, 11215.

48 I. K. Petrushenko and K. B. Petrushenko, *Spectrochim. Acta. A.*, 2015, **138**, 623–7.

49 M. Baruah, W. Qin, N. Basarić, W. M. De Borggraeve and N. Boens, *J. Org. Chem.*, 2005, **70**, 4152–4157.

50 X. Liang, J. Mack, L. Zheng, Z. Shen and N. Kobayashi, *Inorg Chem,* 2014, **53**, 2797-2802.

51 J. Isaad and A. El Achari, *Dye. Pigment.*, 2013, **99**, 878–886.

52 S. Liu, Z. Shi, W. Xu, H. Yang, N. Xi, X. Liu, Q. Zhao and W. Huang, *Dye. Pigm.*, 2014, **103**, 145–153.

53 F. E. Alemdaroglu, S. C. Alexander, D. Ji, D. K. Prusty, M. Börsch and A. Herrmann, *Macromolecules*, 2009, **42**, 6529–6536.

54 L. Jiao, W. Pang, J. Zhou, Y. Wei, X. Mu, G. Bai and E. Hao, *J. Org. Chem.*, 2011, **76**, 9988–9996.

55 O. Buyukcakir, O. A. Bozdemir, S. Kolemen, S. Erbas and E. U. Akkaya, *Org. Lett.*, 2009, **11**, 4644–4647.

56 V. Lakshmi, M. Rajeswara Rao and M. Ravikanth, *Org. Biomol.*, 2015, **13**, 2501–17.

57 T. Komatsu, Y. Urano, Y. Fujikawa, T. Kobayashi, H. Kojima, T. Terai, K. Hanaoka and T. Nagano, *Chem. Commun.*, 2009, 7015–7.

58 L. Gai, J. Mack, H. Lu, H. Yamada, D. Kuzuhara, G. Lai, Z. Li and Z. Shen, *Chem. Eur. J.*,

2014, **20**, 1091–1102.

59 S. Zhu, J. Bi, G. Vegesna, J. Zhang, F.-T. Luo, L. Valenzano and H. Liu, *RSC Adv.*, 2013, **3**, 4793.

60 Y. Hayashi, S. Yamaguchi, W. Y. Cha, D. Kim and H. Shinokubo, *Org. Lett.*, 2011, **13**, 2992–2995.

61 A. Cihaner and F. Algi, *React. Funct. Polym.*, 2009, **69**, 62–67.

62 L. Jiao, C. Yu, M. Liu, Y. Wu, K. Cong, T. Meng, Y. Wang and E. Hao, *J. Org. Chem.*, 2010, **75**, 6035–6038.

63 K. Rurack, M. Kollmannsberger and J. Daub, *Angew. Chem. Int. Ed.*, 2001, **40**, 385–387.

64 Ö. Dilek and S. L. Bane, *Bioorg. Med. Chem. Lett.*, 2009, **19**, 6911–6913.

65 M. Vincent, E. Beabout, R. Bennett and P. Hewavitharanage, *Tetrahedron Lett.*, 2013, **54**, 2050–2054.

66 T. Jiang, P. Zhang, C. Yu, J. Yin, L. Jiao, E. Dai, J. Wang, Y. Wei, X. Mu and E. Hao, *Org. Lett.*, 2014, **16**, 1952–1955.

67 L. Jiao, W. Pang, J. Zhou, Y. Wei, X. Mu, G. Bai and E. Hao, *J. Org. Chem.*, 2011, **76**, 9988-9996.

68 L. Jiao, C. Yu, T. Uppal, M. Liu, Y. Li, Y. Zhou, E. Hao, X. Hu and M. G. H. Vicente, *Org. Biomol. Chem.*, 2010, **8**, 2517–2519.

69 V. Leen, P. Yuan, L. Wang, N. Boens and W. Dehaen, *Org. Lett.*, 2012, **14**, 6150–3.

70 C.-W. Wan, A. Burghart, J. Chen, F. Bergström, L. B.-Å. Johansson, M. F. Wolford, T. G. Kim, M. R. Topp, R. M. Hochstrasser and K. Burgess, *Chem. Eur. J.*, 2003, **9**, 4430–4441.

71 S. Atilgan, Z. Ekmekci, a L. Dogan, D. Guc and E. U. Akkaya, *Chem. Commun.*, 2006, 4398–4400.

72 R. P. Sabatini, T. M. McCormick, T. Lazarides, K. C. Wilson, R. Eisenberg and D. W.

McCamant, *J. Phys. Chem. Lett.*, 2011, **2**, 223–227.

73 X.-F. Zhang, X. Yang, K. Niu and H. Geng, *J. Photochem. Photobiol. A.*, 2014, **285**, 16–20.

74 T. Deligeorgiev, A. Vasilev, S. Kaloyanova and J. J. Vaquero, *Color. Technol.*, 2010, **126**, 55–80.

75 A. M. Hansen, A. L. Sewell, R. H. Pedersen, D. L. Long, N. Gadegaard and R. Marquez, *Tetrahedron*, 2013, **69**, 8527–8533.

76 J. S. Lee, N. Y. Kang, K. K. Yun, A. Samanta, S. Feng, K. K. Hyeong, M. Vendrell, H. P. Jung and Y. T. Chang, *J. Am. Chem. Soc.*, 2009, **131**, 10077–10082.

77 M. Baruah, W. Qin, C. Flors, J. Hofkens, R. a L. Vallée, D. Beljonne, M. Van Der Auweraer, W. M. De Borggraeve and N. Boens, *J. Phys. Chem. A*, 2006, **110**, 5998–6009.

78 O. A. Bozdemir, R. Guliyev, O. Buyukcakir, S. Selcuk, S. Kolemen, G. Gulseren, T. Nalbantoglu, H. Boyaci and E. U. Akkaya, *J. Am. Chem. Soc.*, 2010, **132**, 8029–8036.

79 A. Coskun, E. Deniz and E. U. Akkaya, *Org. Lett.*, 2005, **7**, 5187–5189.

80 H. Son, H. Y. Lee, J. M. Lim, D. Kang, W. S. Han, S. S. Lee and J. H. Jung, *Chem. Eur. J.*, 2010, **16**, 11549–11553.

81 J. Fan, M. Hu, P. Zhan and X. Peng, *Chem. Soc. Rev.*, 2013, **42**, 29–43.

82 S. Atilgan, I. Kutuk and T. Ozdemir, *Tetrahedron Lett.*, 2010, **51**, 892–894.

83 J. K. Hyun, H. K. Sang, H. K. Ja, E. H. Lee, K. W. Kim and S. K. Jong, *Bull. Korean Chem. Soc.*, 2008, **29**, 1831–1834.

84 S. Ozlem and E. U. Akkaya, *J. Am. Chem. Soc.*, 2009, **131**, 48–49.

85 W. Qin, M. Baruah, M. Sliwa, M. Den Van Auweraer, W. M. De Borggraeve, D. Beljonne, B. Van Averbeke and N. Boens, *J. Phys. Chem. A*, 2008, **112**, 6104–6114.

86 I. Móczár, P. Huszthy, Z. Maidics, M. Kádár and Klára Tóth, *Tetrahedron*, 2009, **65**,

8250–8258.

87 M. Yuan, Y. Li, J. Li, C. Li, X. Liu, J. Lv, J. Xu, H. Liu, S. Wang and D. Zhu, *Org. Lett.*, 2007, **9**, 2313–2316.

88 J. Isaad and A. El Achari, *Analyst*, 2013, **138**, 3809–3819.

89 C. J. Pedersen, *J. Am. Chem. Soc.*, 1967, **89**, 7017–7036.

90 R. Adams and L. N. Whitehill, *J. Am. Chem. Soc.,* 1941, **63**, 2073−2078.

91 J. S. Bradshaw and P. E. Stott, *Tetrahedron*, 1979, **36**, 461-510.

92 K. E. Krakowiak, J. S. Bradshaw and D. J. Zamecka-Krakowiak, *Chem. Rev.,* 1989, **89**, 929-972.

93 G. W. Gokel, W. M. Leevy and M. E. Weber, *Chem. Rev.*, 2004, **104**, 2723–2750.

94 Y. Wu, H. An, J. Tao, J. S. Bradshaw and R. M. Izatt, *J. Incl. Phenom. Macro.*, 1990, **9**, 267–274.

95 V. Beachley and X. Wen, *Mater. Sci. Eng. C.*, 2011, **29**, 1–17.

96 S. Homaeigohar and M. Elbahri, *Mater.*, 2014, **7**, 1017-1045.

97 D. H. Reneker and I. Chun, *Nanotechnology*, 1999, **7**, 216–223.

98 S. Agarwal, A. Greiner and J. H. Wendorff, *Prog. Polym. Sci.*, 2013, **38**, 963–991.

99 R. Zugle, C. Litwinski, N. Torto and T. Nyokong, *New J. Chem.*, 2011, **35**, 1588.

100 A. Goethals, T. Mugadza, Y. Arslanoglu, R. Zugle, E. Antunes, S. W. H. Van Hulle, T. Nyokong and K. De Clerck, *J. Appl. Polym. Sci.*, 2014, **131**, 1–7.

101 P. Modisha and T. Nyokong, *J. Mol. Catal. A.*, 2014, **381**, 132–137.

102 M. Fischer and J. Georges, *Chem. Phys. Lett.*, 1996, **260**, 115–118.

103 T. Nyokong, *Coord. Chem. Rev.*, 2007, **251**, 1707–1722.

104 http://goldbook.iupac.org (2006-) created by M. Nic, J. Jirat, B. Kosata; updates compiled by A. Jenkins. ISBN 0-9678550-9-8. doi:10.1351/goldbook.

105 E.L. Clennan, Tetrahedron, 2000, **56**, 9151-9179.

106 P. Modisha, T. Nyokong and E. Antunes, *J. Mol. Catal. A.*, 2013, **380**, 131–138.

107 X.-Z. Wang, Q.-Y. Meng, J.-J. Zhong, X.-W. Gao, T. Lei, L.-M. Zhao, Z.-J. Li, B. Chen, C.-H. Tung and L.-Z. Wu, *Chem. Commun.*, 2015, **51**, 11256–9.

108 M. Managa, E. Antunes and T. Nyokong, *Polyhedron*, 2014, **76**, 94–101.

109 S. Tombe, E. Antunes and T. Nyokong, *New J. Chem.*, 2013, **37**, 679.

110 D. C. Neckers, *J. Photochem. Photobiol. A.*, 1989, **47**, 1–29.

111 N. A. Kuznetsova, N. S. Gretsova, E. Kalmykova, E. Makarova, S. Dashkevich, V. Negrimovskii, O. Kaliya and E. Luk'yanets, *Russ. J. Gen. Chem.*, 2000, **70**, 133–140.

112 D. L. Bish, D. F. Blake, D. T. Vaniman, S. J. Chipera, R. V. Morris, D. W. Ming, A. H. Treiman, P. Sarrazin, S. M. Morrison, R. T. Downs, C. N. Achillies, A. S. Yen, T. F. Bristow, J. A. Crisp, J. M. Morookain, J. D. Farmer, E. B. Rampe, E. M. Stolper and N. Spanovich, *Science*, 2013, **341**, 1-5.

113 C. Würth, M. G. González, R. Niessner, U. Panne, C. Haisch and U. R. Genger, *Talanta*, 2012, **90**, 30–37.

114 H. Langhals, D. Zgela and T. Schlücker, *G S C*, 2015, **5**, 92-100.

115 Gaussian 09, Revision D.01, M. J. Frisch, G. W. Trucks, H. B. Schlegel, G. E. Scuseria, M. A. Robb, J. R. Cheeseman, G. Scalmani, V. Barone, B. Mennucci, G. A. Petersson, H. Nakatsuji, M. Caricato, X. Li, H. P. Hratchian, A. F. Izmaylov, J. Bloino, G. Zheng, J. L. Sonnenberg, M. Hada, M. Ehara, K. Toyota, R. Fukuda, J. Hasegawa, M. Ishida, T. Nakajima, Y. Honda, O. Kitao, H. Nakai, T. Vreven, J. A. Montgomery, Jr., J. E. Peralta, F.

Ogliaro, M. Bearpark, J. J. Heyd, E. Brothers, K. N. Kudin, V. N. Staroverov, T. Keith, R. Kobayashi, J. Normand, K. Raghavachari, A. Rendell, J. C. Burant, S. S. Iyengar, J. Tomasi, M. Cossi, N. Rega, J. M. Millam, M. Klene, J. E. Knox, J. B. Cross, V. Bakken, C. Adamo, J. Jaramillo, R. Gomperts, R. E. Stratmann, O. Yazyev, A. J. Austin, R. Cammi, C. Pomelli, J. W. Ochterski, R. L. Martin, K. Morokuma, V. G. Zakrzewski, G. A. Voth, P. Salvador, J. J. Dannenberg, S. Dapprich, A. D. Daniels, O. Farkas, J. B. Foresman, J. V. Ortiz, J. Cioslowski, and D. J. Fox, Gaussian, Inc., Wallingford CT, 2013.

116 T. Uppal, N. V. S. D. K. Bhupathiraju and M. G. H. Vicente, *Tetrahedron*, 2013, **69**, 4687–4693.

117 C. Sousa, C. Freire and B. de Castro, *Molecules*, 2003, **8**, 894–900.

118 W. Qin, M. Baruah, A. Stefan, M. Van der Auweraer and N. Boens, *ChemPhysChem*, 2005, **6**, 2343–2351.

119 T. Yanai, D. P. Tew and N. C. Handy, *Chem. Phsy. Lett.*, 2004, **393**, 51-57.

120 C. Fischer, S. F. Helas, W. Seichter, E. Weber and B. T. Ibragimov, *Acta Crystallogr. E.*, 2008, **64**, 1556–1556.

121 T. Yanai, D. P. Tew and N. C. Handy, *Chem. Phys. Lett.*, 2004, **393**, 51–57.